REGIONAL FINITE STRAIN PATTERNS IN PROTEROZOIC SLATES AND QUARTZITES: IMPLICATIONS FOR HETEROGENEOUS STRAIN RELATED TO FLEXURAL SLIP FOLDING IN THE MARQUETTE SYNCLINORIUM

By

David B. Westjohn

A DISSERTATION

Submitted to
Michigan State University
in partial fulfillment of the requirements
for the degree of

DOCTOR OF PHILOSOPHY

Department of Geological Sciences

1990

ABSTRACT

REGIONAL FINITE STRAIN PATTERNS IN PROTEROZOIC SLATES AND QUARTZITES: IMPLICATIONS FOR HETEROGENEOUS STRAIN RELATED TO FLEXURAL SLIP FOLDING IN THE MARQUETTE SYNCLINORIUM

By

D.B. Westjohn

Proterozoic rocks in the Marquette synclinorium are part of a sequence of deformed metasediments that extends from northern Michigan (Marquette Range Supergroup; MRSG) to Minnesota (Animikie Group). Slates in the MRSG near Marquette, Michigan, contain reduction spots, sandstone dikes, and deformed veins. Quartzites contain conglomerates, ellipsoidal spots, deformed veins, deformed rutile needles, and grain aggregates. These strain indicators are present in rocks that experienced weak to substantial distortions, and they were used to characterize regional strain patterns.

Quartzites in open folds show no indication of being strained. Strains in quartzites can be discerned where fold limbs dip greater than 60 degrees, and the largest

strain ratios were observed in steep and overturned limbs. Strains in quartzite are heterogeneous, and the deformation style ranges from slight constriction to slight flattening; strain ratios are less than 1.3.

Argillites suffered early compactional strain and slight distortions related to the development of open flexures. Strains developed in early stages of folding, since veins are buckled or stretched even in weakly deformed argillites. Strains are heterogeneous, particularly along contacts between units that have large ductility contrasts. Angular shear strain estimates indicate extensions locally exceed 200 percent. These strains are localized in slate beds, and are not representative for the MRSG at the regional scale.

Strain ratios for slates are approximately twice those observed for quartzites in closed and overturned folds. The orientation of the principal strain axes in fold limbs show a consistent relation to fold geometry (except near major shear zones); the XY plane is approximately parallel to the axial trend of the Marquette trough, and X (maximum stretch) is subvertical.

Major structural features in the MRSG appear to have been inherited from the Archean basement. Fold geometry is consistent with basement controlled tectonics involving translations along faults and shear zones in the Archean blocks. Regional strain patterns and orientations of penetrative fabric support a heterogeneous strain model that includes folding related to flexural slip.

This dissertation is dedicated to Bev. She raised our children so I could go to school; she makes things happen!

ACKNOWLEDGMENTS

Dr. F.W. Cambray patiently guided me through both graduate degrees. I thank him most for the early stimulation he provided regarding all aspects of science, but particularly Precambrian geology. His support made completion of this dissertation possible.

The education in real geology, that is hard rock geology, provided by Dr. T.A. Vogel has kept me marketable during tough times for geologists.

My excitement with field geology was stimulated by Dr. J.T. Wilband. He managed to maintain patience while making me computer literate. He deferred his research dozens of weekends, and wrote and fixed computer programs that made analyzing structural data possible. Thank you Dr. Wilband for the bells and whistles.

Dr. K. Fujita shredded the first copy of the dissertation, demanded a rewrite, and bless him for that. He provided a detailed critical review of the final version, and helped improve the text in numerous ways. Thanks to Kaz and T.A.V.; their critical review of this work proves that scrutiny is one force of progress.

Dr. D.F. Sibley joined the committee late, but provided many helpful suggestions that served to improve the

dissertation.

My colleagues helped me through the culture shock related to leaving success and becoming an old student, and Paul Carter and Steve Young deserve special thanks.

Mark Breithart listened to countless hours of babbling about finite strain, and always managed to seem interested.

To my buddies J.P. Ansted, Mark Smith, and Andy Parr; thanks for all the geofantasy we have shared.

P.T. Benson deserves special recognition; his friendship over the years has helped me keep life in balance.

A special acknowledgement to Loretta; she helped solve problems no one else could, and to Cathy who helped set up our structural geology computer lab (and helped keep it on line). Diane graciously helped hundereds of times direct me along the correct path in the library, and helped me decipher TAV's cryptic slang.

Mike, Laurie, Christopher, and Leah put up with my impatience, and always accepted an absentee father during the course of my education; I love you guys and I appreciate all the help and support you have provided. Mike and Mary Jo Brien supported Bev and I in rough times, and their encouragement helped me make this very important goal.

Francis Grutrude Schlorff and Leonard Henry Westjohn would be proud to see this work complete, and this dissertation is a tribute to them.

TABLE OF CONTENTS

TABLE OF CONTENTS (continued)

TABLE OF CONTENTS (continued)

LIST OF TABLES

LIST OF FIGURES

LIST OF FIGURES (continued)

LIST OF FIGURES (continued)

LIST OF FIGURES (continued)

LIST OF FIGURES (continued)

LIST OF FIGURES (continued)

LIST OF FIGURES (continued)

LIST OF FIGURES (continued)

LIST OF FIGURES (continued)

LIST OF FIGURES (continued)

LIST OF PLATES

INTRODUCTION

The concept that strain variation in folded rock sequences is related to differences in lithology (ductility contrasts between rock types) and the presence of planar anisotropies (orientation of primary and secondary layering, degree of cohesion between layers, etc.) is supported by data from experimental investigations. Donath (1970) demonstrates that sandstone, shale, limestone, and dolomite follow substantially different strain paths when deformed in controlled laboratory experiments. Bulk strains for the rock suite tested differ by more than 350 percent, when strained at moderate confining stresses (2 kilobars). Donath and Parker (1964) relate observations from experimental work to show that relative ductilities and planar anisotropies dictate the mechanisms that produce the internal characteristics (strain patterns) and the geometry of folds. These authors (Donath and Parker, 1964) classify folds by the mechanisms that produce them (flexural slip, flexural flow, passive slip, and passive flow), and show that each mechanism results in different geometrical features.

One general model that is consistent with experimental data (Donath, 1962; Donath and others, 1971; Griggs, 1940) is that intercalated slates and quartzites in folds should have suffered different finite strains because of ductility contrasts. In addition to the effect of ductility contrasts between slates and quartzites, the orientation of primary layering changes relative to the principal stress direction as folds develop, so that the effect of planar anisostropies also changes during deformation. It is expected that these factors should be reflected in strain style and fold geometry. As folding progresses in this general model, the stress changes from layer normal to layer parallel; the predicted result is that in the early stages of fold development quartzites should act as a buttress and limit strains suffered by intercalated slates. In the last stage of the development of upright folds, stress is layer normal, and slates should experience greater bulk strain than quartzites because of the contrast in rheological properties. The predicted result of this model is that strain magnitude should differ in quartzites and slates as a function of relative position within the folded rock sequence, but the orientations of the principal strain axes should show little variation.

In order to test this general model, this dissertation relies on accepted techniques of strain analysis and the presence of multiple strain indicators, to characterize internal distortions in Proterozoic quartzites and slates.

Deformed metasediments near Marquette, Michigan, are part of a sequence of supracrustal rocks that extend from the east-central upper peninsula of Michigan (Marquette Range Supergroup) to northern Minnesota (Animikie Group). Collectively, these have been referred to as the Lake Superior Association (Baragar and Scoates, 1981). The stratigraphic sequences that comprise the Lake Superior Association resemble sedimentary successions that develop on modern passive continental plate margins (Cambray, 1977). By assessing the details of fold geometry, and the nature of internal distortions related to deformation, it should be possible to predict the mechanism responsible for the generation of folds in the MRSG.

It has been suggested that the Lake Superior Association may be one remnant of a continuous series of foldbelts (Circum-Superior Foldbelt) that rimmed the Archean craton during mid-Proterozoic time (Baragar and Scoates, 1981). Baragar and Scoates (1981) show that the Proterozoic foldbelts that partially rim the Archean Superior Province are similar in age, structural style, related igneous activity, and sedimentary history. These relationships support a suggestion that the Circum-Superior Belt is a Proterozoic analog for the style of sedimentation and deformation seen at modern plate margins (Baragar and Scoates, 1981, for the Superior Province; Cambray, 1977, and 1984, for foldbelts along the southern margin of the Canadian Shield).

Six types of finite strain indicators are present in quartzites and slates of the Marquette Range Supergroup. These strain gauges provide a record of the internal distortions experienced by quartzites and slates during folding. Slates in the MRSG contain reduction spots, sandstone dikes, and deformed veins. Quartzites in the same foldbelt contain conglomerate clasts, ferruginous ellipsoidal spots, deformed veins, folded and buckled rutile needles (within deformed quartz grains), and packed grain aggregates. These natural strain indicators are present in rocks that experienced internal distortions that range from weak to substantial, and they occur in a diversity of structural settings. Multiple gauges at single outcrops allow for strain determinations using two or more methods that do not rely on the same assumptions. The widespread distribution of strain gauges provides an opportunity to assess regional patterns of finite strain in rock types that have different rheological properties.

Finite strain analyses, and a detailed assessment of structural fabrics for slates and quartzites are combined with observations made at the outcrop and map scale to (1) address problems in structural geology concerning strain style, deformation mechanisms, strain magnitude, strain variation, strain partitioning, strain heterogeneity, and the effect of volume loss on strain estimates; (2) develop a model for the origin of fold styles observed in the Marquette synclinorium; and (3) test models that have been proposed for the origin of Proterozoic foldbelts in the

Circum-Superior Province.

Strain determinations from multiple strain gauges support a heterogeneous strain model that has many elements in common with a model proposed by Cambray (1977). The heterogeneous strain model, as applied to the study area, consists of a sequence of events that includes (1) layer-normal shortening (compaction) of sediments that accumulated in ensialic rift basins; (2) continued sedimentation with progressive extension along normal faults in Archean basement, with coeval development of near-vertical, east-trending vein sets and sandstone dikes; (3) volume redistribution and rotation of veins and sandstone dikes with early development of buckle folds during initial trough closure; (4) the onset of flattening strains and continued vein and sand-dike rotation driven by angular shear related to flexural-slip folding; (5) continued vertical movement along steep reverse faults (shears) in Archean blocks, but localized along the greenstone trend, with concomitant development of flower structures below the deforming pile; and (6) minor readjustment along the northern trough margin involving left-lateral shear with the local production of superposed folds, and the development of brittle extension veins in quartzites.

GEOLOGICAL SETTING

The geology of the Marquette-Ishpeming area is described by Van Hise and Leith (1911), Gair (1975), Gair and Thaden (1968), and Puffett (1974). A summary of the regional geologic setting is presented by Cambray (1977, 1984), who provides a list of references of the geological investigations that have led to the current understanding of the region. These materials provide details of the geology at all scales. Below, a brief summary of the geology of the Marquette-Ishpeming region is presented.

The area studied is part of the southern Superior Province of the Canadian Shield (Figure 1). Archean rocks consist of greenstone (Mona Schist) and granitoid gneiss (Bell Creek and Compeau Creek Gneiss). These units are locally overlain by a sequence of supracrustal rocks that are assigned to the MRSG (Cannon and Gair, 1970). The supergroup consists of conglomerates, quartzites, carbonates, slates, and banded iron formations. The MRSG includes the Chocolay, Menominee, and Baraga Groups (Cannon and Gair, 1970). Coarse clastics form the basal unit of each group and the repetition of similar stratigraphic sequences is interpreted to indicate that multiple episodes of crustal instability resulted in the development of these

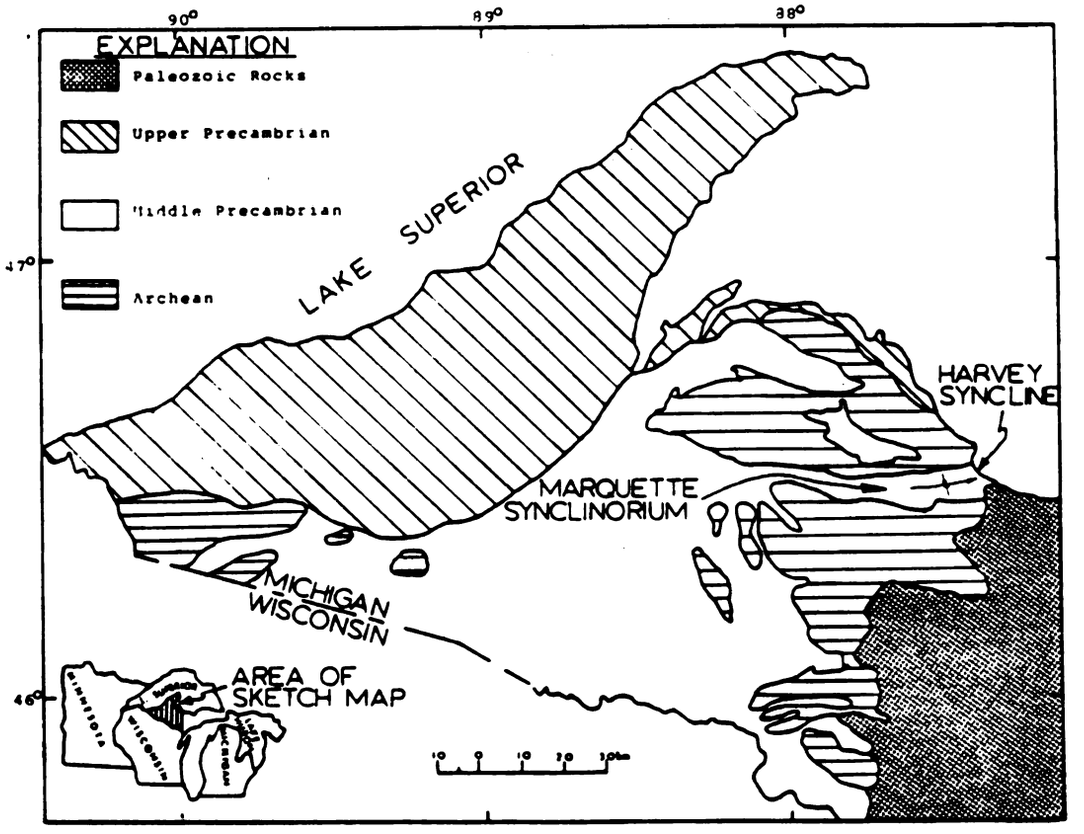

Figure 1. **Geologic sketch map of the western portion of the upper peninsula of Michigan, showing study area.**

successions (Cambray, 1977).

The MRSG sedimentary sequence has many characteristics common to modern miogeoclinal assemblages and transitional facies that develop along passive plate margins. The upright, open to close fold style characteristic of the MRSG resembles fold morphologies common to the Taconic and Wales slatebelts (Wood, 1973); these Paleozoic foldbelts are assumed to be comprised of deformed metasediments that formed along early Paleozoic passive plate margins. The fold style and depositional history of MRSG resembles that of Paleozoic foldbelts associated with continental margin collision type tectonism, and Cambray (1977) cites these similarities as evidence to support a passive plate depositional setting and subsequent deformation model for the MRSG.

Supracrustal rocks in the Marquette synclinorium unconformably overlie Archean basement in the southern fringes of the trough, while the northern contact of Archean and Proterozoic rocks is a steep fault boundary that parallels the synclinorium axis. Penetrative deformation during the Penokean Orogeny (1860-1820 Ma; Van Schmus and Bickford, 1981) produced generally simple fold patterns. The west-trending Marquette synclinorium is characterized by upright to slightly overturned doubly plunging asymmetric anticlinal and synclinal folds. Axial traces for primary folds roughly parallel the trough margins. Second generation folds and structural fabrics

characteristic of polyphase deformation are apparent in the western portion of the synclinorium (Larue and Cambray, 1978), but these are relatively uncommon in the eastern most part of the Marquette trough.

Several models have been proposed to explain the fold patterns in the deformed Proterozoic supracrustal package. Noteworthy models include (1) deposition of the supracrustal units in a passive plate margin setting followed by deformation in a back-arc environment related to subduction of oceanic crust (Van Schmus, 1976); (2) totally intracratonic deposition and deformation (Morey and Sims, 1976); (3) sedimentation in rift-related troughs that were partially closed during a later collisional event (Cambray, 1977); (4) passive drape-folding of the sediments in grabens that developed in rifted Archean basement (Cannon, 1974); (5) deformation involving collision between an arc terrane and a miogeoclinal assemblage (Cambray, 1977; Larue, 1983); and (6) a rifted continental margin with subsequent continent-continent collision (Cambray, 1977; Sims and Peterman, 1983).

DATA COLLECTION AND PROCESSING

Geological maps of the Marquette-Ishpeming area have been published by the U.S. Geological Survey (Gair and Thaden, 1968; Puffett, 1974; Clark and others, 1975; Gair, 1975). These maps served as planning guides for sampling strategy and outcrop location, and helped to expedite efficient field work. The most useful single work is that of Taylor (1973). Taylor's (1973) detailed stratigraphic analysis of the Kona Dolomite, and the geological map that accompanies his dissertation facilitated the location of key outcrops of Kona slate.

The strategy for sample collection was designed to address a fundamental question in structural geology. Do rock types with different rheological properties in various structural positions in foldbelts record internal distortions that provide insight regarding the mechanisms of deformation and fold development? To contribute to this question, research was focused on a continuum of structural environments that include settings where quartzites and slates are sub-horizontal and slightly deformed, and progressed in a sequential fashion to situations where internal distortions appear to be substantial and folds are tight and slightly overturned.

Field mapping of major and minor structures was conducted in conjunction with collection of oriented specimens for laboratory analysis. The orientations of certain structures (slaty cleavage, crenulation cleavage, veins, bedding, and sandstone dikes) provide insight regarding strain style and strain geometry, and the trends of penetrative fabric elements are shown on stereonet plots as a supplement to the strain data. Stereonet plots are included in the text where appropriate, and all are included in Plates 1-4 so that regional structural trends can be compared to strain data.

The procedure followed to extract strain data from oriented field samples involved a sequence of steps; these are summarized in Appendix A. Computer programs designed for applied studies in structural geology were relied on to process all data. The programs used to process data, the source of each program, and a list of "data in data out" are also summarized in Appendix A.

Finite strain values for all samples were determined using accepted methods of strain analysis (Talbot, 1970; Fry, 1979; Erslev, 1988; Lisle, 1985; Borradaile, 1977; and Mitra, 1977). The techniques used are described in conjunction with each type of strain gauge as it is introduced. However, the Rf/Phi (Ramsay, 1967) and Flinn (1962) methods of data display and analysis are discussed here, because these techniques are referred to throughout the text.

THE RF/PHI METHOD OF STRAIN ANALYSIS

Ramsay (1967, p. 211-221) devised a two-dimensional, graphical technique of strain analysis, whereby ellipsoids with variable orientations and axial lengths can be used to estimate finite strain. Dunnet (1969) elaborated on this method, and demonstrated the practical use of the technique that is commonly referred to as the Rf/Phi method of strain analysis. Many modifications and improvements followed Ramsay's (1967) first approach (Dunnett and Siddans, 1971; Elliot, 1970; Holst, 1982; Lisle, 1985; Milton, 1980; Onasch, 1984; Owens, 1984; Patterson, 1983; Ribeiro and others, 1983; Siddans, 1980; Siddans, 1981; De Paor, 1980; De Paor, 1981). The example given by Ramsay and Huber (1983) is used to demonstrate the important aspects of the Rf/Phi method (Figure 2a).

The Rf/Phi method involves determining the ellipticity and orientation of an ellipse that represents the strain ellipse for a given plane. The example shown (Figure 2a) is a plot of the orientation of long axes for seven ellipses relative to a horizontal reference line, plotted against the ellipticity of each feature. The ellipticity before strain (Figure 2a, Rs is the strain ratio, which is 1 for the unstrained case) is the same for each ellipse (Ri

Figure 2a. Diagram illustrating the Rf/Phi method of strain analysis. Block A is the undeformed case showing seven ellipses, each with Ri (initial ellipticity, or long to short axis ratio) equal to 2.0. Blocks B and C show ellipse positions and shapes after increments of strain (Rs=1.5, and Rs=3.0). Blocks A', B', and C' show ellipticities (Rf) after strain, plotted as a function of long axis orientation (angle Phi) for each case. The fluctuation (F) is the variation in the angle Phi. (Modified from Ramsay and Huber, 1985, p. 75).

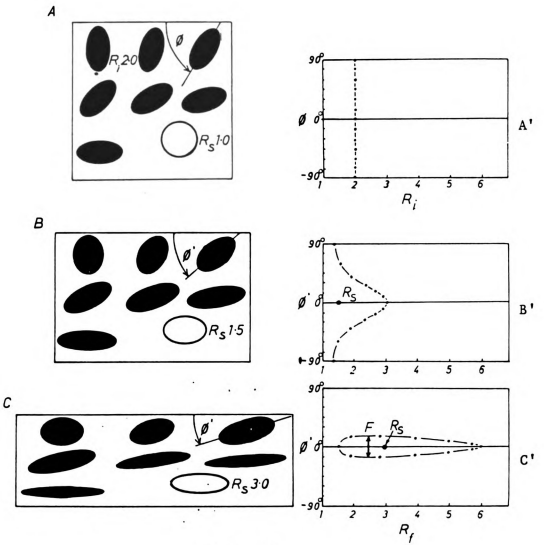

Figure 2a.

is the initial ellipticity, which is 2 for the example), while the acute angle the long axis makes with the reference line (angle Phi) is variable. The Rf/Phi plot for the "unstrained" case is a straight line, because ellipticity (Rf) is constant over a range of variable Phi angles.

After an increment of strain (Figure 2a, Rs=1.5), the ratio of the long axis to short axis (Rf or ellipticity) increases for some ellipses, while it decreases for others. The Rf/Phi plot that represents this increment of strain is illustrated in Figure 2a. Additional strain leads a less dispersed pattern of points on the Rf/Phi diagram, because the fluctuation (F), or variation in the angle Phi decreases with increasing strain.

The shape of the Rf/Phi plot, and the distribution of points is assigned a strain ratio, with the aid of nomograms (Lisle, 1985) that are based on hypothetical examples. Lisle (1985) compiled a series of nomograms based on variable initial ellipticities, and incremental increases of strain. Lisle (1985) also develops equations that allow for statistical treatment of Rf/Phi data. The Lisle (1985) manual should be referred to for details, while the following is a brief discussion of the parameters that are viewed pertinent.

There are numerous Rf/Phi plots included in this dissertation; they illustrate differences in strain magnitude interpreted for different structural settings, as well as strain variation seen in rock types with ductility

contrasts. The following applies to all Rf/Phi diagrams. The right hand corner of each Rf/Phi plot displays statistical data, as well as the number of features (ellipses sections) plotted per diagram. The variables listed for each Rf/Phi diagram include 1) the calculated strain ellipse (Rs); 2) the harmonic mean (Hm); 3) the standard deviation (Sd) for the angle Phi; 4) the calculated symmetry factor (Sym); and 5) the strain ratio determined from the nomograms (MG) based on methods described by Lisle (1985). These variables were calculated for each Rf/Phi diagram, using the equations listed in Lisle (1985), and computer programs shown in the flow chart (Appendix A).

As Lisle (1985) points out, the harmonic mean does provide a rough approximation of the strain ratio. However, the array of Rf/Phi plots included in this text demonstrate that the harmonic mean (Hm), or the calculated strain ellipse (Rs) are not accurate estimators for the strain ratio. In cases where there is substantial fluctuation (variation in the angle Phi), strain ratios interpreted from the Lisle (1985) nomograms are less than either the harmonic mean or the strain ratio.

The nomograms prepared by Lisle (1985) are based on numerical models, and each displays two families of curves. Figure 2b is the nomogram for a strain ratio (Rs) of 1.8, and this plot illustrates curves that are determined using two simple numerical models. Theta curves radiate from the center point of the plot, and these

Figure 2b. Example plot of Rf/Phi diagram from Lisle (1985). See text for explanation.

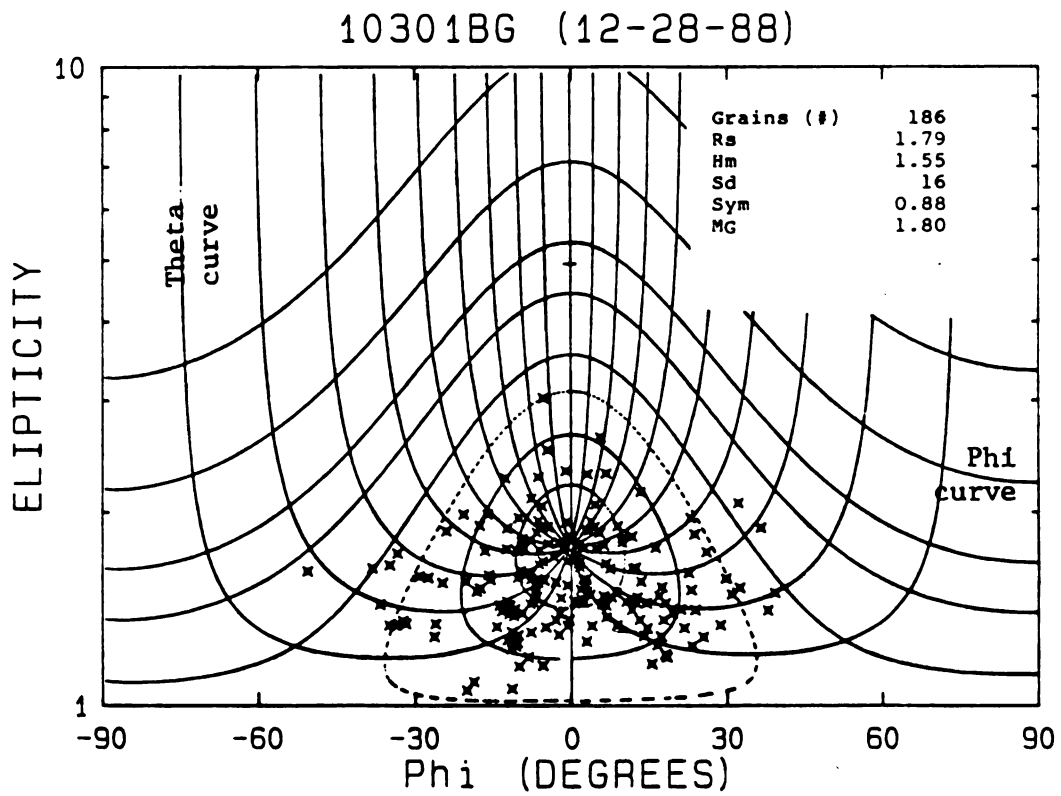
10301BG (12-28-88)
10
1
ELIPTICITY
Theta curve
Phi curve
Grains (#) 186
Rs 1.79
Hm 1.55
Sd 16
Sym 0.88
MG 1.80
-90
-60
-30
0
30
60
90
Phi (DEGREES)

Figure 2b.

represent calculated ellipticity ratios for initially elliptical features, after an increment of strain where Rs=1.8. This strain is imposed on ellipses where the initial ellipticity is variable, and the orientation of the ellipses before deformation is constant. The Ri curves originate at the ordinate axis of the plot, and reach a maximum value at Phi equal to zero. The maximum deviation from the abscissa is at the Phi value of zero degrees, because an ellipse with the long axis before deformation at Phi equal to zero would suffer the greatest extension. Ellipses originally oriented at -90 or 90 degrees Phi would experience some shortening, thus the Ri curves begin with some deflection toward the abscissa, before climbing to the maximum value at Phi equals zero (Figure 2b).

Lisle (1985) includes nomograms for strain ratios that range from 1.05 to 10. It is the distribution of the points plotted on the Rf/Phi diagram that is used to interpret the appropriate strain ratio; the strain ratio is from the nomogram that best matches the Rf/Phi plot. It is necessary to plot the ellipticity and orientation of the elliptical features on semi-log scale, because the nomograms of Lisle (1985) were prepared in this manner. To accomplish the comparison task, transparent overlays were made for each nomogram. For each Rf/Phi plot (plotted at exactly the same scale the Lisle nomograms), a series of transparencies were overlain on the plot until the nomogram that best fit the distribution of Rf/Phi

points was found. In summary, it is necessary to compare the distribution of Rf/Phi points with the Lisle (1985) nomograms, or strain solutions will be exaggerated.

The appropriate strain ellipse for a two-dimensional case can be determined using any elements that can be assigned long and short axes lengths, and an orientation of long axes relative to some reference line (Ramsay and Huber, 1983). The number of features required to define a strain ellipse depends on several factors. It was suggested (Ramsay and Huber, 1983) that 100 ellipse sections per plane should be sufficient, but it was determined in this study that the number required ranges from 50 to +400, depending on the type of strain gauge used.

To extend the Rf/Phi analysis to three dimensions, it is necessary to know strain ratios, and orientations of long axes for three strain ellipses from three planes, relative to a reference plane (field orientation). For this research, the three planes on each sample were orthogonal (generally two vertical and one horizontal), although it is not necessary that the planes be mutually perpendicular (Owens, 1984). The three dimensional strain solutions are based on the two dimensional data determined from the Lisle (1985) nomograms; the best fit strain ellipsoid is computed using software provided by Bauer (1985, written commun.). Elliot (1970) demonstrates mathematically that knowledge of ellipse ratios and orientations for three planes uniquely defines the shape and orientation of the parent ellipsoid for a hypothetical case. The programs used (Bauer, 1985,

written commun.) are based on the equations derived by Elliot (1970).

Strain estimates from ellipsoidal bodies observed in MRSG slates and quartzites (reduction spots, conglomerate clasts, and quartz-grain shapes) are the result of a combination of procedures outlined above, (Lisle nomograms, computer processing of two dimensional data, etc.), and the steps required are given in Appendix A. A summary of the statistics calculated using the equations listed in Lisle (1985) is provided in Appendix B (for quartzites only).

The axial ratios for the best fit ellipsoid are plotted on Flinn (1962) diagrams, and the relevant features of the Flinn plot are the subject of the next section.

THE FLINN STRAIN RATIO PLOT

Structural geologists cannot determine exact magnitudes of natural strain in deformed rocks. Lack of knowledge concerning predeformation geometry of strain markers or gauges, and uncertainties regarding the timing and degree of volume loss are the most serious limitations in strain analysis. Strain ratios and relative strain magnitudes are the most instructive means available to report strain data, and this section summarizes the Flinn (1962) strain ratio plot, which is the most commonly used means to display data.

Estimates of strain magnitude have been made by Wood (1973, 1974) for Taconic and Caledonian slate belts, and by Westjohn (1978) for Proterzoic slates. However, the strain estimates reported by these investigators are based on a constant volume deformation model. It is unlikely that the deformation that rocks experience during folding is a constant volume process, and it is less controversial to report strain ratios, without implying strain magnitude. A convenient way to plot strain ratios was derived by Flinn (1962), and the ratio-ratio plot he devised is used to show all strain data for MRSG slates and quartzites. The Flinn plot (Figure 3) is based on ratios of the principal strain

Figure 3. Graphical plots of the Flinn parameters, and corresponding 3-D blocks to illustrate different k values, and strain fields. (From Ramsay, 1967, Figure 4-11, p. 136).

Figure 4. General shape of five ellipsoid type, and corresponding Flinn k values. (From Ramsay, 1967, p. 157).

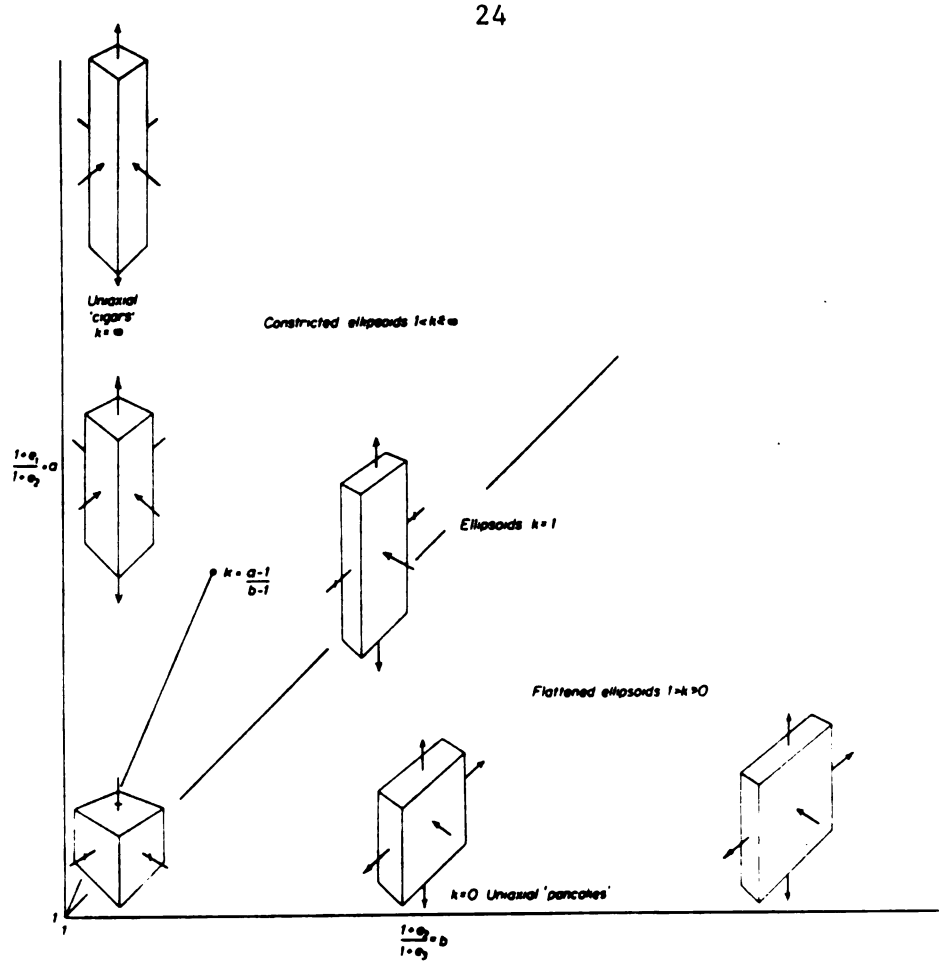

Figure 3.

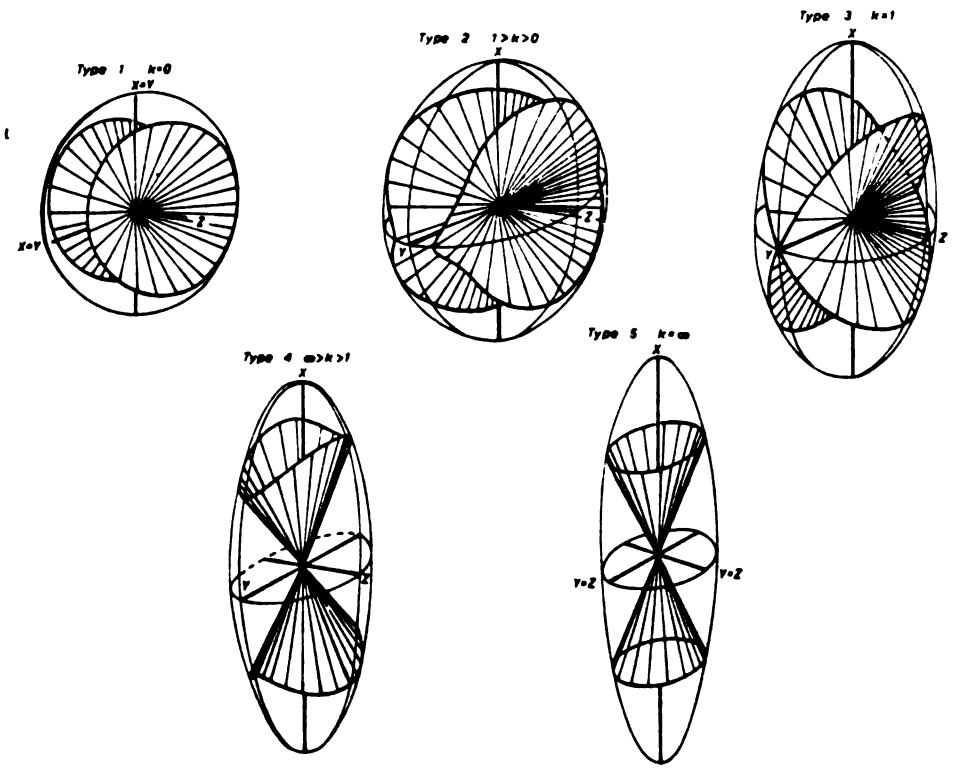

Figure 4.

axes. The convention of denoting the maximum, intermediate, and minimum strain axes of the strain ellipsoid as X, Y, and Z, respectively, is followed in this text. The Flinn diagram is a plot that pairs values "b" (b=Y/Z, or the ratio of intermediate axis divided by the axis of shortening) against "a" (a=X/Y, or the ratio of principal extension divided by the intermediate axis). An algebraic expression (a-1/b-1) in these terms is called the Flinn parameter, or "k" value. Flinn (1962) describes five basic ellipsoid shapes (Figure 4), and each is assigned a k value that corresponds to one of five types; these range from pure flattening (k=0) to pure constriction (k=infinity). One feature of the Flinn plot that is referred to in portions of the upcoming text is the division of "strain fields" that indicate deformation style. Two fields (Figure 3) that indicate constrictional (X>Y<1>Z) and flattening (X>Y>1>Z) strains are separated by a line that represents plane strain (X>Y=1>Z; and k=1).

The orientations of the principal strain axes for all determinations are shown on equal area stereonet plots, and the strain ratios derived from Rf/Phi analyses are plotted on Flinn diagrams (see Plates 1-4 for a summary of all data). This is the convention accepted by most structural geologists.

The next four sections provide descriptions and a discussion of deformed veins and structural fabric in slates and quartzites. Vein textures and structural trends support interpretations of strain style and deformation mechanisms;

the attitudes of deformed veins can also be used to compute strain ratios. These subjects are addressed as a prelude to strain analysis using elliptical strain indicators.

TEXTURE, MORPHOLOGY, AND STRUCTURAL TRENDS OF VEINS IN ARGILLITES AND SLATES

Quartz-carbonate veins are common in MRSG slates and argillites. These are important finite strain indicators, because they occur in rocks that have experienced a substantial range of internal distortion. The presence of undeformed veins in flat-lying argillites provides insight regarding the origin and predeformation character of the veins. With some knowledge of pretectonic configuration and texture of early formed veins, it is possible to use internal distortions recorded by folded and boudinaged veins to interpret strain style, as well as estimate strain ratios using a method devised by Talbot (1970).

This section begins with some general observations of veins at the outcrop scale. These observations are combined with structural fabric orientation data and thin section petrography to support the argument that veins in slates deform progressively with development of folds. It is suggested that vein textures and morphology provide a record of increments of shear strain experienced by MRSG slates. Veins (and host rocks) that appear to be undeformed or weakly deformed are described first, followed by a discussion of veins in open folds. The most deformed

veins occur in slates in tight to slightly overturned folds, and these are discussed last.

Veins In Subhorizontal Argillites

Veins in sub-horizontal argillites in the southern fringes of the Marquette synclinorium are syntaxial in form. It is interpeted that the veins are syntaxial (that is, veins nucleate on the fracture walls, and grow toward the center of the fracture open space), because quartz fibers (first mineral to nucleate) viewed in thin section often have pyramidal terminations that are unidirectional, and oriented normal to the fracture walls. Ramsay and Huber (1983, p. 241-2) illustrate the common features of syntaxial veins, and discuss pertinent implications that these veins textures have regarding the interpretation of vein origin for other geological settings.

Syntaxial veins in Kona argillites show symmetrical growth patterns, and in this regard can be considered composite, after the classification scheme suggested by Ramsay and Huber (1983, p. 243). Kona vein textures are characterized by (1) a selvage of fine-grained quartz; (2) latter fibrous quartz crystals; and (3) complete infilling by zoned carbonate crystals (Figure 5). Discrete iron-rich bands alternate with calcite or ferroan dolomite zones within carbonate rhombohedrons. Zones of high iron (formerly siderite or ankerite?) within carbonate rhombs are oxidized to hematite. These textural relations

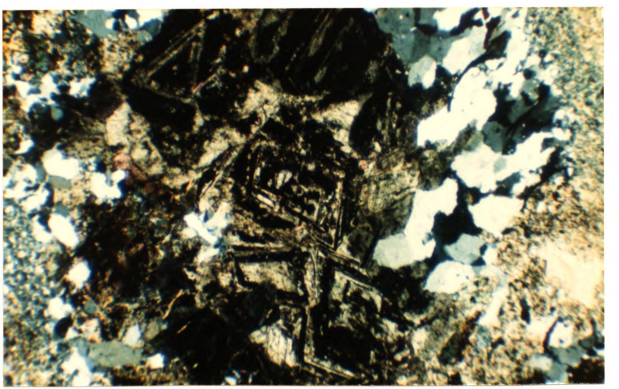

Figure 5. Photomicrograph showing syntaxial vein morphology. Vein width approximately 4 millimeters. Note fine-grained quartz grains form selvage on fracture wall, unidirectional quartz growths, and late zoned carbonate grains. Sample from Lindberg quarry (Kona argillite).

exclude a replacement origin, and textures of veins in sub-horizontal argillites are assumed to be primary.

Veins are rare in sub-horizontal argillites, but where present are vertical to sub-vertical. The number of veins in this geological setting is insufficient to determine statistically (by stereonet analysis) if there is a preferred strike direction. Regardless, vein textures have undeformed primary textures, and it is interpreted that these argillites did not experience any recognizable deformation since vein emplacement. The presence of gypsum casts (replaced by calcite), and cubic casts assumed to originally have been halite, and the absence of slaty cleavage or any structural fabric are additional indications that these rocks have not experienced any significant internal distortion. Meyer (1983) reports the presence of spaced cleavage at the Lindberg quarry; however, the vertical structures observed at the quarry are interpreted by this author as joints rather that spaced cleavage.

Argillites at the Lindberg quarry are obviously recrystallized. Meyer (1983) noted the presence of a decussate fabric in the argillites from the Lindberg quarry (See Plate 1), and this fabric was noted in all thin sections of argillites examined (this research). However, an explanation cannot be offered for the origin of this microfabric. In summary, the lack of any significant deformation fabric, the presence of what appears to be undeformed primary sedimentary textures, and the presence

of veins that have primary textures are indications that argillites in the flat-lying southern limb of the Marquette trough (Lindberg quarry area) suffered minor if any internal distortion during folding of the supracrustal package.

Veins In Shallow-Dipping Argillites

Veins in shallow-dipping (20 to 30 degrees) argillites near the Lindberg quarry (Plate 1) are more abundant, and most are near vertical and planar (Figure 6). There are veins that are slightly boudinaged, and these have a strong east-northeast preferred orientation. There are also veins (Figure 6, 10 percent of the veins measured) that are slightly buckled, and the wavy appearance of these features may (1) represent primary morphology; (2) record the product of slight compactional strain that post dates vein emplacement; or (3) represent tectonic strains induced after vein formation. The slightly buckled veins are also steep in attitude, and have trends that overlap with planar and boudinaged veins (Figure 6). The overlap of boudinaged, planar, and buckled veins in this apparent low strain environment is an enigma. The same situation is noted for the steep south dipping limb at Harvey (Figure 7). This apparent enigma has at least one explanation that is considered in the discussion that follows this descriptive section.

Figure 6. Equal area stereonet plot of poles to enveloping surfaces of veins; sample from shallow-dipping Kona, roadside outcrop on Highway 480, northwest of Lindberg quarry (sample 1031867). (Squares, poles to planar veins; plus symbols, poles to slightly boudinaged veins; triangles, poles to slightly buckled veins).

Figure 7. Equal area stereonet plot of 137 veins trends from the north limb of the Harvey syncline. (Plus symbols, poles to boudinage veins; squares, poles to folded veins; triangles, poles to planar veins).

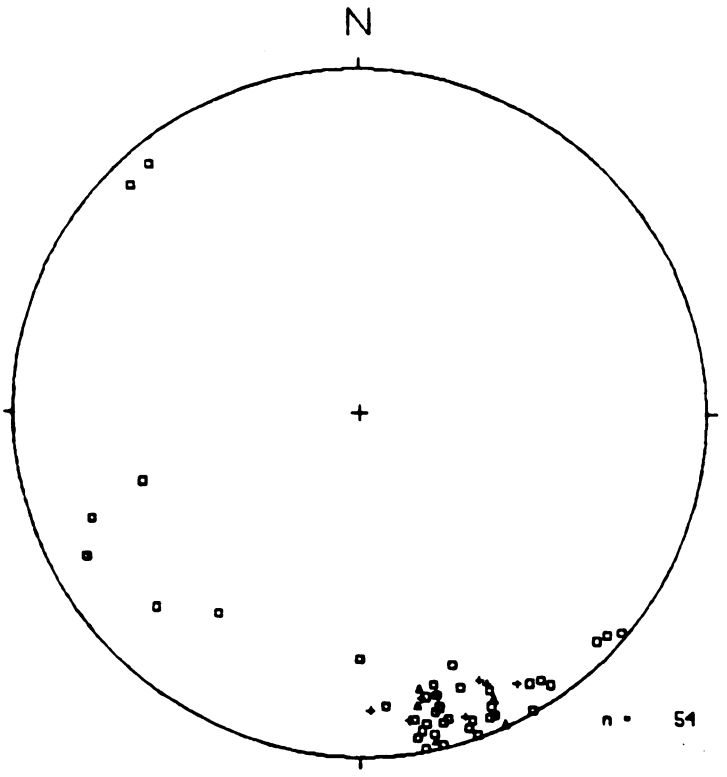

Figure 6.

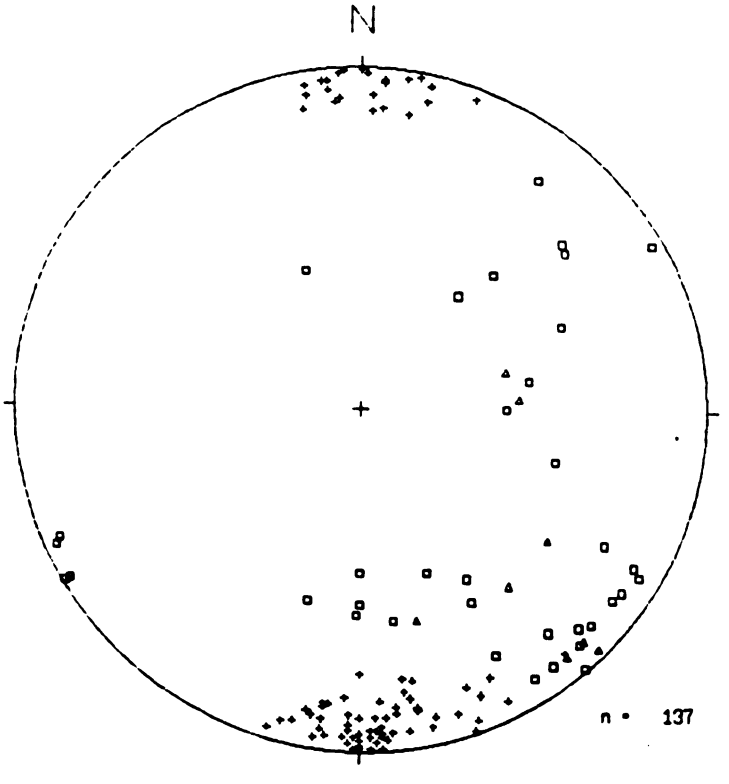

Figure 7.

Veins In Slates

Veins in slates are usually deformed (either folded or boudinaged). Planar veins are rare in rocks with well developed slaty cleavage. In contrast to the assumed primary textures of veins in flat-lying argillites, petrographic examination of deformed veins in slates show substantially different textural relations. Boudinaged veins are the most common type observed (Figure 7). Where boudins show complete separation, which is the general case, necked-areas are in-filled with fibrous quartz (Figure 8). The fibrous growths are similar in appearance to quartz (and/or mica) beards that are interpreted as mineral growths parallel to the maximum extension direction in so-called pressure shadow regions (Ramsay, 1967, p. 181). The importance of the fibrous quartz grains is that these are interpreted to grow parallel to the principal stretching direction during deformation.

Carbonate grains in these veins are twinned, and zoned crystals are absent (Figure 9). Iron appears to be homogeneously distributed in carbonate grains, and the oxidation of former iron-rich carbonate is the suggested origin of the deep-red color common to these grains. Folded veins are dominated by carbonate minerals, and deformation twins are symmetrically arranged within individual folds. Grain boundaries between carbonate grains are also symmetric (Figure 9), and these form

Figure 8. Photomicrograph of fold core from deformed carbonate vein. Thin section cut normal to fold axis. Carbonate grain boundaries form microcleavage fans, and twins inclined at various angles tograin boundaries. Sample Harvey syncline north limb.

Figure 9. Photomicrograph of fibrous quartz crystals from necked area of boudinaged vein. Crystals approxiamtely 1 millimeter in length. Sample from Harvey syncline, north limb.

Figure 8.

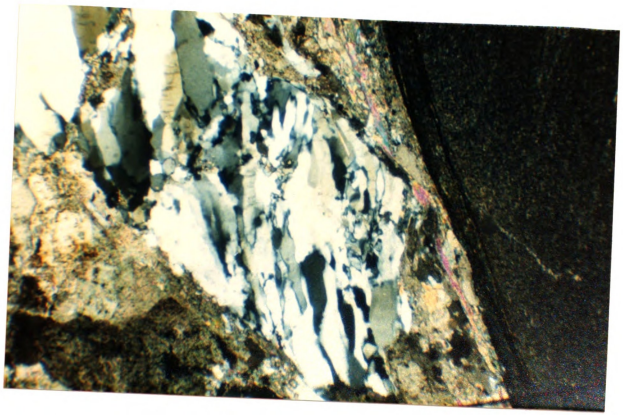

Figure 9.

microcleavage fans about the fold hinges. It is known that the carbonate grain boundaries have the orientation of microcleavage surfaces, because the thin sections were cut normal the the XY principal plane (determined from strain analyses). Deformation twins are inclined at various angles to carbonate grain boundaries (Figure 9), but most show a consistent trend so that the acute angle between grain boundary and twin ranges from 20 to 40 degrees.

Folded veins have been observed offset along cleavage planes. There are at least three explanations for the origin of the offsets; (1) folding predates the development of slaty cleavage; (2) differential slip occurred parallel to cleavage, after the development of folds in veins; or (3) vein material was dissolved in the cleavage plane. Cleavage is deformed against offset veins, and the direction of offset is not consistent with the direction expected if vein material was removed by dissolution (inconsistent with explanation 3), so explanation 2 is consistent with observed microstructures.

FINITE STRAIN ESTIMATES FROM DEFORMED VEINS

Deformed veins have been used as finite strain indicators in previous investigations (Talbot, 1970; Beutner, 1978; Beach, 1974). The method devised by Talbot (1970) involves determining orientations of folded and boudinaged veins; these features represent shortened and extended planes within the host rock body. Talbot (1970) took advantage of mathematical relations derived by Flinn (1962) to develop a technique to use folded and boudinaged veins to determine the shape and orientation of the minimum finite strain ellipsoid (m.f.s.e.). This method characterizes the shape and orientation of a surface of no finite longitudinal strain (s.n.f.l.s.). This theoretical surface contains all lines that have the same length before and after deformation, and the geometry of this surface is a function of deformation style. Strains that are homogeneous and geologically realistic produce a s.n.f.l.s. that has the shape of a double cone (Ramsay, 1967, p. 157). The apices of these cones join at the center of the strain ellipsoid (also the center of the parent sphere), and the cone rims represent the intersection of the ellipsoid with the parent sphere. The geometrical features of the Talbot (1970) method are illustrated in Figure 10.

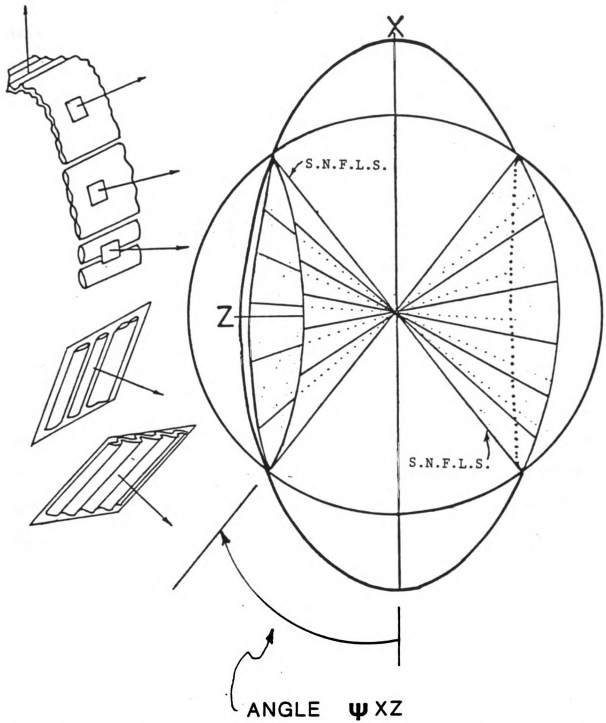

Figure 10. Diagram illustrating some geometrical aspects of the Talbot method. Circle represents the undeformed state. Ellipse is deformed product, and the surface of no finite longitudinal strain (s.n.f.l.s.) is the double cone. Cone apices meet at center point, and cone rims intersect at join of circle and ellipse. Schematic (left side of diagram) is hypothetical boudinaged and folded vein segments, and poles to enveloping surfaces.

The orientations of the principal strain axes can be determined, if the number of deformed veins in a deformation domain is sufficient to define the shape of the s.n.f.l.s. A deformation domain is defined as an area that deformed homogeneously (Talbot, 1970). It is not possible to determine strain magnitude, but the method (Talbot, 1970) does produce ratios of the maximum to intermediate, and intermediate to minimum principal strain axes.

Ratios of the principal strain axes are determined from the shape and orientation of the overall area of elongation (OAE), as defined by Talbot (1970, p. 54). The OAE is determined from a stereonet projection of poles to deformed veins, and represents the projection of the s.n.f.l.s. on the stereonet. This area is constructed to separate poles that represent shortened elements from extended elements, and the ability to constrain the geometry of the OAE is a function of the number of veins measured. Strain ratios are graphically determined using the angles psi XY and psi YZ (Talbot, 1970). These angles are measured from the OAE, relative to the principal strain axes. In practice, these angles are measured relative to the principal planes XY and YZ, and they are determined from the angles of intersection the strain ellipsoid makes with the parent sphere.

Deformed veins were used as a means to estimate strain in an investigation by Westjohn (1978). Orientations were measured on samples cut to expose veins on three orthogonal planes, which facilitated accurate determinations. These data proved to be insufficient (Sanderson, written commun.,

1986), because too few data were included to adequately constrain the shape of the s.n.f.l.s. Additional data have been collected during the course of this research to supplement previous work of Westjohn (1978). These data are relied on to support interpretations concerning strain style and magnitude, but a brief review of previous work (Westjohn, 1978) is warranted.

The deformation domain selected by Westjohn (1978) is along the north limb of the Harvey syncline (Plate 1). Slate samples (eight total samples) with multiple veins were collected, and vein attitudes were determined with contact goniometry measurements and stereonet solutions. For the domain selected, poles to extended elements cluster near the north and south portions of the equal area projection (Figure 11), while the poles to folded elements display substantial scatter. Multiple solutions can be interpreted from the same data set, because the data are insufficient to exactly define the position and shape of the OAE. For example, consider the following two examples. For the first solution, the trace of the s.n.f.l.s. is constructed to exclude poles to shortened elements (Figure 11, solution A). For the second solution, the trace of the s.n.f.l.s. is drawn to include all poles to extended elements (Figure 11, solution B); this is the accepted practice (Talbot, 1970). Axial extensions and orientations for the two solutions are plotted on appropriate Flinn diagrams and equal area stereonets (Plate 1). The two solutions are assumed to represent extremes,

Figure 11. Equal area stereonet plot of poles to deformed veins. Triangles, poles to folded veins; filled circles, poles to boudinaged veins. Also shown are plunge directions (open circles) determined from bedding cleavage intersections, and overall areas of elongation (solutions A and B), determined using the Talbot method of strain analysis. Xv, Yv, and Zv are plots of strain axes orientations (same for solutions A and B). Data from Westjohn (1978); laboratory determination of vein trends, six samples of slate from the north limb of Harvey syncline.

FIgure 12. Equal area stereonet plot of poles to deformed veins; all from field measurements at the north limb of the Harvey sincline. Overall area of elongation (solution C) drawn to tightly enclose all poles to extended (boudinaged veins) elements. Squares, poles to folded veins; pluses, poles to boudinaged veins; triangles, poles to planar veins.

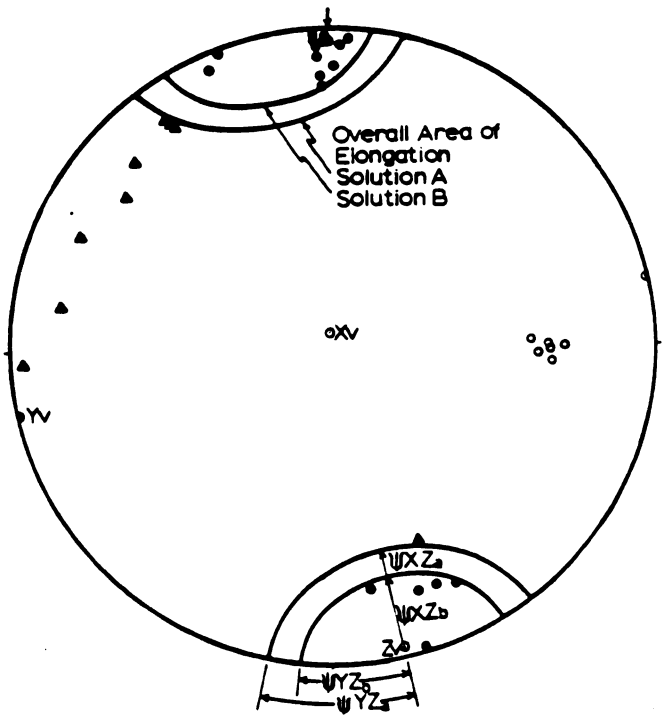

Figure 11.

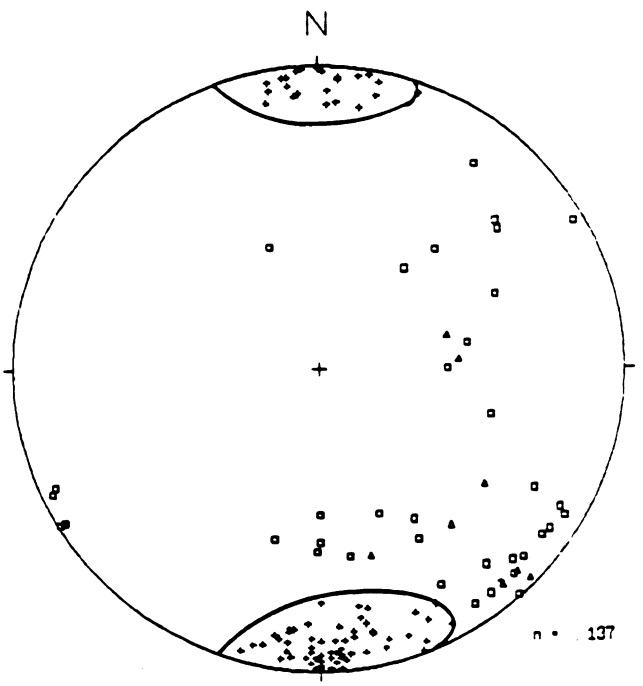

Figure 12.

and the actual s.n.f.l.s. probably lies within the area where folded veins are excluded, and extended veins are tightly enclosed (Figure 11). Although the solutions are realistic, additional data are needed to substantiate the strain determination from deformed veins.

A review of preliminary data (Westjohn, 1978) leads to the conclusion that in an attempt to be precise, there was some oversight regarding the scale of observations. The samples collected for laboratory analysis were from a limited area (the reduction spot zone at Harvey), and it is probable that calculated strains are not representative of distortions recorded at the outcrop scale. To treat the problem at an appropriate scale, all folded and boudinaged veins at the Harvey area road-cut outcrop (355 feet continuous outcrop, see Gair and Thaden, 1968, Plate 5, survey stations 420 to 775) were measured to provide sufficient data for strain determination. There are 137 deformed veins exposed in an area (1,800 square-feet) along the north limb of the Harvey syncline. It is assumed that this area meets the criteria suggested by Talbot (1970) for a deformation domain, because the slates that contain deformed veins are massive, and dip is uniform (65 to 70 degrees) throughout the selected domain.

The orientations of all veins measured at the north limb of the Harvey syncline were used to construct the orientation of the s.n.f.l.s. The overall area of elongation constructed from the field data (Figure 12) falls within the areas reported by Westjohn (1978);

therefore axial ratios computed from the field data are also within the reported range. However, the orientations of the principal strain axes are somewhat different (c.f., Figures 11 and 12). The important point is that the construction of any OAE that is consistent with the data will produce a solution that falls in the flattening field. This qualitative and quantitative evidence supports one suggestion; slates in the MRSG experienced flattening-type strains during Penokean deformation.

Limitations In Strain Analysis Using Deformed Veins

All methods of strain analysis have inherent limitations. The usual situation is that assumptions must be made that cannot be directly or indirectly demonstrated. Assumptions inherent in Talbot's (1970) method of estimating strain using deformed veins are (1) constant volume homogeneous deformation; (2) a large range of predeformation orientations for veins; (3) initial planar vein morphology; and (4) homogeneous deformation at the domain scale, but inhomogeneous deformation at the vein scale. The constant volume assumption continues to receive attention (Wright and Platt, 1982; Bell, 1985, for example). This topic has important implications regarding deformation style and strain magnitude, and it is discussed in the section on deformation mechanisms. Assumption 4 is accepted, because of relations observed between veins and primary sedimentary features. Bedding in slates is

distorted locally near the contact with deformed veins, but this distortion is not seen at distances more than one centimeter away from the vein margin. Considering the fine-grained nature of Kona slates, it is expected that deformation is homogeneous at the centimeter scale. However, because of the ductility contrast between coarse-grained vein material and the fine-grained matrix of the host slate, deformation must be heterogeneous at and near the margin of the vein. Assumptions 2 and 3 are addressed in light of observations made at several outcrops in the Marquette synclinorium.

The fact that vein textures appear to be primary and undistorted in flat-lying argillites (Lindberg quarry, Plate 1) is evidence for a pretectonic origin for at least some of the veins. This observation does not exclude the possibility that the flat-lying argillites suffered some increment of distortion prior to vein emplacement. The number and density of veins appears to increase relative to a corresponding increase in bed dip (and degree of vein distortion). This supports a suggestion that veins form as a continuous process during folding. It is assumed that some veins form progressively with fold development, as a function of dewatering of the sedimentary pile during deformation. Veins in this case could be interpreted as the product of material redistribution during folding, and it is implicit that these veins record only part of the strain history.

The observation that veins are primarily vertical in

both flat-lying and shallow dipping argillites deserves mention. The absence of shallow to moderately dipping veins excludes the possibility that a large range of orientations existed before deformation (assumption 2 must be rejected). Unfortunately, strain ratios derived from deformed veins using the Talbot (1970) are viewed as suspect, because required assumptions cannot be demonstrated.

A Simple Shear Model For Vein Deformation

A comparison of vein orientations in steep-dipping limbs (Harvey, Plate 1), and shallow-dipping limbs leads to some interesting considerations. The relatively tight distribution of poles to planar, slightly boudinaged, and slightly buckled veins for the shallow limb (Figure 6) is similar in form to the cluster of poles to boudinaged veins where limb dip is steep (Figure 7). These similarities in vein attitudes for contrasting structural settings are interpreted to be a function of their pretectonic configuration.

One possibility for the origin of early veins is supported by indirect geological evidence. Plates 1-4 illustrate the major geological features of the Marquette-Ishpeming area, and is a compilation from several U.S. Geological Survey maps (Gair and Thaden 1968, Plates 1, 2, and 4; Puffett, 1974, Plates 1 and 2; Clark and others, 1975; Gair, 1975, Plate 1). This map shows

contacts between Archean and Proterozoic units, trends of major fold axes, and major fault trends. Geographical and minor geological details were not included, so that stereonets and Flinn strain ratio plots of data can be more clearly seen. Plate 1 was prepared at the same scale as detailed U.S. Geological Survey maps, and many reference points common to both map sets provide a means for easy comparison, as well as accurate cross-reference for outcrops and sample locations.

There is a preponderance of west trending structures in the Archean blocks that bound the synclinorium, as well as in the MRSG. Metadiabase dikes of uncertain age (multiple stages of dike emplacement), and dikes mapped as Keweenawan have a persistent east-west trend. Major shear zones and faults also have this common trend, and foliations in Archean rocks (see Gair and Thaden, 1968, p. 64) also have a dominant east-west trend. A pronounced near-vertical east-west structural weakness in both Archean and supracrustal rocks is indicated by these structures. This leads to the inference that a strong preferred near-vertical, westerly structural trend of veins persisted prior to deformation. It is suggested that veins developed within the sedimentary pile during coeval sedimentation and extension, and that the dominant structural trends were inherited from the Archean basement.

If a predeformation vertical attitude is assumed (east-west trend), veins can be used as angular shear strain gauges, in a manner similar to the analysis Cambray

(1978) described for estimating strain from sandstone dikes in the Siamo Slate. Angular shear strain is a measure of the deflection two perpendicular lines record after some increment of distortion (Ramsay, 1967, p. 53). The general equation that relates angular shear to shear strain is:

$$\gamma = \tan \psi$$

where psi is the angle between elements that were perpendicular before deformation, and gamma is the shear strain.

When veins are considered and a initial orthogonal relation to bedding is assumed, the simple shear strains that correspond to increments of angular shear can be modeled in a simple two-dimensional fashion (constant area). The shear strain for shallow-dipping argillites (angular shear of 20 degrees, and gamma = 0.37) is substantially less than that estimated for the steep limb (angular shear of 70 degrees, gamma = 2.74), an observation that is consistent with the degree of boudinage described for the two settings.

A simple shear strain model can also be invoked to account for the overlap of poles to slightly folded and slightly buckled veins (Figures 6 and 7). Rather than assuming a vertical attitude for all veins, a more likely case is that the bulk of early veins were sub-vertical. For this case, veins inclined at steep angles to the north would experience an initial increment of shortening related to simple shear. Additional deformation (simple shear) of these features would result in rotation into the extension

field and subsequent unfolding. At the same time, steep south-dipping veins would record only extension. However, extensions calculated for slate beds at the Harvey syncline using this simple shear model seem extreme (192 percent extension for the steep limb), and are generally in poor agreement with axial ratios estimated from reduction spot Rf/Phi plots.

This rudimentary simple shear model sufficiently demonstrates the general case, but details of individual veins show the deformation is more complex. Figure 13 illustrates a common situation, where the trend of a single vein is variable, and includes a reversal in dip direction (Figure 14). This example is from Kona slate (Harvey syncline), and shows that angular shear strain differs as a function of proximity of the vein to beds that have a contrast in ductility. The slate bed illustrated in Figure 13 is intercalated between calcareous quartzite beds. The component of angular shear reaches a maximum (70 degrees) near lithologic contacts. Also illustrated (Figure 13) is the situation of apparent bed offset. The direction of apparent offset is consistent throughout the fold limb. The offset is along a plane that is approximately parallel to cleavage, but the direction of offset is not consistent with a pressure dissolution origin. Offset along cleavage is not an uncommon situation (Sack, 1988). If the offset is actual (slip parallel to cleavage) rather than apparent (pressure dissolution of part of the vein), then cleavage is not parallel to the XY

Figure 13. Diagram of boudinaged vein configuration based on field note sketch. Dip and dip direction of segments of vein (for example, 77/188) listed on diagram, and poles to these segments plotted in Figure 14. Shear angles (41 and 70 degrees) determined from simple shear model, by assuming an original orthogonal relation of vein and bedding. Also shown is direction of offset of bedding. Vein in Kona slate, north limb of Harvey syncline.

Figure 14. Equal area stereonet plot of poles to segments of boudinaged vein, showing reversal in dip direction.

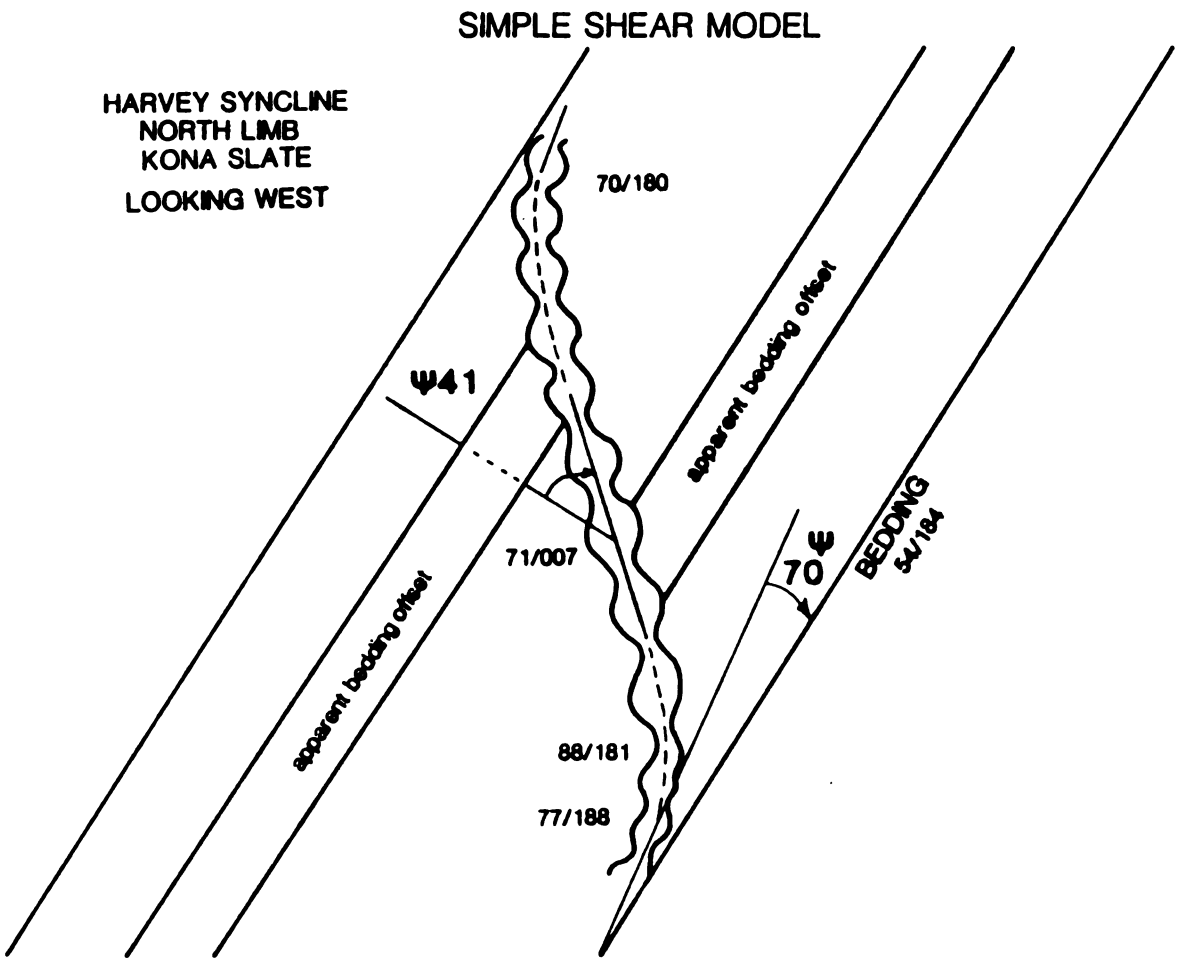

Figure 13.

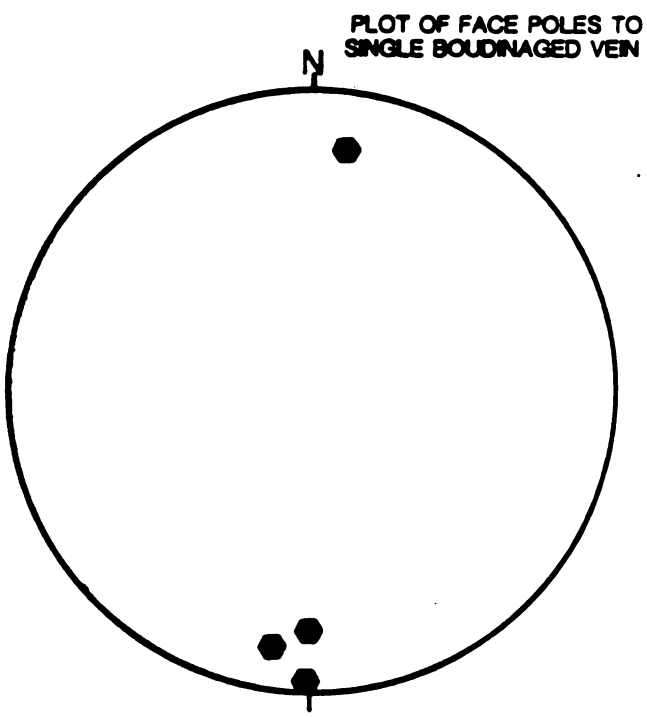

Figure 14.

plane of the finite strain ellipsoid throughout folding, as has been postulated by some (Wood, 1974, for example), and argued against by others (Treagus, 1987). The vein offsets observed appear to be actual displacements, and this supports the suggestion that some deformation in the MRSG post-dates the development of slaty cleavage.

This more realistic model of simple shear (Figure 13) dictates that deformation is heterogeneous at the bed scale. It is suggested that shear strains associated with flexural-slip folding are indicated by vein morphology. Shear strains are clearly partitioned within individual slate beds, with high strains concentrated near lithologic contacts. Significantly smaller shear strains (central part of slate beds) are recorded away from the contacts.

The morphology of boudinaged veins provides additional indications of strain style. All boudinaged veins at the Harvey location are chocolate-tablet structures. The chocolate-tablet vein morphology is characterized by a network of crossing boudin necks that indicate stretching in all directions in the plane of the deformed vein. The term chocolate tablet is descriptive (Ramsay and Huber, 1983, p. 66); for the general case boudins are isolated remnants of original vein material that are surrounded by secondary minerals growths. The secondary minerals fill the voids generated during stretching. Chocolate-tablet veins in Kona slates and quartzites are characterized by fibrous-quartz that fills necked areas that surround individual boudins (tablets). The fibrous quartz growths

when viewed in thin section have the appearance pressure shadows; Ramsay and Huber (1983, p. 273) attribute similar features seen in other deformed rocks to mineral growths that occur in low strain regions. The regions of low strain result because rigid material (boudins) protects local areas (shadows) from imposed strain. Pressure shadows are visible in any thin section cut normal to the plane of boudinaged veins (Kona slates, and calcareous quartzites). This observation supports the argument that some component of flattening is necessary to explain the deformation style documented in slates.

MORPHOLOGY, TEXTURES, AND ATTITUDES OF VEINS IN CALCAREOUS QUARTZITES AND ORTHOQUARTZITES

Veins are less common in quartzites than in slates, and there are differences in morphology that preclude the use of veins in quartzite to estimate strain using the Talbot (1970) method. This is primarily because folded or boudinaged veins are rare in quartzites, so it is not generally possible to interpret the orientations of extended and shortened planes. However, vein textures and dominant structural trends do provide qualitative evidence that is interpreted to indicate the strain style experienced by quartzites. In certain respects, veins in calcareous quartzites resemble deformed veins in slates; these are discussed first, followed by a similar treatment of veins in orthoquartzites.

Calcareous quartzites that are intercalated with Kona slates locally contain quartz-carbonate veins that show signs of internal deformation. Chocolate-tablet boudinage structures are not uncommon in quartzites where limbs are steep (Harvey, Eagle Mills, and Ski Hill Anticline), although the degree of necking is visibly less in quartzites than that observed in slates. The presence of chocolate-tablet boudins is clear, although qualitative

evidence that calcareous-quartzites also suffered a flattening style of strain.

The method described by Voight (1964) was used to determine longitudinal strain along profiles that are assumed to be parallel to the maximum and intermediate principle strain axes (these axial orientations were determined from reduction spots in slates at the same outcrop). Equations by Voight (1964) include:

$$Wno = An/to$$

$$e = (Wn - Wno)/Wno$$

where Wno is the original neck width,
An is the area of the necked portion of the vein,
to is original vein thickness, not less than the maximum boudin thickness
Wn is the present width of the neck, and
e is the longitudinal strain.

There is substantial variation in the degree of necking, as well as in areas of boudinage necks. Longitudinal strains calculated using this approach range from 18 to 68 percent extension, and this range indicates that strains experienced by boudinaged veins are very heterogeneous. Consideration of the method (Voight, 1964) leads to the suggestion that longitudinal strain estimates are qualitative, because important controls of deformation style such as ductility contrasts cannot be assessed by

this method. However, the textures do support the suggestion that flattening is the style of deformation experienced by calcareous quartzites.

Veins in orthoquartzites appear to have no relation to structures observed in slates. Veins in orthoquartzites are always planar, and consist of quartz. The intensity of quartz veining and preferred orientations differ from outcrop to outcrop. Along the north limb of the Harvey syncline (Mt. Mesnard), hundreds of vertical quartz veins show a strong north-northeast preferred orientation (Figures 15 and 16). A similar situation although less pronounced also occurs at the north limb of the Eagle Mills Syncline (Figure 17, and Plate 2). Deformed veins (folded or boudinaged) are absent in orthoquartzites, an observation that leads to the suggestion that mechanisms by which slates and quartzites deform may be fundamentally different. Alternatively, veins in orthoquartzites may have been emplaced very late in the deformation history. For this case, veins would record only the increment of distortion related to brittle deformation, in contrast to the ductile distortion recorded by veins in slates.

Stereonet plots of quartz veins in quartzite (Figures 16 and 17) show trends that are interpreted to represent south-southwest trending extensional vein sets. There are only 75 poles to planes plotted for the Mt. Mesnard outcrop (Figure 16, and Plate 1), but each pole represents no fewer than five vein trends (fracture-set mapping, Peters, 1978, p. 151). Single veins are not considered important in this

Figure 15. Contoured equal area stereonet plot of poles to planar quartz veins, based on field measurements made at Mt. Mesnard (single veins trends included).

Figure 16. Contoured equal area stereonet plot of veins set data (five or more veins per set) for planar veins at Mt. Mesnard (70 vein sets).

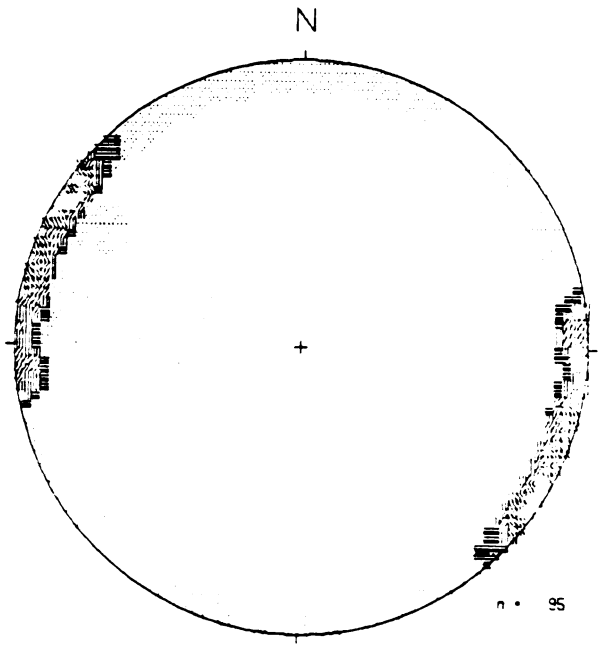

Figure 15.

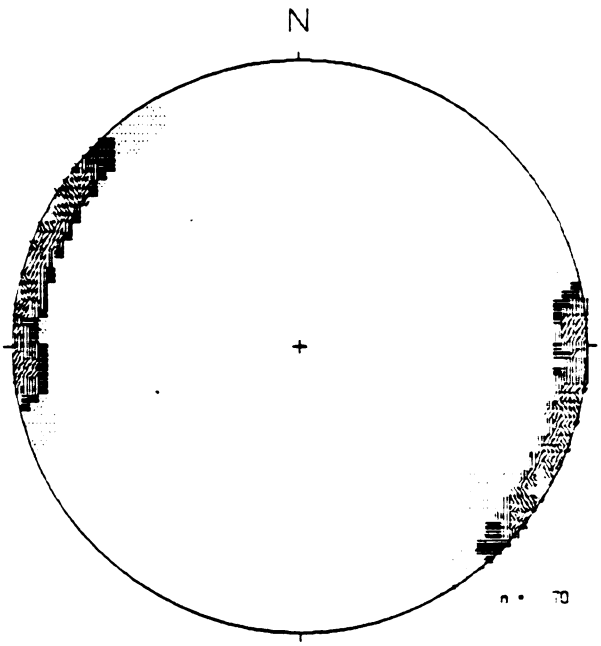

Figure 16.

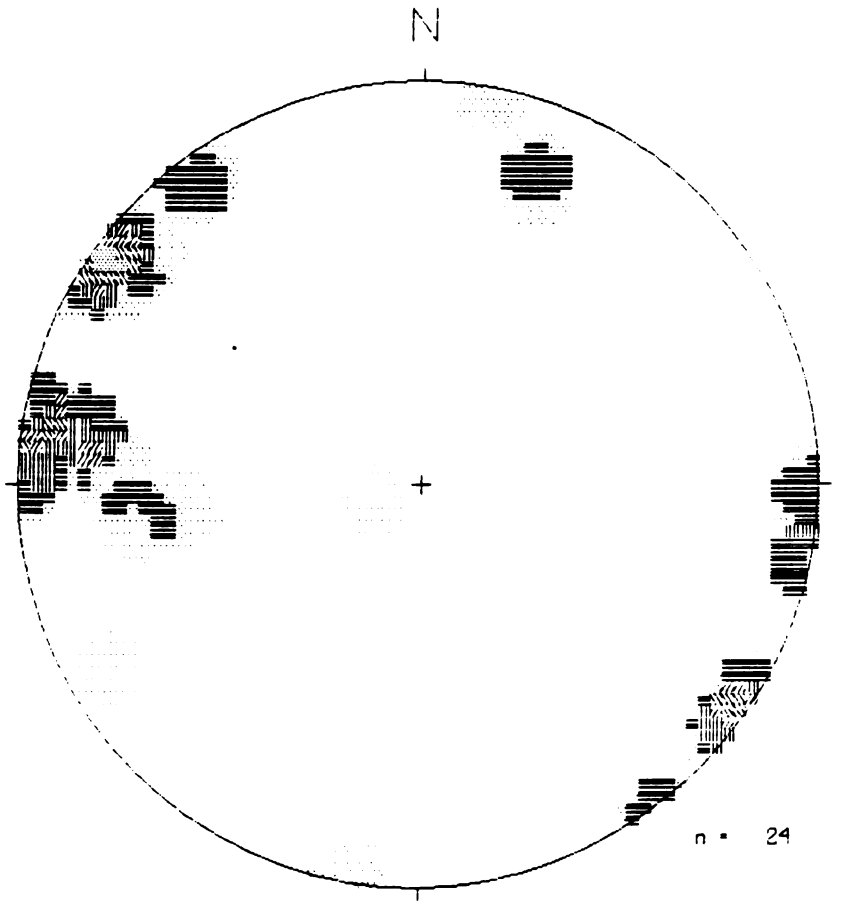

Figure 17. **Contoured equal area stereonet plot of quartz vein sets in Ajibik Quartzite, Eagle Mills syncline (24 vein sets).**

analysis, but the trends of all veins are contoured in Figure 15 for comparison.

Vein sets in orthoquartzites are interpreted to have an origin late in the history of fold development. The strong preferred trends documented for quartzites at the east and west ends of the study area are consistent with a west-southwesterly extension late in the development of the synclinorium. These predominant structural trends, and the lack of deformation of veins in quartzites, are evidence that the maximum principal stress was south-southwest north-northeast during their formation. This suggestion is consistent with the model proposed by Cambray (1984).

In summary, vein textures and structural trends support a deformation model that consists of 1) early emplacement of veins in argillites and calcareous quartzites related to extension and tectonic dewatering; 2) subsequent rotation of initially subvertical veins in response to heterogeneous shear during flexural slip folding; 3) development of internal distortions in veins that indicate a flattening mode of deformation; and 4) emplacement of late quartz veins in extension fractures.

CLEAVAGE AND SANDSTONE DIKES IN MRSG SLATES: ADDITIONAL INDICATORS OF STRAIN GEOMETRY

It has been argued that slaty cleavage is precisely parallel to the principal XY plane of the finite strain ellipsoid (Wood, 1974), and thus represents a plane of flattening. Others dispute this suggestion (Wright and Platt, 1982; Bell, 1985), and propose a volume loss model for the origin of slaty cleavage. This section concentrates on the relation of cleavage orientation in MRSG slates, to patterns of boudinaged veins and strain geometry.

Slaty Cleavage In Kona Slates

The relationship of slaty cleavage orientation to strain geometry has been a subject of interest and debate since the early work of Sharp (1847) and Sorby (1853). Sorby (1853, 1855) recognized the mechanical significance of slaty cleavage, and noted that the direction of maximum shortening in Cambrian slates was perpendicular to slaty cleavage. Sorby (1855) also demonstrated that the plane of maximum extension delineated using ellipsoidal green spots was parallel to cleavage orientation. More recent

investigations have focused on the origin of slaty cleavage, and its relation to the principal strain axes throughout deformation (Wood, 1974; Williams, 1976; Treagus, 1987). There are similarities in cleavage orientation to boudinaged veins trends in Kona slates (Harvey location, Plate 1), and these similarities are illustrated in Figures 18 and 19.

Slaty cleavage at the Harvey syncline is variable in trend. Figure 18 is a contoured equal area stereonet plot of 179 poles to cleavage planes. These cleavage trends were measured in the same domain that contains folded and boudinaged veins. Inspection of Figure 19 shows that there is a positive correlation of trends of boudinaged veins and slaty cleavage. The presence of chocolate tablet boudinaged veins has been suggested to indicate extension in all directions in the plane of deformed veins. The trends common to cleavage and veins (boudinaged) supports the argument that cleavage is a structural fabric that indicates flattening.

Most structural geologists agree that cleavage is approximately parallel to the principal (XY) plane of the finite strain ellipsoid (Ramsay, 1976), and some propose that cleavage is precisely parallel to the principal plane (Wood, 1974). There is substantial variation is cleavage orientation at the Harvey quarry, and is it assumed that the principal axes of the finite strain ellipsoid also vary in the same fashion. This is evidence that strains are heterogeneous at the outcrop scale, and the principal plane

Figure 18. Contoured equal area stereonet plot of poles to slaty cleavage. Cleavage trends measured in the same deformation domain that contains deformed veins at the north limb of the Harvey syncline (179 cleavage trends).

Figure 19. Contoured equal area stereonet plot of poles to surfaces that envelope boudinaged veins at the north limb of the Harvey syncline (121 veins).

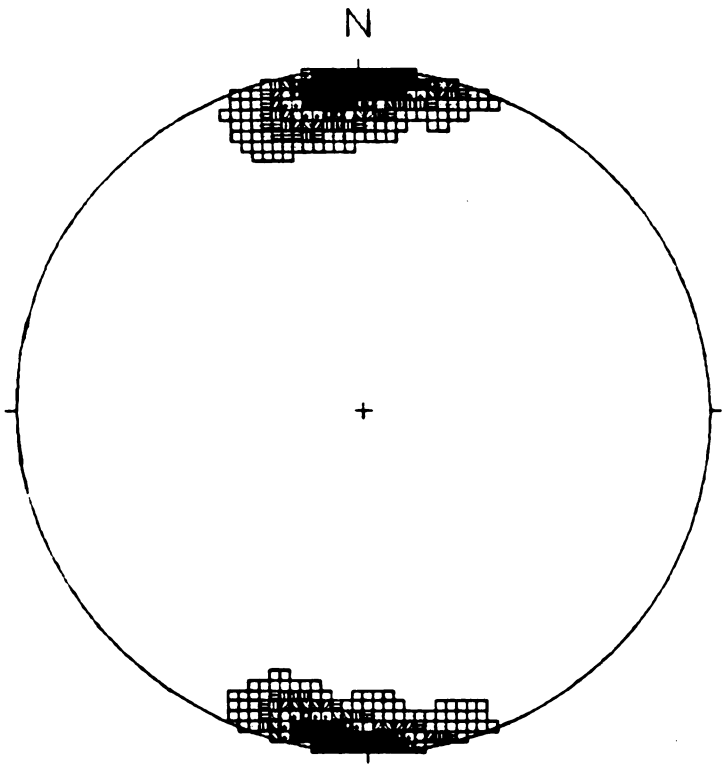

Figure 18.

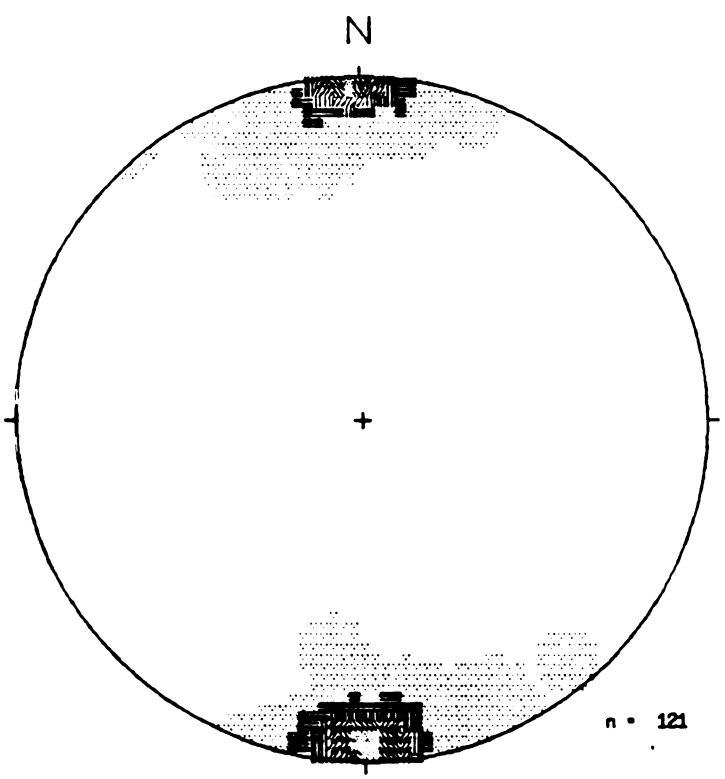

Figure 19.

of the strain ellipsoid is of the flattening type.

Sandstone Dikes In The Siamo Slate

Sandstone dikes in MRSG slates have been noted by other writers (Cambray, 1977, 1978; Klasner, 1978; Powell, 1972). Borradaile (1974, 1977) devised a technique to use the relations between cleavage, bedding, and sandstone dike trends as a means to estimate finite strain. This technique is similar in most respects to the Talbot (1970) method, with inherent assumptions that include (1) a pretectonic origin and initial random trend of sand dikes; (2) homogeneous deformation at the domain scale; and (3) the presence of a ductility contrast between dike and matrix. The occurrence of sandstone dikes provides an additional means to estimate strain in MRSG slates. The importance of this situation is that fundamental concepts of the Talbot (1970) and Borradaile (1974) methods dictate that each strain gauge should have recorded the same finite strain.

Cleavage, bedding and sand dike orientations from Siamo Slate (Figure 20) were analyzed in the manner described by Borradaile (1974), and the interesting outcome is that the predicted strain style is of the pure flattening type. Borradaile (1974, 1977) reports pure flattening for two slate belts (Scottish Highlands, and Rhine slatebelt, West Germany), on the basis of strain estimates derived from deformed sand dikes. Pure flattening is rarely reported in

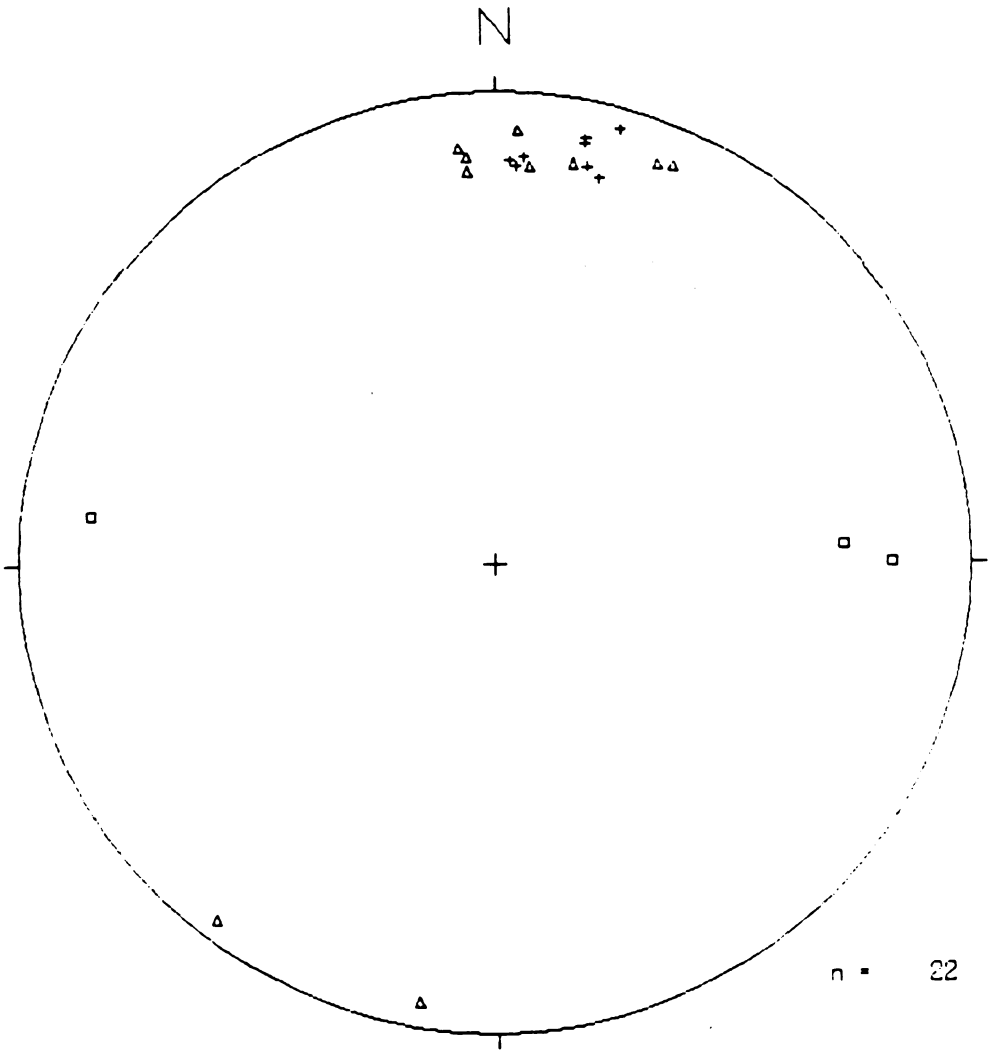

Figure 20. Equal area stereonet plot of poles to cleavage (plus symbols), poles to sandstone dikes (triangles), and plunge of minor buckles in folded sandstone dikes (Siamo Slate at Negaunee roadside outcrop).

geological literature, and it remains controversial whether or not this mode of deformation operates during folding. A pure flattening strain style is controversial because this type of deformation involves unidirectional shortening (Z axis), with corresponding extensions that are exactly the same for the X and Y axes of the strain ellipsoid.

A diversity in pretectonic orientations of sand dikes (assumption 1 above) is a requirement to determine three dimensional strain geometry using the Borradaile (1974) method. A random pattern of sand dike orientations might be expected if the stress field was isotropic during dike emplacement. Contrary to an isotropic stress field, the elongate (west oriented) geometry of the Marquette trough, and the preponderance of west trending vertical vein sets in weakly deformed (or undeformed) argillites are indications that north-south extension was coeval with sedimentation. It is proposed that dikes were emplaced in an orderly, non-random manner during loading as the sedimentary pile accumulated, and developed with a strong preferred vertical to sub-vertical, westerly orientation. This configuration is the expected result if north-south directed extension continued during sedimentation. Because of the assumed pretectonic preferred orientation of the sand dikes, it is accepted that strain estimates derived from these features using the method described by Borradaile (1974) are suspect.

In the case of sand dikes in the Siamo Slate, dike injection (and vein emplacement) must have taken place

after the mudstones were sufficiently lithified to fracture. This is supported by observations of angular argillite clasts that are within the sand-dike matrix. The important observations are that mudstones were at some stage of lithification before dike and vein emplacement, and that some volume reduction preceded the development of these structures. If the assumed west-trending pretectonic configuration of sandstone dikes is correct, angular shear strains can be computed using the method described in the section on veins. There is a consistent relation between deformed slates along trend from Marquette to Ishpeming. The angle between bedding and angular shear strain gauges (veins or sand dikes) is consistent with the amount of deflection expected if the strain indicators were orthogonal to bedding prior to deformation. The style of rotation is consistent with folding by the mechanism of flexural slip.

The Rf/Phi method and its application in determining finite strain from elliptical strain indicators was introduced in a previous section. Reduction spots are one type of ellipsoidal strain indicator present in MRSG slates and quartzites. These features are distributed throughout the Marquette synclinorium, and reduction spots and their application in strain analysis are discussed as a prelude to other ellipsoidal strain gauges that occur only in local settings.

REDUCTION SPOTS IN SLATES

Summary Of Previous Investigations

Sorby (1855) was the first to note reduction spots in slates, and he formulated some of the fundamental concepts that structural geologists continue to debate. Sorby (1855) reported the correlation of the orientation of the principal XY extension plane of ellipsoidal green spots, and the orientation of slaty cleavage. Wood (1974) devised a quantitative method to calculate finite strain from reduction spots, and used these to estimate strain in Caledonian and Teconic slatebelts. Wood (1974) reports a precise, positive correlation of slaty cleavage orientation and the XY principal plane of strain calculated from deformed spots. The use of the word precise (Wood, 1974, p. 375) stimulated many critical comments (see Williams, 1977 for review and discussion).

Tullis and Wood (1975) provide additional evidence to support the relation of slaty cleavage and the XY plane orientation determined by reduction spot strain analyses. This correlation is based on X-ray goniometry analysis of microfabrics in slates, and is suggested to be a positive test of the layer-silicate rotation model proposed by March (1932). These investigators (Wood, 1973, 1974; Tullis and

Wood, 1975) report principal extensions that exceed 170 percent for slate in Wales, and somewhat less for Taconic slatebelts (150 percent).

Wood (1973, 1974) and Tullis and Wood (1975) report the ability to demonstrate a predeformation origin, and a pretectonic spherical shape for reduction spots. These investigators relied on geometrical arguments to establish a predeformation spherical form. The basis for arguing a spherical form include the documentation of perfect ellipsoidal form of reduction spots in deformed slates, and the lack of significant differences in the shape of spots for particular geological settings. Westjohn (1978) relied on arguments posed by these authors in his study of finite strain in the MRSG, and also assumed initial sphericity. Extensions reported by Westjohn (1978) for Proterozoic slates (maximum of 70 percent) are substantially less than Wood (1974) reports for Phanerozoic slatebelts, while the degree of shortening is similar (45 percent, Westjohn, 1978, 50-70 percent, Wood, 1974).

The assumption of initial sphericity simplifies the calculation of the extensions of the principal strain axes, given the additional assumption that deformation is accomplished under constant volume conditions. The equation used is:

$$r^3=XYZ$$

where r is the radius of the parent sphere

X is the maximum principal strain axis length

Y is the intermediate strain axis length

and Z is the minimum strain axis length.

The lengths of long (X), intermediate (Y), and short (Z) axes measured from individual reduction spots allow for the computation of strain, given that the original axis length is equal to the radius of the original sphere.

A recent investigation provides evidence that conflicts with a proposed pretectonic spherical form. Mykura and Hampton (1984) report observations of ellipsoidal spots in undeformed redbeds. The spots described are oblate (roughly circular in the bedding plane) ellipsoids flattened normal to bedding, with axial ratios that range from 1.06 to 1.3 (average of 1.15). This flattening is assumed to be the result of compaction, and is consistent with a slight layer-normal shortening of 7 percent (for the average case). This shortening is estimated given the assumption that sub-spherical reduction spots form near the sediment-water interface in entirely unconsolidated sediments. It is also possible that the ellipsoidal shape of the spots observed by Mykura and Hampton (1984) might be the result of preferential fluid flow (reducing fluid) parallel to bedding in the mudstones. If preferential fluid flow is the process responsible for the ellipsoidal shape of reduction spots, then reducing fluids must have migrated after compaction of the mudstones. Either mechanism is possible, and it is assumed that reduction spots in Kona slates were ellipsoids before deformation.

Although the possibility that reduction spots were sub-spherical at some stage cannot be excluded, substantial deviation from a pretectonic spherical form poses problems in the use of these features to calculate finite strain using the methods devised by Wood (1974) and Westjohn (1978). In fact, any homogeneous volume reduction slates experience leads to overestimates of extensions calculated using reduction spots, when using the Wood (1974) or Westjohn (1978) methods. However, the Rf/Phi method of strain analysis eliminates the need to assume initial sphericity.

Observations of reduction spots in MRSG argillites and slates provide some insight regarding their origin; this topic is addressed next, followed by a discussion of strain analyses for undeformed argillites, argillites with weakly developed cleavage, and slates with well formed slaty cleavage.

Reduction Spots In Kona Slates

The presence of reduction spots in MRSG slates is an unusual situation in that these strain indicators provide a third means to assess the style of internal distortions suffered by slates during Penokean deformation. Reduction spots are dispersed in the domain that contains deformed veins, and this allows for the comparison of strain estimates derived from alternate methods.

Westjohn (1978) recognized a regional distribution of spots in the gray-green argillite member of the Kona Formation (Taylor, 1973), and Meyer (1983) reported the presence of spots in the big cusp algal dolomite member as delineated by Taylor (1973). The reduction spots are pale-green to pale-yellow triaxial ellipsoids, but zones of reduced iron are not always ellipsoidal in form. Bodies of reduced iron locally have irregular form, and often bedding surfaces show color contrast that indicates reduction of iron occurred parallel to bed surfaces. This situation is usually observed in sub-horizontal argillites. Also common is the coalescence of two or more reduction spots. This can be demonstrated in cases where oxidized or partially reduced cores remain within the coalesced spots. For this situation, the reduction bodies are substantially more elliptical than single spots observed in the same sample. This circumstance poses problems in Rf/Phi analysis, because ellipticities of the coalesced spots measured in any plane are exaggerated.

Reduction of iron in ferruginous Kona slate has been observed as thin films and/or selvages that parallel cleavage surfaces. This observation is one indication that reducing solutions were mobilized late and perhaps during folding, if it is assumed that cleavage is a fabric element that forms late. It is assumed that there is more than one stage where fluids with a reducing capacity were mobile.

Although there is some doubt regarding the stage of diagenesis (or deformation?) in which reduction spots form, their presence in undeformed, unmetamorphosed rocks supports the suggestion that they form early (Mykura and Hampton, 1984). The favored origin for reduction spots in Kona slates is that they formed near the sediment-water interface. This origin is consistent with diagenetic conditions expected for the Kona mudstones. It is likely that the abundant sulfides in the Kona (Taylor, 1973) originated under near euxcinic conditions (bacteria reduction of sulfate), an environment that would foster reducing conditions at the sediment-water interface.

Rf/Phi Strain Analyses Using Reduction Spots

Slates at seven locations contain sufficient numbers of reduction spots for strain determination. The strain ratios for seven determinations are plotted on a Flinn diagram (Figure 21), and the axial orientations for the principal strain axes are shown on stereonet plots (Plates 1 and 2). It would be redundant to include all Rf/Phi plots prepared from measurements of reduction spots, because most are similar in form. However, there are important differences between Rf/Phi diagrams for slates at the Harvey and Lindberg quarries. Examples of plots for these locations are included for comparison (Figures 22-27).

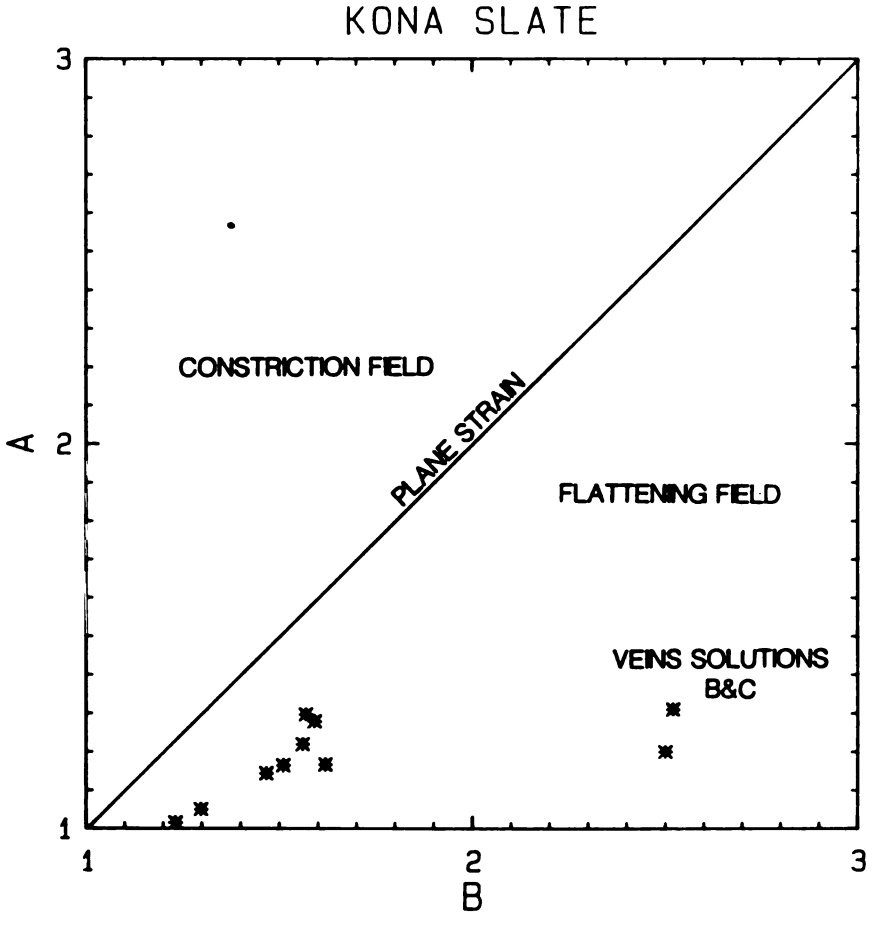

Figure 21. Flinn plot showing strain ratios for Kona slates.

Figure 22. Rf/Phi plot of 51 reduction spots from the north limb of the Harvey syncline (sample 1030863). Plane is vertical and nornal to cleavage. (Lisle nomogram (abbreviated MG for marker grid) MG=2.7)

Figure 23. Rf/Phi plot for 50 reduction spots, same sample as Figure 22, but plane is horizontal and normal to cleavage. Lisle nomogram, MG= 2.40.

Figure 24. Rf/Phi plots for 69 reduction spots, same sample as Figure 22, but plane is vertical and parallel to cleavage.

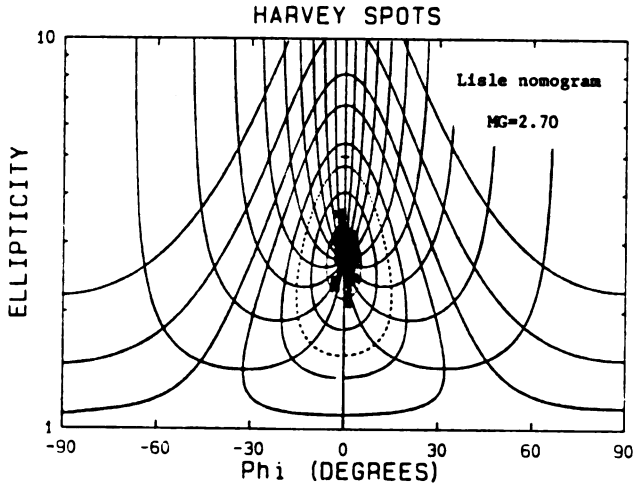

Figure 22.

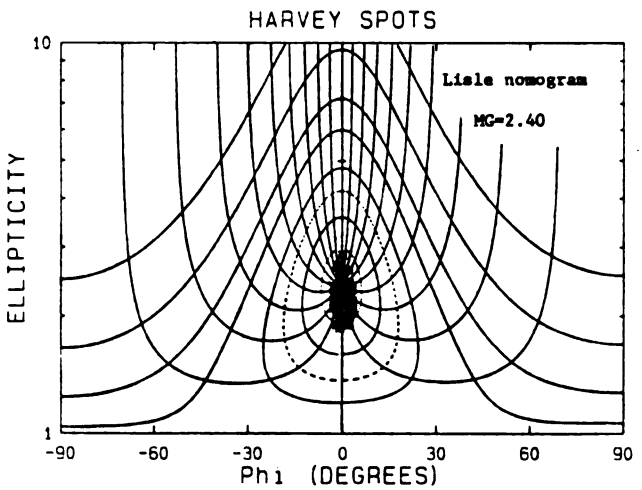

Figure 23.

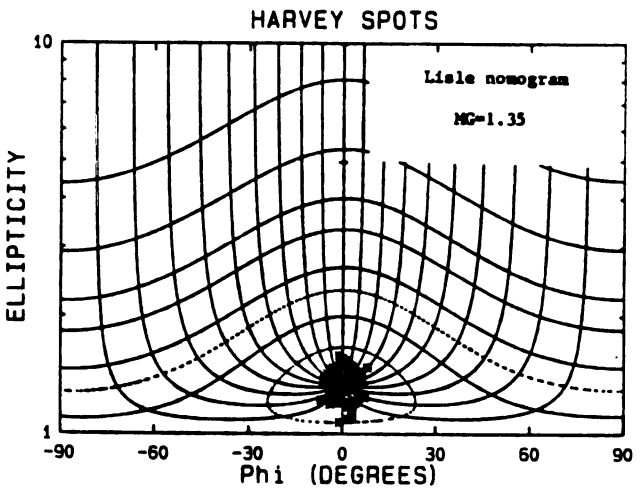

Figure 24.

Figure 25. Rf/Phi plot for 50 reduction spots at the Lindberg quarry (Kona argillites). Plane is vertical (strike 310 degrees). Lisle nomogram value MG=1.60.

Figure 26. Rf/Phi plot for 45 reduction spots, same sample as Figure 25, plane is parallel to bedding. Lisle nomogram value MG=1.10.

Figure 27. Rf/Phi plot for 51 reduction spots, same sample as Figure 25, plane is vertical (strike 130 degrees). Lisle nomogram value MG=1.70.

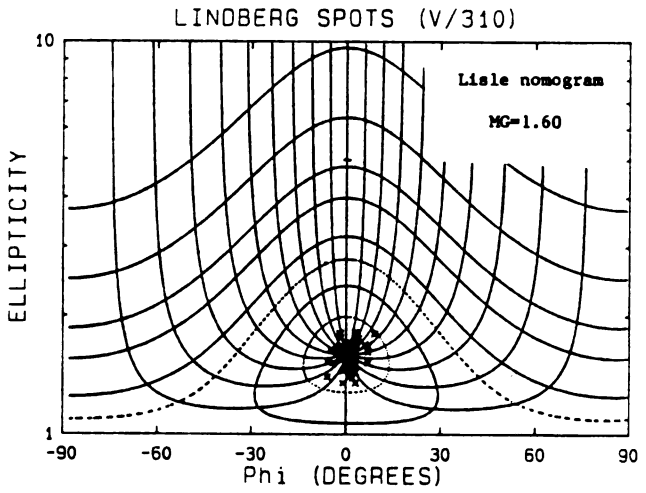

Figure 25.

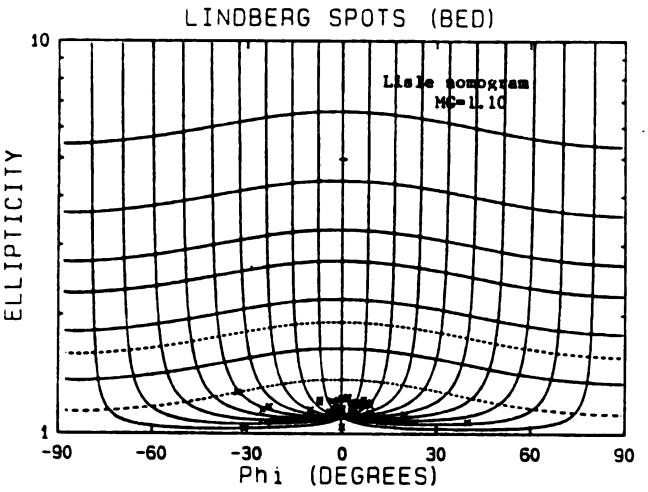

Figure 26.

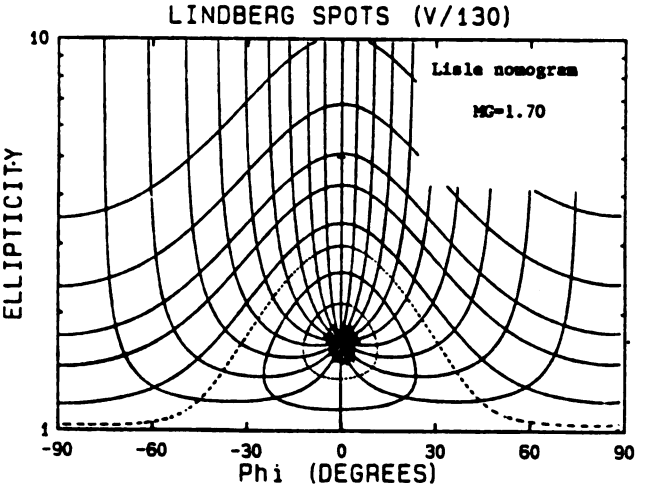

Figure 27.

The structural setting of slates that contain reduction spots differs from site to site. Inclination of bedding ranges from flat to slightly overturned, and fold plunge variation includes shallow west plunging synclines, moderate (55 degrees) west plunging anticlines, moderate (35 degrees) east plunging synclines, and upright non-plunging folds. The orientation of the principal strain axes shows a systematic relation to fold geometry at most locations (Plates 1-4). Where observed in steep limbs of folds, the long axis (X) always plunges east, and is near-vertical. Generally, long axes plunge in the same direction as fold axes, but at a steeper angle. There are two instances where folds and principal extension directions plunge in opposite directions (Ski Hill anticline, and Eagle Mills syncline, Plates 1 and 2), and one case where the plunge direction of these is the same (Harvey syncline core).

In flat-lying and apparently weakly deformed argillites (Lindberg Quarry, Plate 1), reduction spot long axes lie in the bedding plane. The spots are flattened parallel to bedding, and Meyer (1983) reports that there is a preferred northwest orientation of long axes of reduction spots. Meyer (1983) used a method of strain analysis devised by Elliot (1970), a technique that is similar in many respects to the Rf/Phi method. To maintain consistency in data analysis, argillites were sampled from the same outcrop Meyer (1983) sampled (Lindberg quarry), and strain analyses were made using the Rf/Phi technique.

Inspection of the Rf/Phi (Figure 26) plot of spots in the bedding plane shows a slight ellipticity, and the stereo net plot of principal strain axes (Plate 1, Lindberg quarry) supports the interpretation of Meyer (1983). The minimum shortening normal to the bedding plane is estimated at 27 percent, a figure that hinges on assuming a sub-spheroidal form that pre-dates compactional strain. This is similar to the result reported by Meyer (1983), although he does not attribute a mechanism to account for initial layer-normal shortening. The sub-oblate ellipsoidal shape is reasonably well established (Meyer, 1983), and verified with an independent determination (Figures 23, 25, 27, and Plate 1).

Reduction spots are present in shallow-dipping argillites at the locality described previously in the section on veins (Hwy. 480 outcrop, northwest of Lindberg quarry, sample site 1031867, Plate 1). The number of spots was insufficient for strain analysis using the Rf/Phi method, but measurements made at the outcrop show the maximum extension (X axis) is vertical, and the XY principal plane is west-northwest in orientation. This trend is the same as that reported by Meyer (1983) for reductions spots measured in shallow-dipping argillites at the Lindberg quarry. It is important to note that even though vein textures (slightly folded and boudinaged) indicate only slight internal distortion, the X axis differs by 90 degrees between these locations. This topic is addressed in the section on the role of volume loss

during deformation.

There are multiple strain indicators in MRSG quartzites; the next section introduces one additional method of strain analysis, the Fry (1979) center-to-center technique. This method was used as a supplement to the Rf/Phi method, to compute strain ratios using packed grain aggregates in quartzites.

QUARTZITES: THE FRY METHOD OF STRAIN ANALYSIS

All quartzites in the Marquette-Ishpeming area are generally featureless at the outcrop and mesoscopic scale (except for occasional quartz veins described previously). However, it is now demonstrated that there are microfabrics and macrofabrics in certain structural environments that are interpreted to be a record of internal distortions quartzites suffered during folding. Microfabrics were assessed using the Rf/Phi method, and these are supplemented with analyses derived from an alternate method (Fry, 1979).

Figure 28 illustrates the principles of the Fry (1979) method, using a two-dimensional case. The method relies on the concept that particle centers in a packed grain aggregate should be displaced proportionately during strain. For example, the distance between nearest-neighbor grain centers should increase in the direction of extension (vertical in Figure 28), while the distance between grain centers should decrease in the direction of shortening (horizontal in Figure 28). In practice, the Fry method involves determining the relative change in lengths of tie lines that connect nearest neighbor grain centers, relative to a grain that is selected as the origin (see Ramsay and

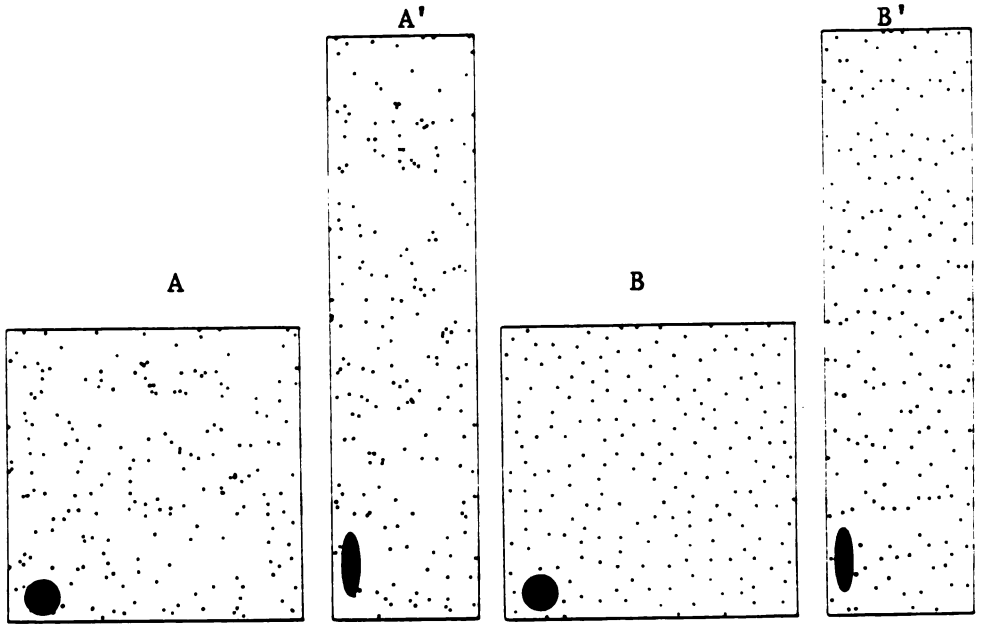

Figure 28. Illustration of random and non-random point distributions. Diagram A shows a Poison random distribution, and A' is the deformed product, also a random distribution. Diagram B shows a statistically uniform distribution of points, and B' illustrates the deformed product. Points in B' are not uniform in distribution. (Modified from Ramsay and Huber, 1985, p. 110).

Huber, 1983, p. 108). This can be accomplished by measurements made on photographic enlargements of grain aggregates (quartzites). This is a time consuming process, and Fry (1979) devised a rapid method that eliminates the need for these measurements. The rapid method involves plotting a sufficient number of grain centers on a transparent overlay. The center of a single grain (selected near the center of the distribution of points) is plotted on a second overlay as a reference point; this reference point is placed over the center of each grain that appears on the first overlay, maintaining a constant azimuth between both overlays, and the locations of all grain centers are plotted on the second transparency. If a sufficient number of grain centers are plotted, a vacancy field, or an area where there are no points should be produced. The vacancy field results, because the distance between grain centers can be no closer than two times the average grain radius. Because the shape and definition of the vacancy field is a function of the grain radius, the method works best if grain size is uniform in the aggregate. Improvements in the Fry (1979) method eliminate this requirement; this topic is addressed in later paragraphs. There are computer programs that can perform the plotting of grain centers, and determine the shape and orientation of the vacancy field (strain ellipse). These programs allow rapid processing of large quantities of data, and programs provided by Bauer (1985, written commun.) were used for strain analyses using the Fry (1979)

method (Appendix A).

Strain ellipses and orientations for three planes are required to compute strain ellipsoid geometry, and the same computer programs that were used for strain determinations from Rf/Phi plots allow this manipulation (Appendix A).

The Fry (1979) and Rf/Phi methods of strain analysis produced comparable results for the orientation of the long axis of the strain ellipse for given planes from the same rock sample, while the strain ratios differ between methods. Figures 29-34 are Rf/Phi and Fry plots that illustrate these points. The discussion that follows supports the selection of strain values derived from the Rf/Phi method, over the Fry (1979) method.

The most serious limitation in the "nearest-neighbor" or center-to-center method (Fry, 1979) is the requirement that objects that make up the packed aggregate cannot be random, and they cannot be clustered or anticlustered (non-uniform). Examples of random and uniform grain center distributions are shown in Figure 28.

Fry (1979) points out that the confidence in being able to assess natural distortions by this method is a function of the degree of departure from an initial pretectonic fabric (the same is true for the Rf/Phi method). It is also implicit that processes such as grain-boundary sliding cannot be appraised by the Fry (1979) technique.

The requirement of homogeneous deformation of an isotropic media (Fry, 1979) might be viewed as a significant limitation. Internal distortions in quartzite

Figure 29. Plots showing comparison of Rf/Phi and Fry analyses of data for same plane (plane A, sample 914875, Eagle Mills syncline). Left diagram based on 361 grain ellipticities. Right diagram based on 361 grain centers.

Figure 30. Plots for plane B4, same sample as Figure 29. Left diagram based on 335 grain ellipticites; Fry plot (right) based on 335 grain centers.

Figure 31. Plots for plane C4, same sammple as Figure 29. Rf/Phi plot (left) based on 412 grain ellipticities; Fry (right) based on 412 grain centers.

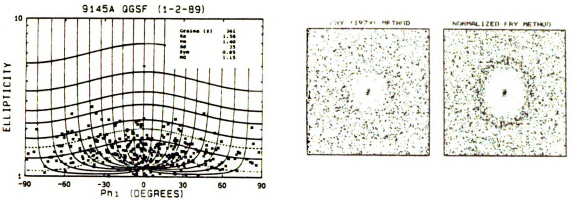

Figure 29.

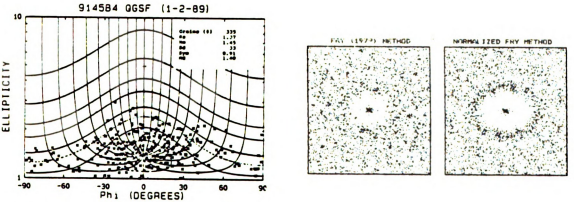

Figure 30.

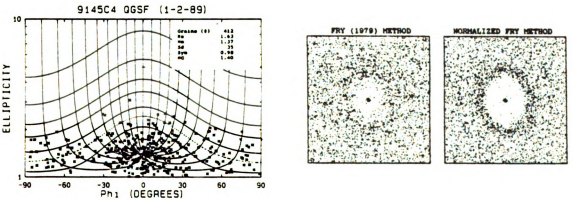

Figure 31.

Figure 32. Pf/Phi (left diagram) for Mesnard Quartzite (sample 1030861) near the DNR in Marquette, based on 186 grain ellipticities, and Fry plot for same plane (right diagram), based on 188 grain centers.

Figure 33. Rf/Phi plot (left diagram) based on 165 quartz grain ellipticities, and Fry plot (right diagram) based on 231 grain centers (both plots based on same plane) for same sample as Figure 33.)

Figure 34. Rf/Phi plot (left diagram) based on 229 quartz grain ellipticities, and Fry plot (right diagram) for the same plane, based on 199 grain centers. (Plots for same sample as Figure 32).

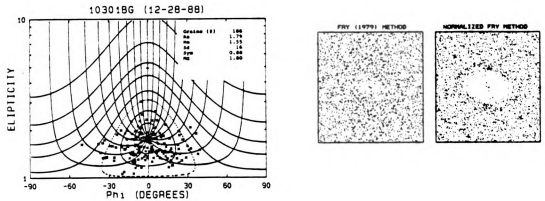

Figure 32.

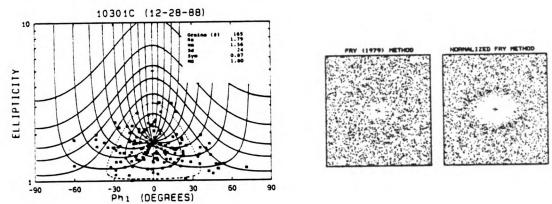

Figure 33.

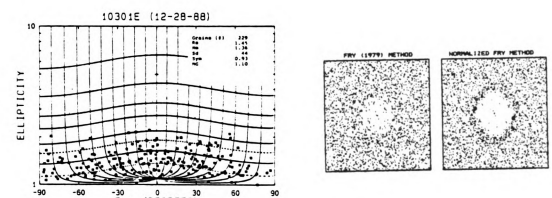

Figure 34.

are likely heterogeneous at the hand sample scale, and probably at the grain scale in certain instances. However, this assumption must be made, and the validity of the strain values estimated using the Fry (1979) and Erslev (1988) methods hinges on the assumption of homogeneous deformation.

Crespi (1986) demonstrates using artificially derived point distributions that there are several aspects of the center-to-center method that need to be considered. Crespi (1986) shows that a clear demarcation of the vacancy field from the field of high point density is a function of the degree of anticlustering. Artificial point distributions with different degrees of anticlustering are used to show that a girdle of high point density results only in cases where pretectonic point distributions are sufficiently anticlustered (Crespi, 1986). A sufficiently anticlustered point distribution is necessary for the center-to-center method to provide meaningful results (Fry, 1979). For the environments studied, anticlustered populations and corresponding well defined vacany fields are indicated only where ellipticites (based on Rf/Phi plots) exceed 1.3. The most important conclusion of Crespi (1986) is that the shape and orientation of the vacancy field does not provide an objective approach to define an appropriate strain ellipse. Quartz grain subfabrics (QGSF) in MRSG quartzites are used to substantiate this conclusion.

Analysis of quartzite microfabrics using computer programs provided by Bauer (1985, written commun., see

Appendix A) produced mixed results in most cases, with the fundamental problem that vacancy fields were poorly defined regardless of the number of objects digitized. Erslev (1988) elaborates on this common problem, and attributes the lack of definition of the vacancy field to size distribution of objects in packed-grain aggregates. To circumvent this problem, Erslev (1988) devised a normalization technique. The center-to-center distance between objects is divided by the sum of the average radii (the normalization technique is a subroutine of INSTRAIN, Appendix A).

Plots generated using the normalization technique of Erslev (1988) illustrate a well defined vacancy field (Figure 29-34), in contrast to the rather poorly defined field from the standard Fry plot. However, the ellipticity of the vacancy field for most samples analyzed has a limited range (1.2 to 1.3). Three planes with the same ellipticity, which is the general case for most plots derived from analyses of MRSG quartzites, cannot describe the shape of any triaxial ellipsoid. It is assumed that in cases where strain magnitudes are low, the normalized center-to-center method (Erslev, 1988) is of limited application in determining the shape of the strain ellipse. However, the orientation of the vacancy field consistently corresponds to the solution generated from Rf/Phi plots for the long axis orientation.

First inspection of the comparitive plots (Figures 29-34, for example) may lead to some confusion regarding

the orientation of the calculated strain ellipse. The orientation of the elliptical vacancy field is plotted relative to the direction the photographic enlargement is placed on the digitizer tablet, hence the apparent lack of relation in orientations of long axes when Rf/Phi plots are compared to normalized Fry plots. In the case of Rf/Phi plots, the angle Phi is always adjusted so the mean is zero, so that the Lisle (1985) strain ratio overlays provide meaningful solutions. The adjustment in the angle Phi is accomplished by a combination of Fortran programs (see Appendix A), whereas the angle Phi (normalized Fry plot) is fixed.

In summary, the Rf/Phi method combined with Lisle (1985) nomograms is preferred to assess fabrics in MRSG quartzites, because the nomograms allow for an objective assignment of ellipticity, and the corresponding strain ratio.

QUARTZITES: STRAIN ANALYSES BY THE RF/PHI METHOD

Photographic enlargements were made from thin sections of quartzite, so that grain shapes could be accurately digitized (see Appendix A). Each quartz grain was assigned long and short axes directions by visual inspection. End points of the long and short dimensions (at contacts with adjacent grains) for each grain were digitized. In general, it is difficult to assign elliptical shapes to quartz grains without bias toward grains that are obvious ellipses, versus those that have other geometrical forms (trapezoids, for example). Ramsay and Huber (1983) demonstrate that the shape of any feature can be assigned values for long and short axes.

In order to eliminate bias toward selecting just elliptical grains, end points of long and short dimensions of all grains were digitized (DIGROCK, Appendix A) for each thin section photo enlargement. The area digitized per photo ranged from 25 to 80 square inches (grain total usually 200 to 400 per plane). A counting grid with 1 inch-square cells was used as a overlay net, to assure all grains per cell were digitized, and to prevent digitizing grains more than once. Recognition of grain boundaries was enhanced using a ten-power magnifying lens, a device often

used to do fine-detail drafting. Grain boundaries are also enhanced in some photos (unfortunately only quartzites with demonstrable fabric), because high-birefringent layer silicates form envelopes that partially surround quartz grains. These partial envelopes contrast substantially in polarized light (crossed polars), and this is reflected in the photo enlargements.

Strain Variation And Petrographic Observations

Quartz grain subfabrics (QGSF) based on Rf/Phi plots are interpreted to show that the degree of distortion is a function of bed dip. Figures 29-38 show the variation observed in Rf/Phi plots of the quartzites sampled from different structural settings, and Figures 39 and 40 are Flinn strain ratio plots and stereonets that show the strain variation. Subhorizontal quartzites (Kona and Ajibik) along the southern limb of the Marquette synclinorium (dips less than 30 degrees) do not have fabrics that can be attributed to internal distortions, or at least any fabric is too obscure to be assessed by the Rf/Phi method. Strain ratios derived from Lisle (1985) nomograms are always less than 1.3 for these quartzites. This degree of ellipticity is within the range of ellipticities reported by Bokman (1959) for sand grains. Data processed for these quartzites cannot be manipulated without large error messages that indicate either heterogeneous strain, or the inability to determine a

Figure 35. Rf/Phi plots for Mesnard Quartzite (sample 915875), Eagle Mills syncline.

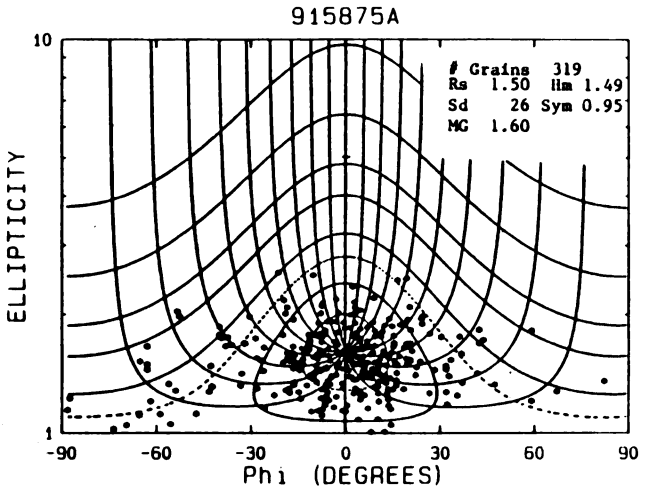
915875A
Grains 319
Rs 1.50 Hm 1.49
Sd 26 Sym 0.95
MG 1.60
ELLIPTICITY
10
1
-90 -60 -30 0 30 60 90
Phi (DEGREES)

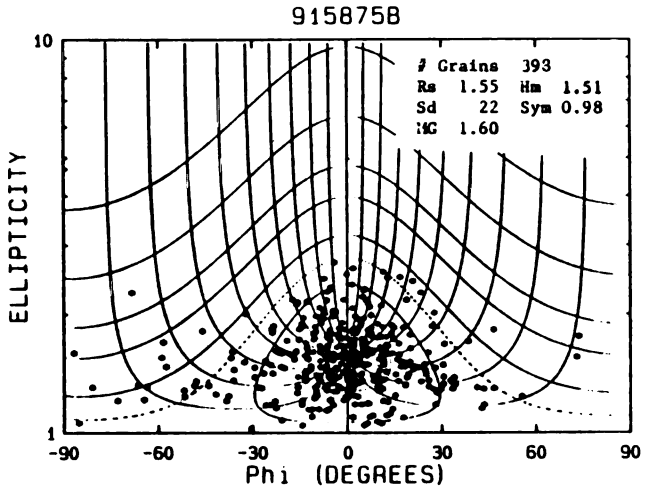
915875B
Grains 393
Rs 1.55 Hm 1.51
Sd 22 Sym 0.98
MG 1.60
ELLIPTICITY
10
1
-90 -60 -30 0 30 60 90
Phi (DEGREES)

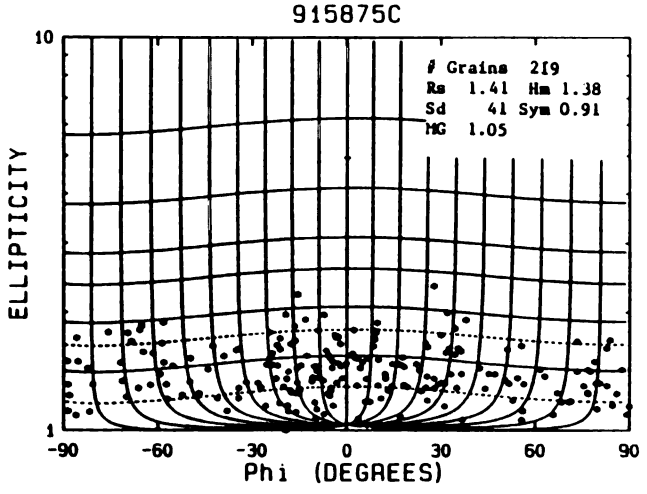
915875C
Grains 219
Rs 1.41 Hm 1.38
Sd 41 Sym 0.91
MG 1.05
ELLIPTICITY
10
1
-90 -60 -30 0 30 60 90
Phi (DEGREES)

Figure 35.

Figure 36. Rf/Phi plots for Mesnard Quartzite (915876), Eagle Mills syncline.

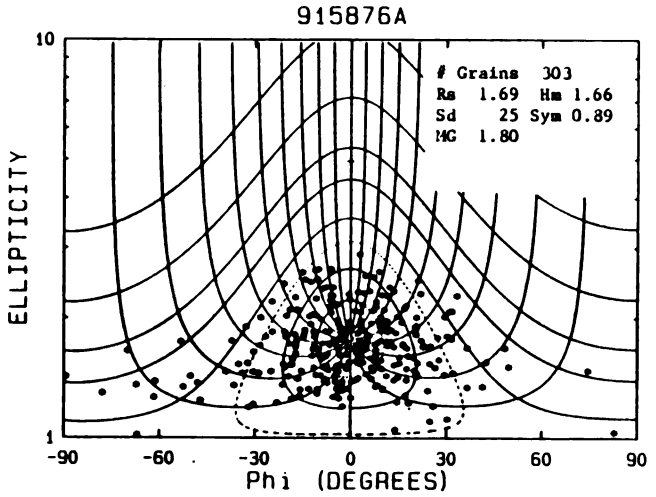
915876A
Grains 303
Rs 1.69 Hm 1.66
Sd 25 Sym 0.89
MG 1.80
ELLIPTICITY
10
1
-90 -60 -30 0 30 60 90
Phi (DEGREES)

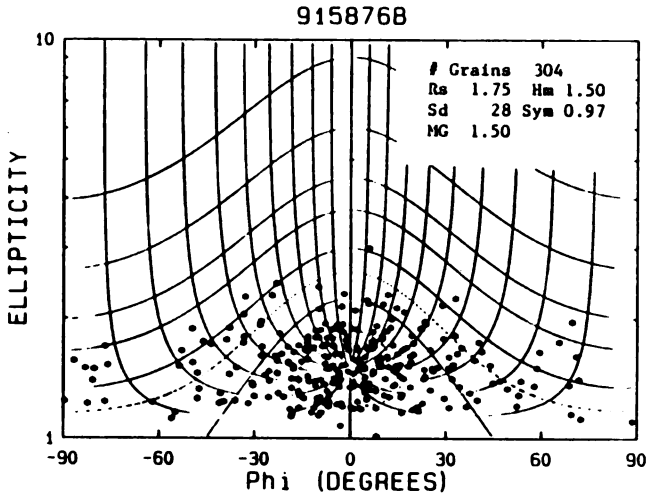
915876B
Grains 304
Rs 1.75 Hm 1.50
Sd 28 Sym 0.97
MG 1.50
ELLIPTICITY
10
1
-90 -60 -30 0 30 60 90
Phi (DEGREES)

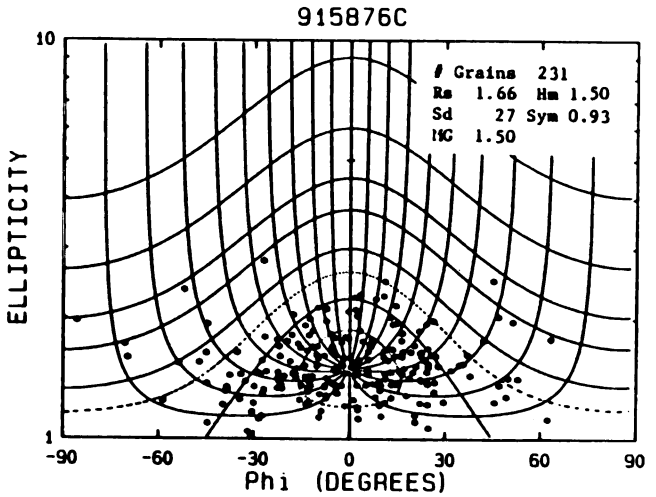
915876C
Grains 231
Rs 1.66 Hm 1.50
Sd 27 Sym 0.93
MG 1.50
ELLIPTICITY
10
1
-90 -60 -30 0 30 60 90
Phi (DEGREES)

Figure 36.

Figure 37. Rf/Phi plots for Ajibik Quartzite (10318611), Cooper Lake outcrop, northwest of Ishpeming.

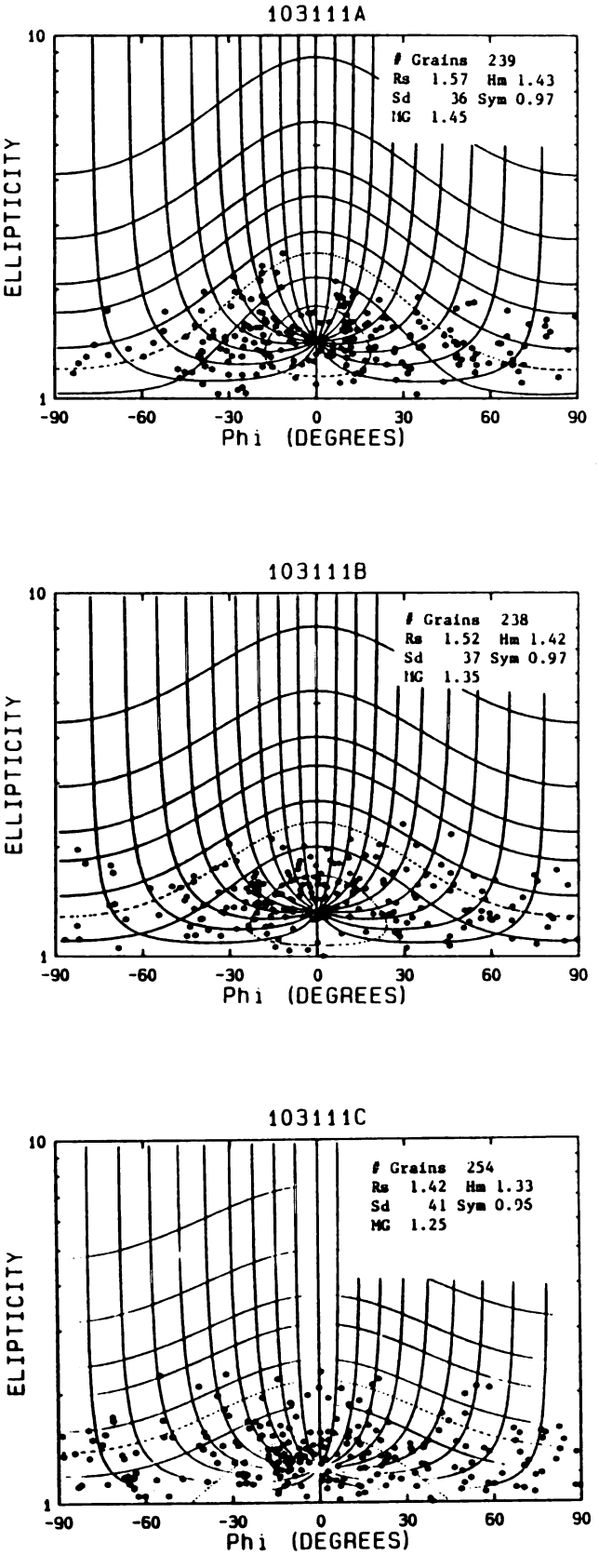
103111A
Grains 239
Rs 1.57 Hm 1.43
Sd 36 Sym 0.97
MG 1.45
ELLIPTICITY
10
1
-90 -60 -30 0 30 60 90
Phi (DEGREES)
103111B
Grains 238
Rs 1.52 Hm 1.42
Sd 37 Sym 0.97
MG 1.35
ELLIPTICITY
10
1
-90 -60 -30 0 30 60 90
Phi (DEGREES)
103111C
Grains 254
Rs 1.42 Hm 1.33
Sd 41 Sym 0.95
MG 1.25
ELIPTICITY
10
1
-90 -60 -30 0 30 60 90
Phi (DEGREES)

Figure 37.

Figure 38. Rf/Phi plots for Ajibik Quartzite (916873), west Cooper Lake outcrop.

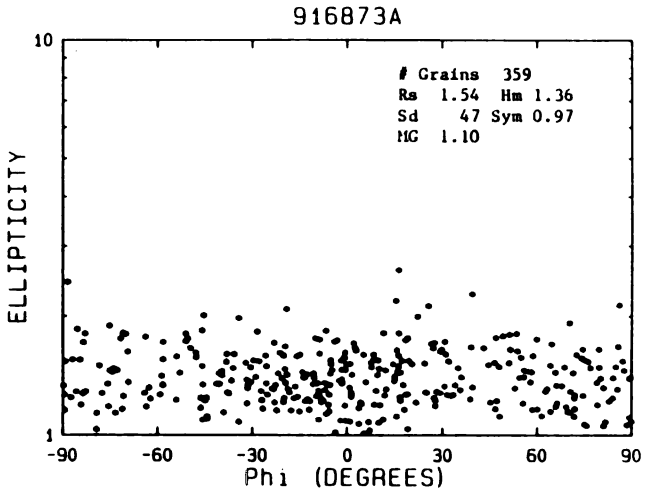
916873A
Grains 359
Rs 1.54 Hm 1.36
Sd 47 Sym 0.97
MG 1.10
ELLIPTICITY
10
1
-90 -60 -30 0 30 60 90
Phi (DEGREES)

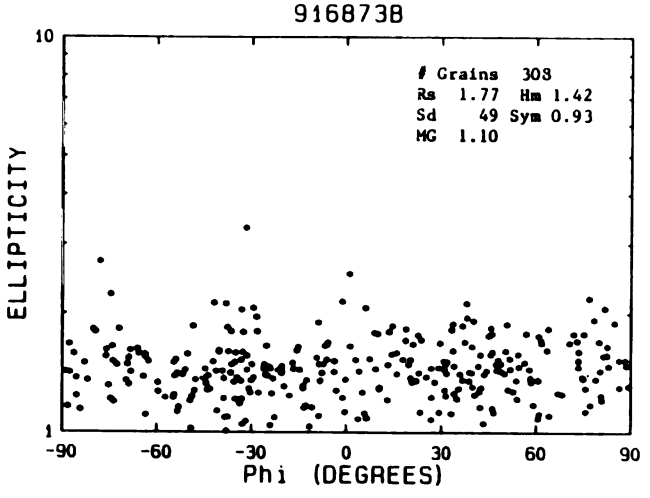
916873B
Grains 308
Rs 1.77 Hm 1.42
Sd 49 Sym 0.93
MG 1.10
ELLIPTICITY
10
1
-90 -60 -30 0 30 60 90
Phi (DEGREES)

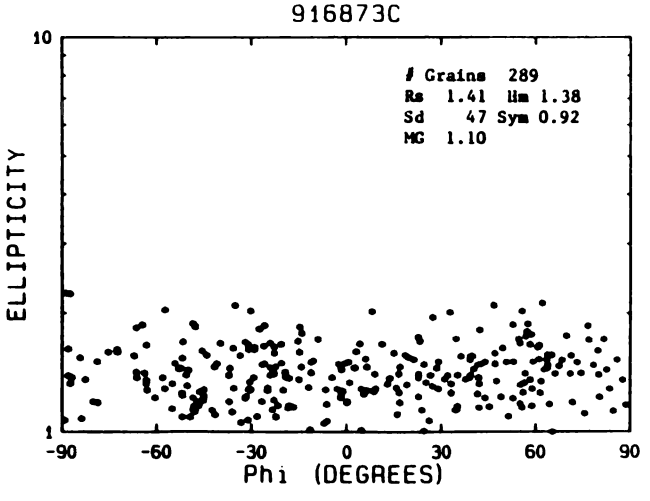
916873C
Grains 289
Rs 1.41 Hm 1.38
Sd 47 Sym 0.92
MG 1.10
ELLIPTICITY
10
1
-90 -60 -30 0 30 60 90
Phi (DEGREES)

Figure 38.

Figure 39. Flinn plot of all strain data for Mesnard and Ajibik Quartzites (see Plate 1 for locations).

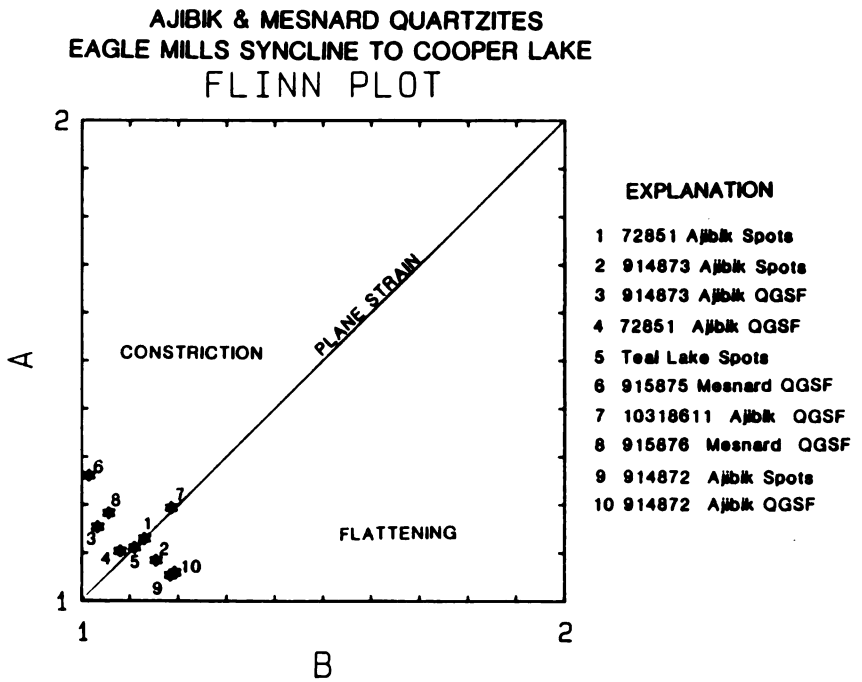
AJIBIK & MESNARD QUARTZITES
EAGLE MILLS SYNCLINE TO COOPER LAKE
FLINN PLOT
2
1
A
1
2
B
CONSTRICTION
PLANE STRAIN
FLATTENING
EXPLANATION
1 72851 Ajibik Spots
2 914873 Ajibik Spots
3 914873 Ajibik QGSF
4 72851 Ajibik QGSF
5 Teal Lake Spots
6 915875 Mesnard QGSF
7 10318611 Ajibik QGSF
8 915876 Mesnard QGSF
9 914872 Ajibik Spots
10 914872 Ajibik QGSF

Figure 39.

Figure 40. Equal area stereonet plots of X, Y, and Z axes for ten strain determinations, Ajibik and Mesnard Quartzites, Negaunee-Ishpeming area. Numbers correspond to samples listed in Figure 39.

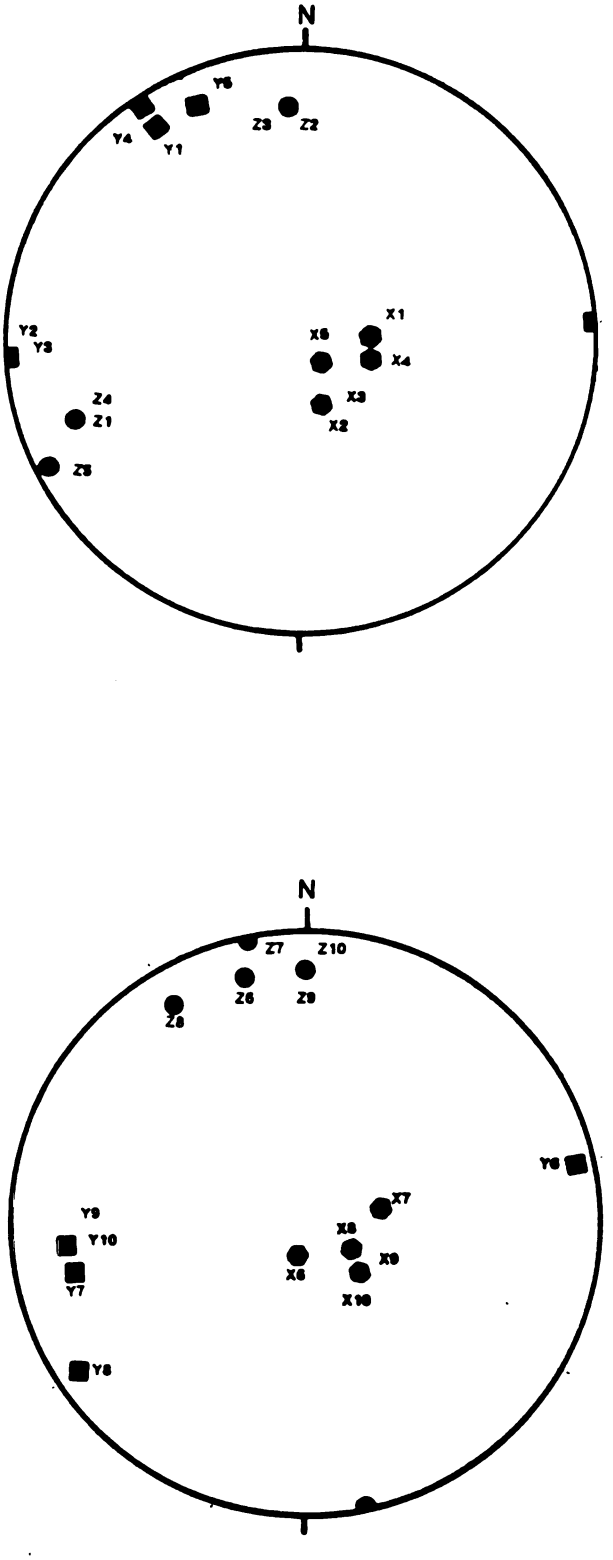
N
Y5
Z3
Z2
Y4
Y1
Y2
Y3
X1
X5
X4
X3
Z4
Z1
X2
Z5
N
Z7
Z10
Z6
Z9
Z8
Y6
Y9
X7
X8
Y10
X6
X9
Y7
X10
Y8

Figure 40.

suitable three dimensional solution.

Thin section observations show both sutured and smooth grain boundaries (as described by Sibley and Blatt, 1976) in all quartzites from flat and shallow dipping limbs, and it is not possible to detect any microfabric in these rocks. Grain contacts are predominantly quartz to quartz, and fibrous quartz-mica growths are lacking in all samples examined. There is no indication of extension in any thin sections examined. The MRSG experienced lower-greenschist facies metamorphism during Penokean deformation (Cannon, 1973). It is assumed that metamorphism generated conditions favorable for internal chemical homogenization, so features that allow for the assessment of pressure solution by cathodoluminescence are absent. As Sibley and Blatt (1976) demonstrate, pressure solution controlled grain boundaries can have either a smooth or sutured morphology, so it is not possible to determine the role of pressure solution and it's relation to the style of grain boundary development. Quartz grains with deformation lamellae are present, but these constitute a minor percentage of the total grain population.

The structural setting where quartzite beds dip from 30 to 55 degrees was not analyzed by the Rf/Phi method, because thin section observations show a microfabric is lacking in these rocks. It is assumed that Rf/Phi analyses of these would produce plots that indicate no internal distortion.

There is a definite fabric developed in cases where bed

dips approach 60 degrees. For quartzites in this environment, the principal extension direction is always sub-vertical with steep east and southeasterly plunge (Figure 40). The XY plane for these quartzites consistently dips steeper than bedding (10 to 15 degrees), and there is substantial variation in the orientation of the XY principal plane (Figure 40).

Considerable effort was directed to quartzites in the north limb of the Eagle Mills syncline, because of the presence of multiple strain gauges. Figure 39 illustrates that strain ratios from five determinations plot near the plane strain field, with some overlap into flattening and constriction fields. These five strain analyses (3 Rf/Phi analyses of reduction spots, and 2 QGSF, duplicate samples of reduction spot zones, for a total of 4544 ellipses digitized) are for three outcrops (Plate 2) of Ajibik quartzite, where moderate dips range from 57 to 63 degrees south. Strain ratios are small for these quartzites, and although the fabric cannot be recognized at the mesoscopic scale (visual inspection of photo enlargements), Rf/Phi plots are reproducible. It is interpreted that internal distortions are first recognizable in MRSG quartzites at this stage in fold development. Deformation lamellae are more common in these quartzites, but still constitute a minor portion of the total grain population.

Strain ratios (Lisle nomogram) reach a maximum (Rs=1.8) where fold limbs are vertical (north limb, Harvey syncline) or slightly overturned (Eagle Mills syncline). Strain

ratios are interpreted to indicate slight flattening in moderately dipping quartzites (65 to 75 degrees), and the degree of flattening increases as a function of limb attitude. Strain determined for Mesnard Quartzite in the vertical limb north of Harvey indicates flattening (Plate 1, and Figure 39). Mesnard Quartzite in the slightly overturned north limb of the Eagle Mills syncline also appears to be flattened (Plate 2). Deformed grains (deformation lamellae) are dominant in structural settings where limb dip is steep. In steep and overturned limbs, quartz grains are predominantly ellipsoidal (Figure 41), and mica beards are common in presumed pressure shadow regions (Figure 42). Quartz-to-quartz grain contacts are generally observed only along the trace of apparent shortening (based on the Rf/Phi plots). In the direction of apparent extension, fine grained quartz-mica "beards" or K-mica occupy the space between quartz grains; these textures correspond to the extension direction predicted by strain computed using the Rf/Phi method.

Internal distortions and flattening strains in near-vertical and overturned limbs are also indicated by observations of rutile needles. Rutile crystals have been noted in most thin sections of quartzite. Rutile needles appear to be undistorted in all shallow to moderately dipping quartzites. Thin sections cut parallel to the calculated flattening plane show segmented rutile crystals (Figure 43) that have the appearance Mitra (1977) ascribed

Figure 41. Photomicrograph of elliptical quartz grain (approximately 1 millimeter long). Thin section of Mesnard Quartzite (DNR outcrop, sample 1030861).

Figure 42. Photomicrograph (close-up) of right end of quartz grain shown in Figure 41, showing white mica mineral growths in pressure shadow region.

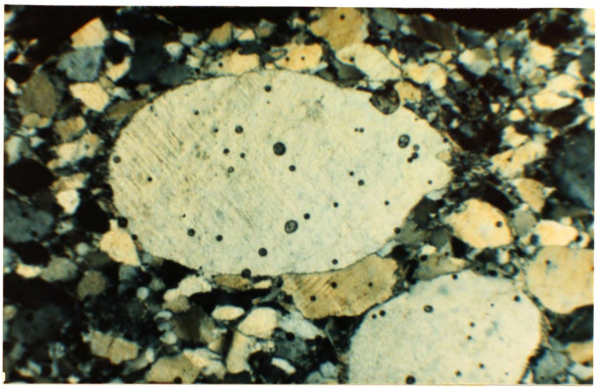

Figure 41.

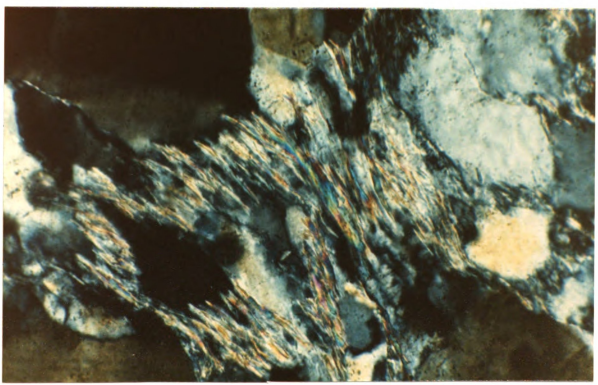

Figure 42.

Figure 43. Photomicrograph of quartz grain, showing extended rutile needle (microboudin). (Sample 1030861, Mesnard Quartzite, near DNR in Marquette).

Figure 44. Photomicrograph of quartz grain showing folded rutile needle (microbuckle). (Sample 1030861, Mesnard Quartzite, near DNR in Marquette).

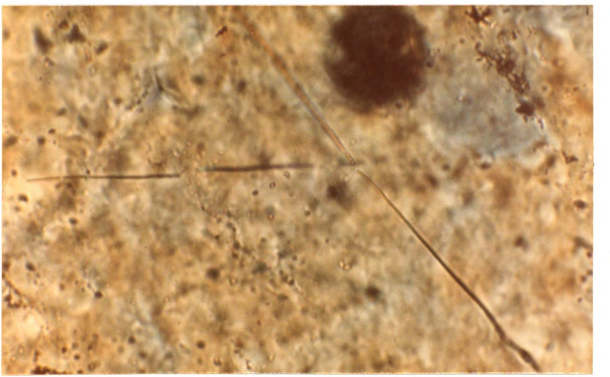

Figure 43.

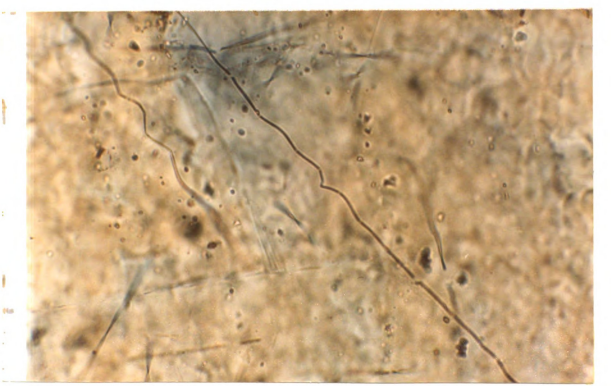

Figure 44.

to extension. These are microboudins. Rutile needles that show indications of shortening (microbuckles) are less common, but these are observed in thin sections cut normal to the apparent flattening plane (Figure 44). These microstructures have been observed only in quartzites from steep or overturned limbs.

One additional line of evidence that supports a flattening strain style is the presence of chocolate-tablet boudinaged veins in calcareous quartzites. However, it is noteworthy that the Rf/Phi plot for all planes examined in calcareous-quartzite have the character common to orthoquartzite samples from the southern fringes of the synclinorium. The fluctuation in the angle Phi (Lisle, 1985, p. 5) is substantial for all planes, a situation that could be incorrectly interpreted to indicate no significant internal distortion. Quartz grains are entirely supported by a matrix of ferroan-carbonate, and it is suggested that recrystallization of the matrix is the mechanism that accommodates distortions for this setting. A reasonable explanation for the lack of alignment of quartz grain long axes cannot be offered, and it is perplexing because elongate grains should have rotated during deformation.

Although pronounced microfabrics can be documented for many localities, there is one case where textures of quartzites in steep dipping limbs (as mapped by the U.S.G.S.) resemble those observed in the flat and shallow dipping limbs. One example is from the Ajibik Quartzite that is in contact with the Archean greenstone belt along

the Carp River Falls shear zone. Ajibik at this location occurs as an obscure "outlier". Although the U.S.G.S. map (Clark and others, 1975) indicates the quartzite dips 80 degrees south, it is clear from the sample (Plate 4, Cooper Lake area, sample number 916873) that beds actually dip less than 50 degrees southeast. Although the Ajibik is close to the Archean (Kitchi Schist) and the Carp River Falls shear zone, Rf/Phi plots for this sample (Figure 38) show substantial fluctuation in the angle Phi that indicates little or no distortion. It is suggested that this outlier of Ajibik was rotated passively, and did not record any significant internal distortion.

In summary, when all strain analyses based on quartz grain subfabrics are considered, it is concluded that finite strains in quartzites are heterogeneous at all scales of observation. Strain styles interpreted include constriction, plane strain and flattening for moderately dipping quartzites, but steep limbs appear to be flattened. Strain ratios increase as a function of increasing bed dip; strain ratios for all samples analyzed are small and internal distortions are minimal.

Strain Analyses Using Conglomerate Clasts

Conglomerate clasts have been used as strain gauges in many previous investigations (Coward, 1976; Etheridge and Vernon, 1981; Gay, 1969; Ghosh and Ramberg, 1976; Holst and Fossen 1987; Lisle, 1979; McClay, 1977; McEwen, 1978;

Mendum, 1976; Miller and Oertel, 1980; Moser, 1976, 1978, 1980; Oertel, 1978; Patterson, 1983; Wood, 1973). The important aspects of some of these studies are summarized (with analyses based on other types of strain indicators) in Table 1. The common application of these features is a function of the widespread distribution of conglomerates in many tectonic settings, coupled with the fact that clasts are preserved even in rocks that have experienced extreme distortions. Recognition of enormous extensions interpreted for certain tectonic settings (Wood, 1973, for example) hinges on interpretations made using deformed conglomerates.

A conglomerate bed occurs near the base of the Ajibik Quartzite (Eagle Mills north limb, Plate 2), and ellipsoidal clasts occur in the same zone (and deformation domain) as ellipsoidal green spots. Ferruginous spots in quartzites occur in at least two environments (Westjohn, 1986, 1987; Bouchez, 1977). For convenience, these spots are referred to as ferruginous spots, since the green color is the product of iron in the reduced state. Ferruginous spots from three localities, and conglomerate clasts from a single location offer the unusual opportunity to estimate strain using three independent gauges (QGSF included) for a single deformation domain.

Rf/Phi plots for conglomerate clasts and QGSF derived from a single sample (Plate 2, sample 914875) are shown in Figures 45-47. Inspection of the Rf/Phi plots shows that clasts in the Ajibik quartzite have a fabric only in the

Table 1. List of strain styles and tectonic environments, based on published data.

Location, age and orogeny	Rock type and fold style	Strain gauge	Strain style and orientation	Strain magnitude	Tectonic setting	Author
Wales Cambrian Caledonian	slate upright symmetric	reduction spots	flattening X vertical	1.7:1:0.26 X=80 to 170% Z=-55 to -75%	autocth.	Wood, 1974
Vermont Cambrian Taconic	slate overturned asymmetric	reduction spots	flattening X inclined	1.7:1:0.17 X=150% Z=-75%	allouch. thrust sheet	Wood, 1974
Rhodesia Archean	greenstone upright isoclinal	pebbles	plane strain X vertical	4.2:1:0.25 X=300% Z=-75%	rim syncline	Wood, 1974
Swiss Alps Jurassic Tertiary	carbonates recumbent	ooids	flattening X horizontal	2.2:1:0.25 Z=-30 to -70%	thrust nappes	Wood, 1974
Scotland Camb. Ordv. Caledonian	conglomerate recumbent	pebbles	constriction X inclined	25:1:0.9 X=1000% Y&Z=-75%	marginal	Wood, 1974
New Jersey	slate upright folds	veins	irrotational pure shear	2.08:1:0.48		Beutner, 1977
New York Appalach. foreland	carbonate	fossils	compaction	10% layer parallel shortening		Engelder, 1977
Australia Cambrian Tabberab- beran Devonian	slate turbidites upright simple	quartz grn. aspect ratios	plane strain constant vol.	100% extension		Waldron & Sandiford 1988

Figure 45. Comparison of Rf/Phi plots for quartz grain ellipticities (left diagram, 361 grains), and pebble ellipticities (142 pebbles) for sample 91487%, plane A. Sample from Eagle Mills syncline.

Figure 46. Rf/Phi plots, for quartz grain ellipticities (335 grains), and pebble ellipticities (105 pebbles), plane B, same sample as Figure 45.

Figure 47. Rf/Phi plots for quartz grain ellipticites (412 grains), and pebble ellipticities (196 pebbles), plane C, same sample as Figure 45.

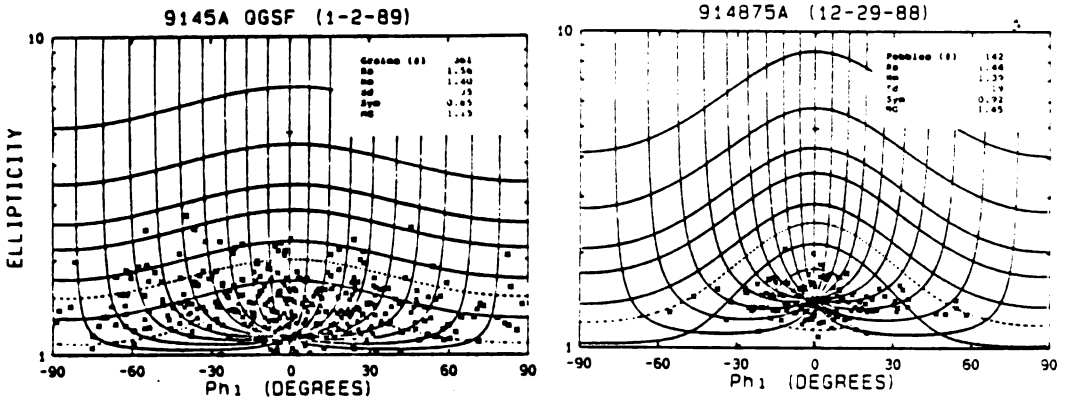

Figure 45.

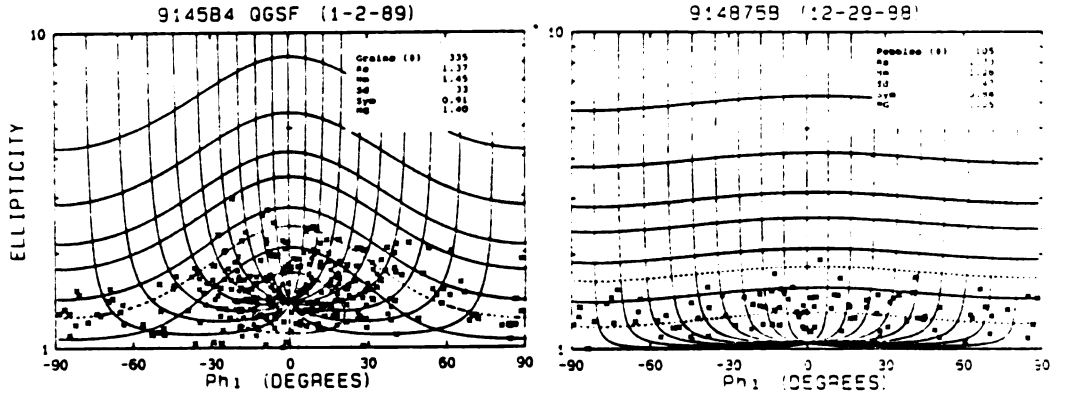

Figure 46.

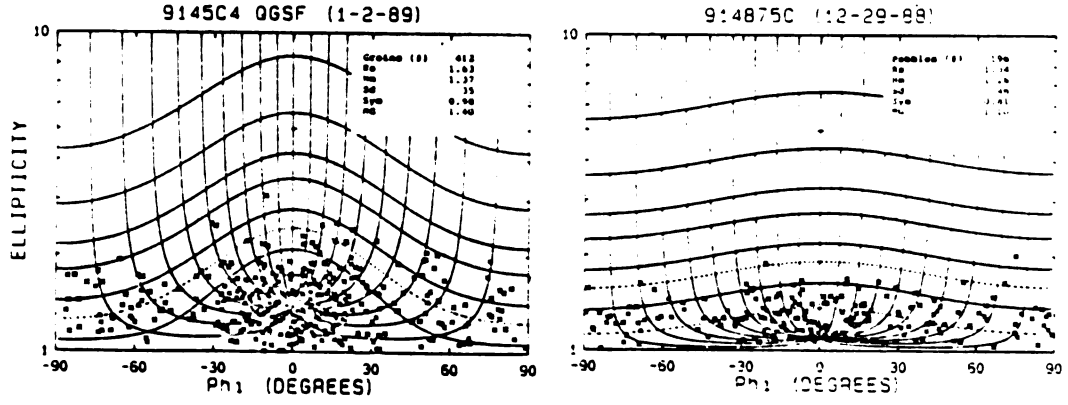

Figure 47.

plane parallel to bedding (Figure 45). Quartz grains in the same plane show a very weak fabric, while planes normal to bedding have a more pronounced fabric. One explanation is that the conglomerate clasts have retained an initial sedimentary fabric, with the long axes showing preferred alignment in the bedding plane. For this case, rotational strains might be interpreted as insignificant. Alternatively, it could be argued that the clasts are not actually pebbles. This alternative case can not be excluded, because recognition of these so-called clasts is a product of color contrasts (Liesegang banding) that are not uncommon in ferruginous quartzites. However, the fact that these proposed pebbles have been observed protruding from weathered surfaces in the quartzites supports the suggestion that they are indeed clasts. Considering the strain ratios indicated by other strain gauges, rotation of clasts is assumed to be an unlikely process, but it is noteworthy that QGSF for the conglomerate sample mimic the fabric documented for other Ajibik samples in the Eagle Mills area.

Strain Analyses Using Ferruginous Spots

There are three outcrops of Ajibik Quartzite (north limb of the Eagle Mills syncline) that contain ellipsoidal ferruginous spots. Rf/Phi plots for each location are shown in Figures 48-53, and Figures 54-56 provide a comparison of Rf/Phi plots for QGSF and reduction spots for

Figure 48. Rf/Phi plot of ferruginous ellipsoidal spots, Ajibik Quartzite, Eagle Mills syncline. (Sample 914872, plane BA, 326 ellipse sections).

Figure 49. Rf/Phi plot of ferruginous spots (same sample as Figure 48, 301 ellipse sections, plane BB).

Figure 50. Rf/Phi plot of ferruginous spots (same sample as Figure 48, 301 ellipse sections, plane BC).

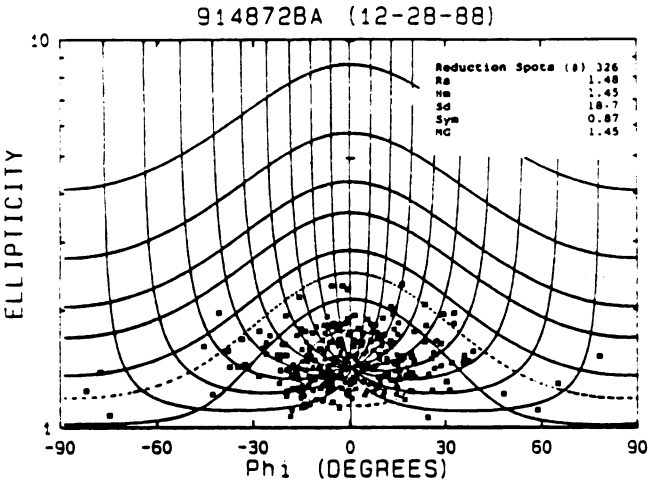

Figure 48.

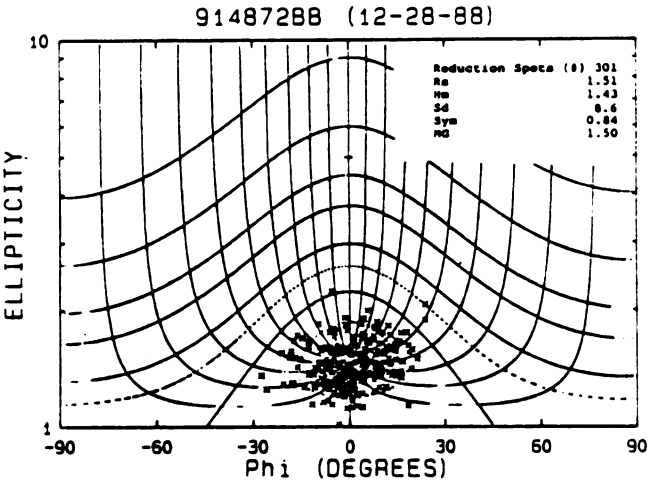

Figure 49.

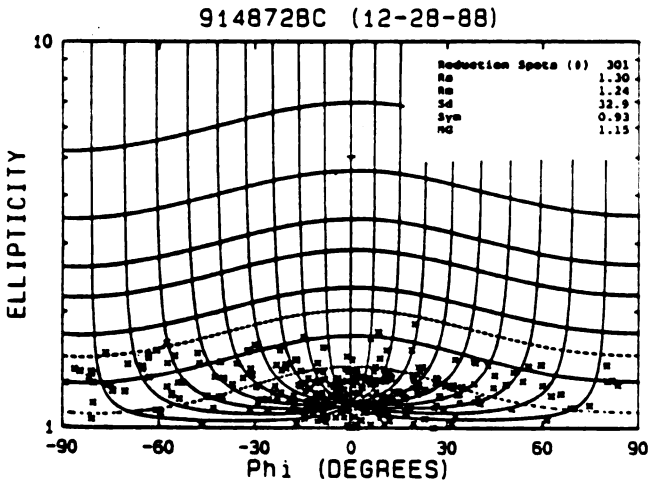

Figure 50.

Figure 51. Rf/Phi plot of ferruginous ellipsoidal spots from Ajibik Quartzite, Eagle Mills syncline (sample NGRS1, plane AF, 211 ellipse sections).

Figure 52. Rf/Phi plot of ferruginous ellipsoidal spots (same sample as Figure 51, 77 ellipse sections, plane FF).

Figure 53. Rf/Phi plot of ferruginous ellipsoidal spots (same sample as Figure 51, 166 ellipse sections, plane IF).

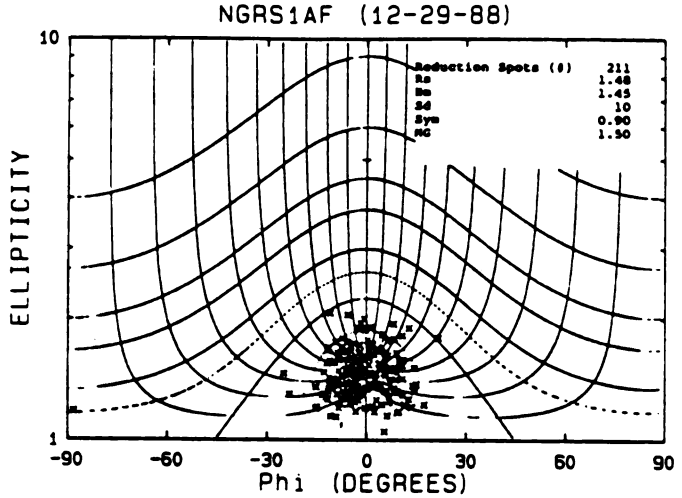

Figure 51.

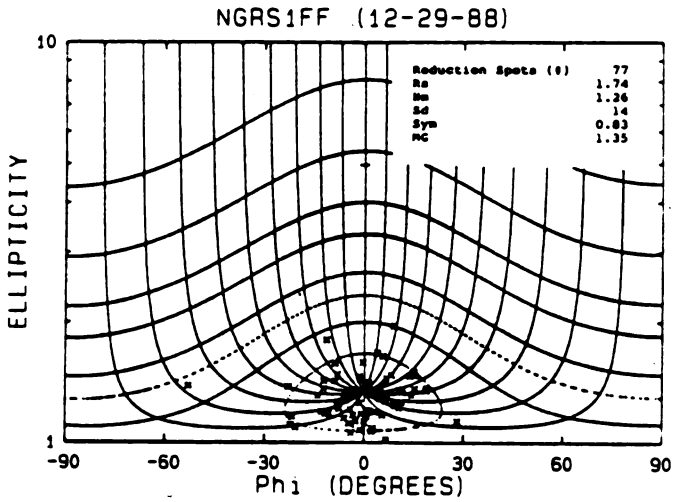

Figure 52.

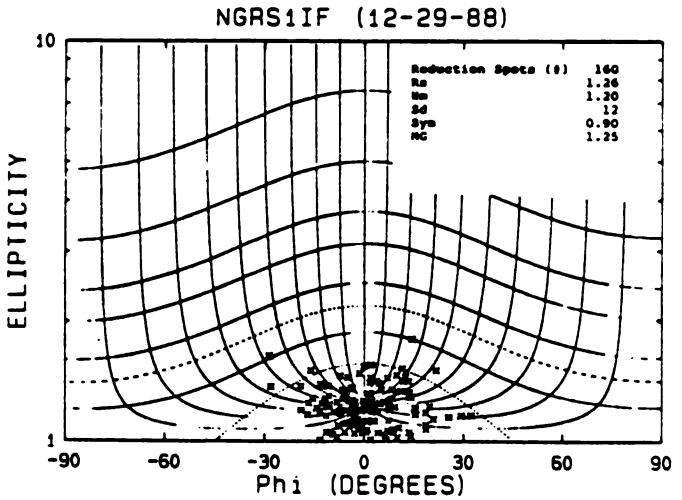

Figure 53.

Figure 54. Rf/Phi plots for 219 reduction spots (left) and 154 quartz grains, Ajibik Quartzite, Eagle Mills syncline (sample 72851, plane AF).

Figure 55. Rf/Phi plots for 111 reduction spots, and 211 quartz grains (same sample as Figure 54, planes F and GF, same orientation, different photograph).

Figure 56. Rf/Phi plots for 155 reduction spots, and 230 quartz grains (same sample as Figure 54, photos J and N, same orientation).

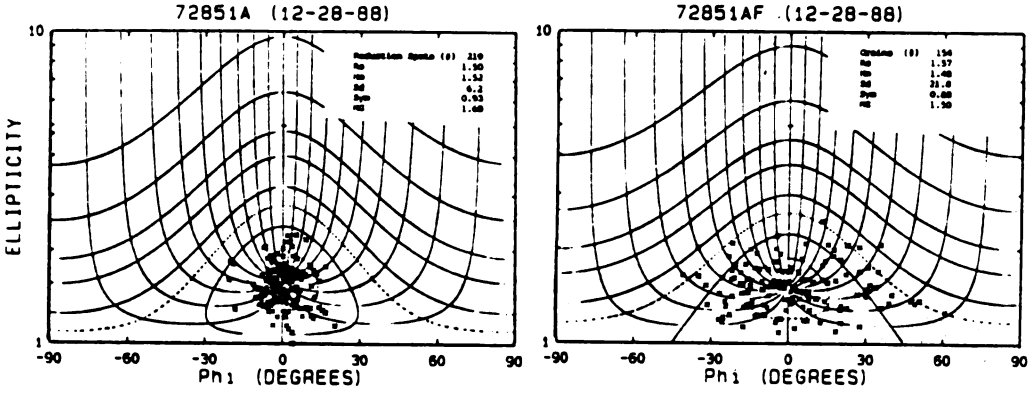

Figure 54.

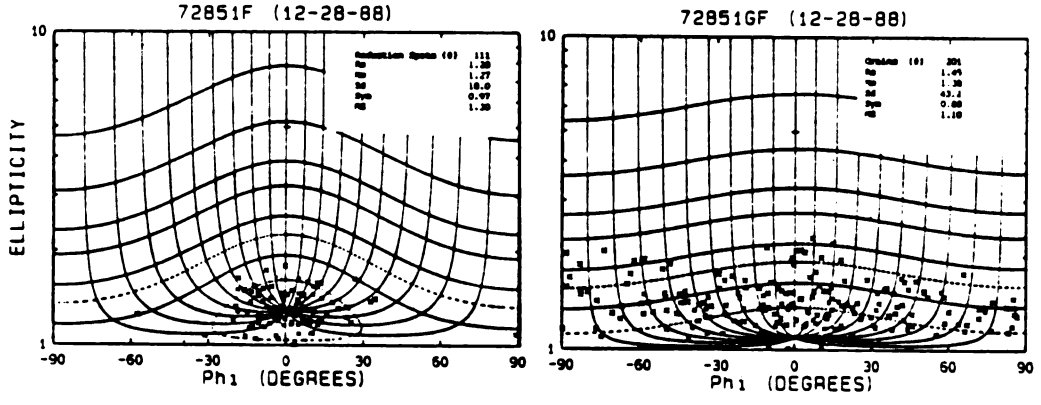

Figure 55.

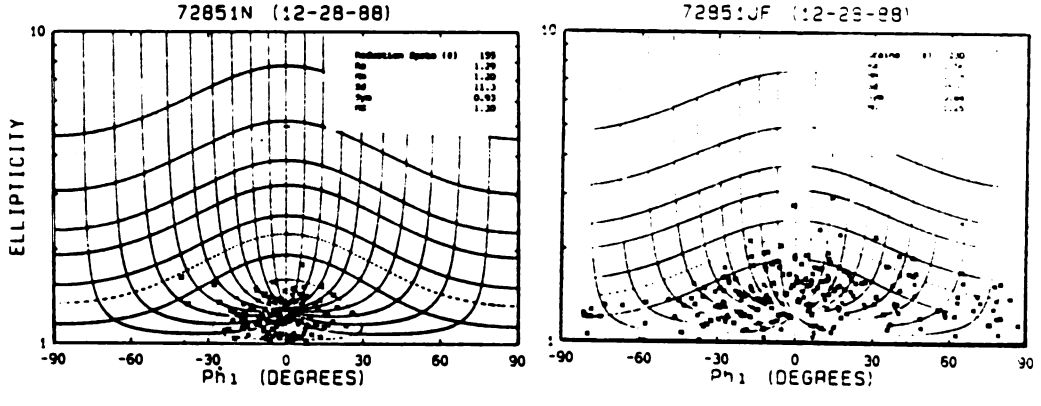

Figure 56.

a single sample. The consistent relationships seen for all quartzites are that ferruginous spot ellipticities are slightly larger than indicated for quartz grains, and spot ellipticities per plane are similar for each location. Ajibik quartzites dip 60 to 70 degrees south at these locations, which are separated by more than one mile along strike. Westjohn (1986) proposed that the difference in ellipticities (reduction spots vs. QGSF) was a function of larger strains recorded by spots, and suggested that spots record the element of grain boundary sliding. Further consideration leads to the suggestion that the differences are not sufficient to support this argument. Inspection of Figure 39 shows that for one sample of Ajibik quartzite (north limb, Eagle Mills syncline, sample 914872), QGSF analyzed by the Rf/Phi method produce nearly the same strain ratio as determined from reduction spots. If grain boundary sliding is an important process, then any strain related to this process cannot be assessed with the methods used.

Many lines of evidence support the conclusion that internal distortions in slates and quartzites developed in an orderly manner, and the strain style is of the flattening type for slates, and ranges from slight constriction to slight flattening for quartzites, except in steep limbs where flattening strains are interpreted for quartzites. Strain ratios increase as a function of increase in dip for both rock types. Several arguments are proposed regarding strain style and deformation mechanisms.

DEFORMATION MECHANISMS

The Role Of Volume Loss

One of the most perplexing problems that must be dealt with in strain analysis is volume loss. The assumption that volume reduction can be neglected in strain analysis (Wood, 1973, 1974; Tullis and Wood; Beutner, 1978; Westjohn, 1978) is viewed as unacceptable by many structural geologists. Wright and Platt (1982) document distortions in Martinsburg Slate using graptolites as strain gauges, and provide convincing evidence demonstrating volume loss during deformation. One of the more controversial arguments posed (Wright and Platt, 1982) is that cleavage forms as a product of pressure dissolution of carbonate and silicate minerals, and hence is a product of volume loss rather than a flattening phenomenon as suggested by others (Wood, 1973, 1974; Westjohn, 1978). The morphology of distorted graptolites (Wright and Platt, 1982) is used to establish that extension in any direction parallel to cleavage is 10 percent or less, and shortening perpendicular to cleavage exceeds 50 percent. This magnitude of shortening is interpreted to be the result of volume loss, rather than a function of flattening strain

(Wright and Platt, 1982). The interpretation of Wright and Platt (1982) is correct only if the distortions measured from graptolites are representative of deformation suffered by the Martinburg slate. Measurements made at the hand sample scale are interpreted to be representative of finite strains at the outcrop scale (Wright and Platt, 1982).

Slates examined in foldbelts worldwide (see Table 1) are reported to have suffered a similar degree of shortening, regardless of the type of strain indicator used. However, the absence of any significant extension noted by Wright and Platt (1982) is in marked contrast to the large magnitude extensions reported by Wood (1973) for Cambrian slates in Wales (170%, for example), and by Westjohn (1978) for Proterozoic slates (approximately 60 percent vertical extension in MRSG slates). In support of the extensions reported by Westjohn (1978), Carter (1989) interprets extensions that range from 40 to 70 percent for Archean greenstones and the lower-most MRSG unit (Enchantment Lake), and he concludes that strains in Archean and Proterozoic supracrustal rocks are not measurably different. However, if volume loss is a mechanism that controls the shape change reduction spots experience during deformation, strain estimates from these features are suspect, particularly regarding the estimated magnitudes of extension. For pressure solution to be a process that results in shape change, dissolution of matrix minerals (carbonates, quartz, and layer silicates) must occur homogeneously, in order to preserve the ellipsoidal

shape of reduction spots.

Bell (1985) demonstrates that commonly proposed deformation models of plane strain without volume loss, and plane strain with incremental volume loss are mechanisms that cannot account for the strain style interpreted for Borrowdale volcanics in the English Lake district. Bell (1985) devised a practical application of theoretical considerations developed by Sanderson (1976), and proposes a pure volume loss component to explain strain style.

Bell (1985) developed a deformation model that involves pure volume loss, followed by plane strain to explain strain style interpreted using accretionary lapilli in deformed volcanic rocks (Table 1). Most structural geologists that invoke large magnitude volume losses related to tectonism prefer the plane strain mode of deformation (Sanderson, 1976, for example). The important features of Bell's (1985) model are illustrated in Figure 57, and also plotted are strain ratios for Kona slates. Reduction spot strain ratios as a function of increasing bed dip are plotted in a second diagram for comparison (Figure 58). Inspection of Figure 57 shows data from this research follows a similar path as the calculated strain path of Bell (1985) where strain ratios are small. The data are interpreted to show that early distortions are consistent with a volume loss deformation mechanism. However, the data (this research) at higher strain ratios deviate from the calculated strain path (Bell, 1985), and the path trends toward the constrictional field of strain.

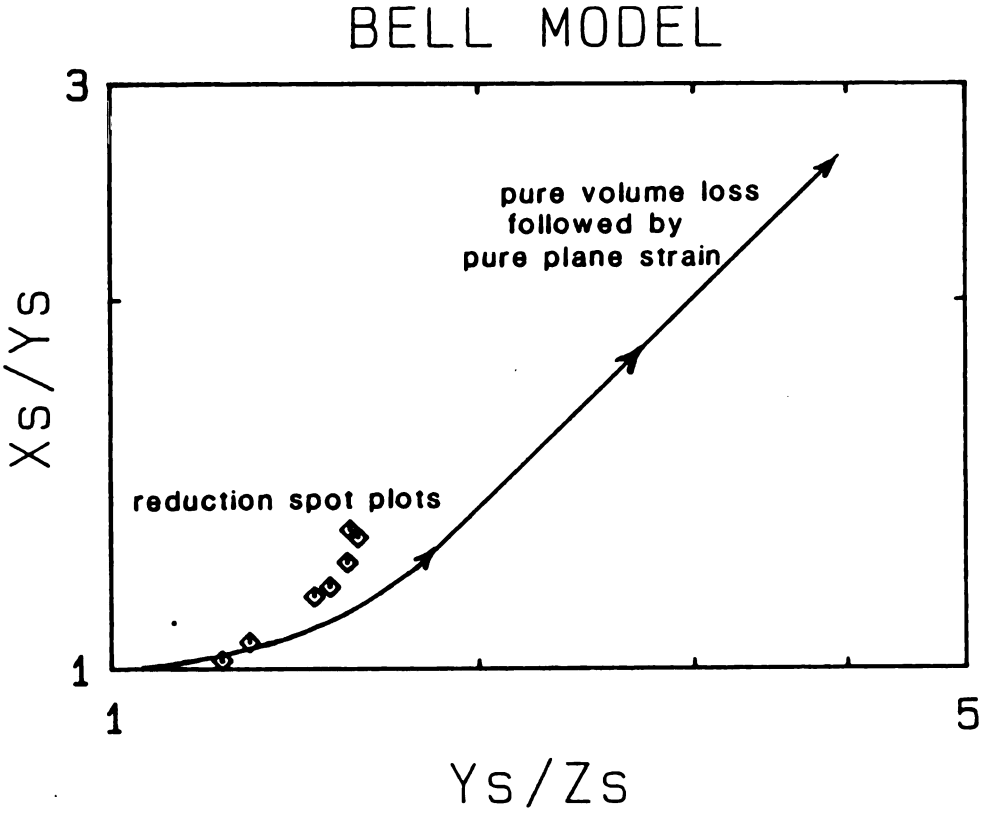

Figure 57. **Logarithmic Flinn plot, based on Bell's (1985) pure volume loss, followed by plane strain model (diamonds are strain ratios from reduction spots in Kona slates).**

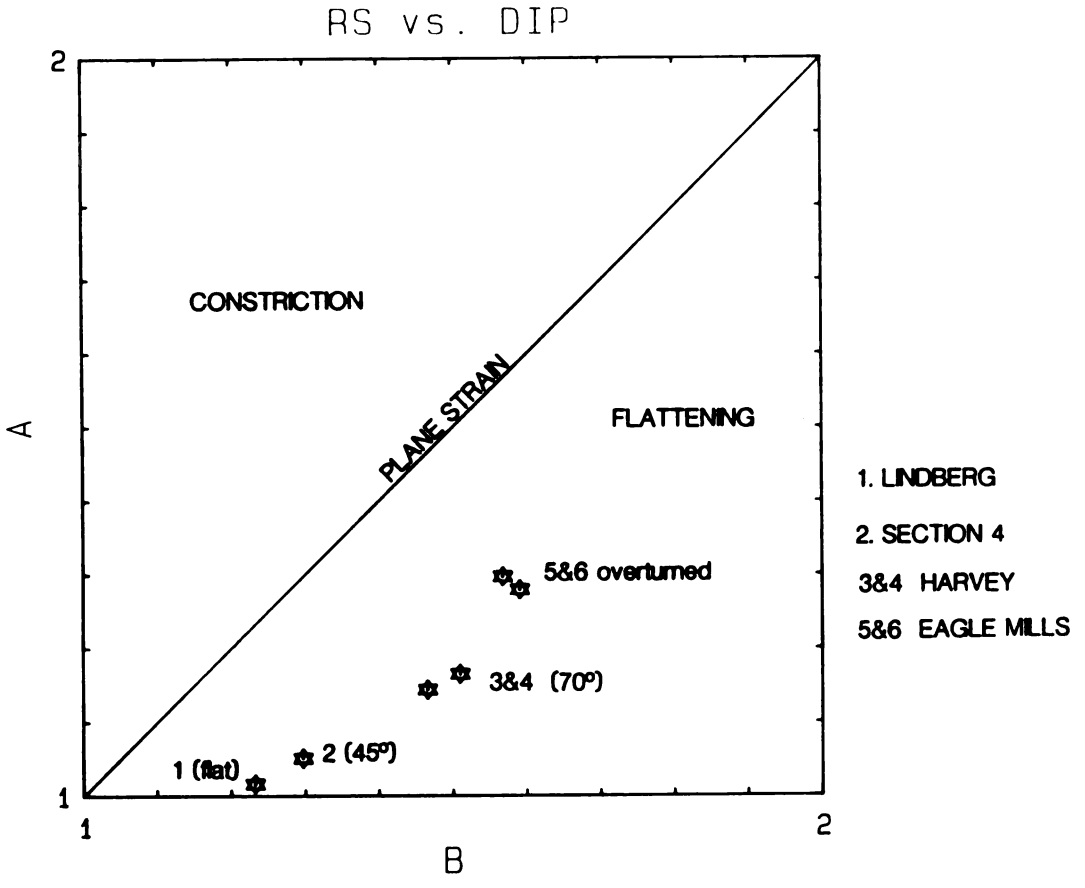

Figure 58. Kona slate reduction spot strain ratios, plotted on a Flinn diagram as a function of bedding dip.

The problem that must be considered is that the preponderance of chocolate tablet boudinaged veins, vein patterns in general, reduction spots in slate, and quartz grain shapes (steep limbs only) cannot be explained by either a plane strain or constrictional model, and all evidence indicates some increment of flattening strain.

There are proponents that continue to argue constant volume deformation. For example, Waldron and Sandiford (1988) argue a constant volume model (closed system) and suggest local dissolution-precipitation reactions to explain the development of P (phyllosilicate) and Q (quartz-rich) domains associated with spaced cleavage development. Quartz grain aspect ratios (similar technique to Rf/Phi method) are used to show that quartz rich domains experienced approximately one-half the distortion recorded by phyllosilicate domains. Waldron and Sandiford (1988) support the constant volume argument with geochemical evidence to show that bulk rock chemistry is constant, although there is redistribution of major and trace elements between P and Q domains. At the other end of the spectrum, Wright and Platt (1982) dispute constant volume deformation, and suggest pore fluid and dissolved constituents move into an overlying sediment pile to form quartz and other vein types.

It is obviously impractical to assume constant volume deformation throughout the history of distortions recorded by MRSG slates and quartzites. The problem is, where is volume loss incorporated in the incremental strain

history? It is obvious that argillites must have been sufficiently lithified to fracture at the stage of vein and sand dike emplacement, so at least partial dewatering must have preceded these structures. Ellipsoidal reduction spots in relatively undeformed argillites (Meyer, 1983) record an increment of layer-parallel shortening that is assumed to be a function of volume loss. Either pore-water loss with corresponding porosity reduction and bulk density increase, or homogeneous pressure dissolution are mechanisms favored to account for the ellipsoidal shape. Consider that reduction spots form in calcareous muds near the sediment-water interface (Beutner, 1978), where the bulk-density may be as low as 1.6 gm/cc, and porosity might exceed 60 percent (Bachman and Edwin, 1976). Slates that represent the deformed product of this assumed precursor (MRSG slates, 2.65 gm/cc density, Klasner and Cannon, 1974) experience a volume reduction that exceeds 60 percent related to expulsion of porewater. This volume reduction is exclusive of material loss due to mass transfer (see section on pressure dissolution).

Westjohn (1989) reports that brine saturated bulk densities in the range of 2.25 to 2.30 gm/cc are common for clean Pennsylvanian and Mississippian sandstones in the Michigan basin, and porosities that range from 25 to 30 percent are associated with this range of bulk density. Klasner (1974) used an average density of 2.65 gm/cc to represent quartzites for gravity models of the Marquette trough. All MRSG quartzites examined have zero porosity.

If a closed system is assumed, and realistic porosity (25 percent) and dry bulk density (1.99 gm/cc, by extracting the effect of brine with density of 1.2 gm/cc) values are assumed, the computed change in bulk density is 33 percent. The small strain ratios measured from quartzites (moderate to steep dipping limbs) could be assigned to distortions that result from this type of material redistribution. Regardless of any of the preceding arguments, MRSG slates and quartzites have zero porosity in their present form, so volume reduction and volume redistribution are considered to be processes that operated during deformation.

One possibility is that the bulk of volume reduction in mudstones (pore water related) takes place in the early stages of fold development. It is likely that at some increment of strain, Kona argillites were entirely dewatered. Consider the hypothesis that cleavage forms in slate only after sufficient or complete dewatering. Figure 58 illustrates an interesting case. Strain ratios for the intermediate dipping limb (45 degrees) and the Lindberg site (flat-lying) are similar, but the principal strain axes differ by 90 degrees between locations. The distortions required to change the principal extension direction from horizontal to vertical are substantially more than one might interpret from the Flinn plot (Figure 53). In terms of general appearance, Kona slate at the Section 4 outcrop (Plate 1) resembles the shallow-dipping argillites, but slaty cleavage is weakly developed. One

approach is to assume that the bulk of volume loss is related to strain increments that are recorded by these two structural settings. The shape change in ellipsoidal reduction spots between the Lindberg quarry and the Section 4 outcrop corresponds to approximately 40 percent horizontal shortening that may be attributable to volume loss. An incremental volume loss model is shown in Figure 59 to demonstrate this case. The volume loss related to pretectonic compaction and early folding is estimated to range from 60 to 70 percent, a figure that exceeds the 50 percent shortening that is commonly interpreted for deformed slates in other tectonic settings (Table 1). However, as Figure 59 illustrates, the strains measured cannot be entirely a function of volume loss, and must include some component of internal distortion. Two independent lines of evidence support this statement. First, as mentioned in the section on vein morphology, most quartz-carbonate veins in shallow dipping Kona argillites are slightly buckled or boudinaged indicating some internal distortion. Second, if the simple shear model for vein rotation (also discussed earlier) is correct, then these deformed veins have experienced a component of angular shear strain.

Pressure Dissolution

Pressure dissolution and its influence on the behavior of rocks during deformation is a subject that continues to

INCREMENT 1

Pure volume loss, represented by reduction spots at the Lindberg quarry:

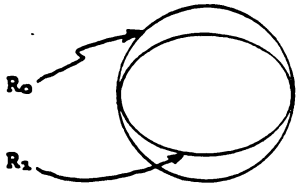

R_o=precompaction spot, XZ plane
R_1=spot w/ increment of volume loss, ellipticity of 1.3
X_{R1}=1.3
Z_{R1}=1.0
e_{z1}=1.0-1.3/1.3=-23%

Increment 1 results in 23 percent layer parallel shortening, related to pure volume loss.

INCREMENT 2

Tectonic produced volume loss accompanied by slight internal distortion, represented by Section 4 outcrop (see Plate 1):

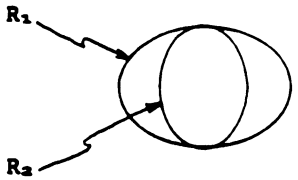

R_1=XZ plane of spot after first increment of volume loss ellipticity 1.3
R_2=XZ plane, after additional volume loss and some internal strain ellipticity 1.36
X_{R1}=1.3
Z_{R1}=1.0
X_{R2}=1.0
X_{R2}/Z_{R2}=1.36
Z_{R2}=1.0/1.36=0.74
e_{z2}=0.74-1.36/1.36=-46%

Increment 2 results in 46 percent horizontal shortening.

INCREMENT 3

Pure shear, constant volume tectonic distortion, represented by reduction spots at the Harvey syncline:

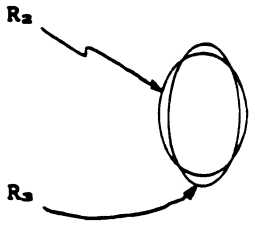

R_3=XZ plane of spots at Harvey
X_{R2}=1.36
Z_{R2}=1.0
area R_2=π(1.3·1.0)=4.27=area R_3
X_{R3}/Z_{R3}=1.68
X_{R3}=Z_{R3}(1.68)
$\pi(Z_{R3}^2 \cdot 1.68)$=4.27
Z_{R3}^2=0.81
Z_{R3}=0.9
X_{R3}=1.51
e_{xR3}=1.51-1.36/1.36=+11%
e_{zR3}=0.9-1.0/1.0=-10%

Increment 3, constant area deformation results in 11 percent vertical extension on X, and 10 percent horizontal shortening on Z, by pure shear.

Figure 59. Composite ellipse model, based on reduction spot strain ratios from three structural settings.

receive attention (see Houseknect, 1988 for example). Sorby (1855) in his early investigation of deformation fabrics in slates proposed that pressure dissolution may have been a process related to slaty cleavage development.

Important observations reported in several articles are briefly reviewed. De Boer (1977) and De Boer and others (1977) demonstrate experimentally that stressed portions of mineral grains are more soluble than "stress-free" parts, which leads to dissolution along grain boundaries, and precipitation in pore space (porosity reduction). Observations from experimental work (De Boer and others, 1977) are extended to suggest that pressure solution may be the mechanism that controls deformation before the onset of plastic straining and dislocation creep in naturally deformed aggregates. Rutter (1983) argues along similar lines, and adds the idea of stress induced chemical gradients, and emphasizes the role of intergranular aqueous films that support shear stress during deformation. Rutter (1983) experimentally produced fibrous crystal growths of amphibole in deformed basalt that are analogous to fibrous growths observed in naturally deformed rocks noted in this dissertation. The fibrous amphibole grains develop preferentially in the direction of maximum finite extension, and are assumed to be the product of pressure-dissolution of basalt.

Etheridge and others (1984) rely on theoretical considerations to implicate the importance of mass material transport and its influence in deformation and

metamorphism. They demonstrate the importance of a high pressure fluid phase on the rheologic properties of the solid phase, and that intergranular mass transport of material (advective mass transport) has significant consequence in explaining the development of internal distortions observed in folded rocks. Etheridge and others (1984) cite the work of Wright and Platt (1982), and use this as an example of large scale transport of material out of the system. They (Etheridige and others, 1984) consider the 50 percent shortening in Martinsburg slate (Wright and Platt, 1982), with no corresponding extension in the plane normal to shortening, evidence that part of the rock mass was mobilized as a result of pressure solution. They also call on examples provided by Stephens and others (1979), and Wall and Cephlecha (1976), who report the common shortening of 50 percent normal to cleavage laminae in folded slates, and suggest the same phenomena applies.

Beach (1974, 1979) approached the pressure solution concept from an alternate viewpoint, to show that the process represents a logical extension of diagenetic processes in sedimentary rocks. It is illustrated (Beach, 1979) that spaced cleavage represents the accumulation of residual insoluble materials, in addition to newly recrystallized mineral phases. Beach (1979) also emphasized that mineral reactions assumed to take place during greenschist facies metamorphism include chlorite to K-mica, and K-spar + epidote to K-mica. Each of these reactions yield water, and it is assumed that release of

this water is another form of volume loss.

It is tempting to suggest that pressure dissolution (volume loss) is a process that dominated the internal distortions recorded by Kona slates, and also played a role in the deformation interpreted for MRSG quartzites. Pressure solution is a process that did operate during the development of folds in the MRSG, but unfortunately its contribution can only be considered qualitatively.

TESTS OF TECTONIC MODELS

It is demonstrated from a variety of quantitative and qualitative evidence that slates of the MRSG experienced a flattening style of strain during folding. Internal distortions appear to develop progressively in quartzites, and the strain style ranges from slight constriction to slight flattening where strain ratios are small. Flattening is more pronounced in steep and overturned limbs. Boudinaged veins show a definite relation to cleavage orientation, and these features are interpreted to support a flattening mode of deformation for slates. The flattening strain style interpreted for slates is supported by the fact that boudinaged veins parallel to cleavage are chocolate-tablet structures, a morphology that requires extension in all directions in the plane of the vein.

Few structural geologists dispute the general relationship of cleavage (and schistocity, see Ramsay, 1967, p. 177) to the principal (XY) plane of the finite strain ellipsoid. On these grounds, it is suggested that the general XY plane for the synclinorium is of the flattening style. The strain ratios are small for all environments, although a general increase in strain ratio corresponds to an increase in limb inclination. Strain

ratios are approximately half for quartzites, compared to slates (steep limbs only). This is in agreement with data reported by others for strain variation between quartzites and phyllites (Waldron and Sandiford, 1988). The concept of angular shear strain applied to deformed veins produced large magnitude extensions, assuming a rotation of 70 degrees is accurate. If the strain ratio for the XZ plane based on reduction spots in the same environment is combined with the appropriate XZ section for the oblate ellipsoids assumed to represent the pretectonic geometry (Lindberg quarry, Plate 1), the resultant composite ellipse indicates an extension of 239 percent. If this magnitude of extension is reasonable, then there is a strain compatibility problem (Sanderson, 1976) that must be considered. Such strains in slates cannot be balanced with those established for quartzites (unless quartzite strain ratios are grossly underestimated) without invoking some mechanism such as volume loss, or the development of similar folds. Any model for the origin of folds in the Marquette trough must be consistent with these general observations.

In terms of models, the data generally support ideas posed by James and others (1961), and Cambray (1977). One fundamental feature common to models proposed by these investigators is that rigid Archean blocks move along reverse faults, and deform the more ductile MRSG units that are trapped in fault bounded troughs. It is difficult to argue against the proposition that Archean blocks played an

instrumental role in the development of the foldbelt, and the resultant strain patterns and style. James and others (1961) illustrate through a series of sketches, models where Archean blocks control deformation patterns in overlying sedimentary rocks. One of James and others (1961) original models (Figure 60) illustrates the extreme case, a situation that is referred to descriptively as the trap-door model (this authors terminology). For this case, the supracrustal rocks could be entirely hidden below opposing Archean blocks. James and others (1961) do not propose a mechanism to explain why basement blocks move. However, compressional stresses consistent with this model would produce the fold geometry observed in the synclinorium.

Cambray (1977, 1984) emphasizes the work of James and others (1961), and shows that the involvement of basement blocks can be considered in light of a modern plate tectonic model. The original model (Cambray, 1977) points to the positive correlation of the MRSG depositional setting and stratigraphic sequence with sedimentary successions seen (seismic profiles) along current plate margins (passive shelf margin, Atlantic coast). In most respects, the Marquette-Ishpeming geologic setting appears to be an ancient analog of a modern plate environment.

Cambray (1984) extends his plate tectonic model to include a component of left-lateral shear to explain superimposed folds in the MRSG. Considerable effort (this research) has been directed to locate areas where

Figure 60. Upper diagram is geologic section showing the relations between Archean and Proterozoic rocks in the Felch trough area, Dickinson county, Michigan (Modified from James and others, 1961). Lower diagram is sketch (from James and others, 1961) showing the trap-door model (this authors nomenclature), and illustrates the possibility that Proterozoic metasediments may be entirely hidden below Archean blocks, and the proposed reverse fault motion.

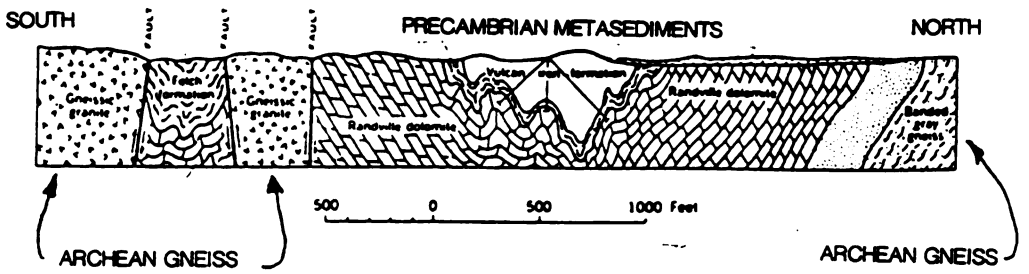
SOUTH
PRECAMBRIAN METASEDIMENTS
NORTH
Randville dolomite
500
0
500
1000 Feet
ARCHEAN GNEISS
ARCHEAN GNEISS

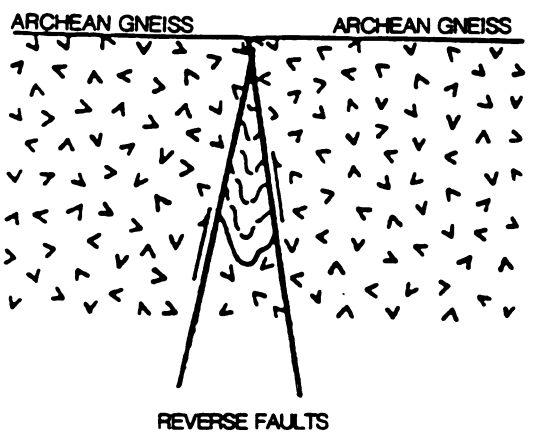
ARCHEAN GNEISS
ARCHEAN GNEISS
REVERSE FAULTS

Figure 60.

superposed folds are prominent, and collect appropriate data to test whether these features are consistent with a model that includes late left-lateral shear. Superposed fold trends that would be consistent with this model necessarily inherit features of the first-formed folds. For example, plunge direction of second generation folds is a function of bed dip of the first order fold. All superposed folds observed have either a near-vertical plunge, or plunge east at moderate angles (40 to 60 degrees). This plunge direction is the same as the plunge of the principal extension direction interpreted from reduction spots in the MRSG. This direction of plunge is also consistent with the style of rotation that would be generated with a left-lateral shear component. However, the left-lateral shear model requires a rotation of the XY principal plane in an anticlockwise fashion, a situation that is only locally observed (Figure 39).

In summary, the trends of superposed folds are consistent with the extended Cambray (1984) model, but strain determinations cannot be used to support or reject the hypothesis of superposed shear along the trough boundaries. The superposed folds are generally sparse, and where observed are always near the contacts with the Archean blocks. These are developed only in fine-grained argillaceous units (Enchantment Lake Formation), a situation that precludes the application of the Rf/Phi technique to assess internal distortions. However, the concept of heterogeneous strain (see heterogeneous strain

model) is proposed to account for the local development of superposed folds in the MRSG. These structures are interpreted to develop only along the trough margins, where shear strains are particularly significant.

In terms of testing additional models that have been proposed to explain fold patterns in the MRSG, there are certain factors that limit the application of the strain data. The data offer no clues to the type of plate margin involved (continent-continent, arc-continent, compression related to subduction of oceanic crust), so none of the compression model variants can be rejected on the basis of the strain data. The absence of volcanic detritus and the dominance of continentally derived sediments (MRSG) cannot be considered evidence contrary to the model proposed by Ueng and Larue (1988), because of the distance between the arc environment and the depositional setting of the MRSG. The arc continental collision model is a realistic model, and consistent with both depositional and deformation styles. However, the extension related drape fold model (Cannon, 1974) is viewed improbable, since structures in general (and strain patterns) are simply not consistent with such a model.

HETEROGENEOUS STRAIN: A GENERAL MODEL

Internal distortions are not homogeneous at the outcrop scale in cases where intercalated lithologic units have substantial ductility contrast. It has been demonstrated that internal distortions are clearly heterogeneous at the bed scale (Figures 13 and 14), and it can be demonstrated that heterogeneous deformation is also recorded at the centimeter scale. One of the fundamental problems in structural geology is that finite extensions, or more particularly finite shortening estimated in a single rock unit is incorrectly suggested to represent the magnitude of distortions that characterize the foldbelt scale.

One approach is to consider that heterogeneous strain patterns are associated with folds observed in the MRSG. Johnson emphasizes that processes involving complex deformation mechanisms can be mathematically modeled (1970, p. 133-172); he illustrates the important role of ductility contrast in the derivation of mathematical expressions to explain fold amplitudes in deformed wax and clay models, and clearly demonstrates that ductility contrasts control fold morphology when material properties differ substantially. Johnson (1970) alludes to analogs in naturally deformed rocks to apply the mathematical

approach. In an effort to explain the increased thickness noted for shales in the hinge zones of folds, while chert beds retain a relatively constant thickness (Franciscan Formation, CA.), Johnson (1970, p. 296) infers that cherts behave as viscous-plastic units (Newtonian viscous behavior). He postulates that cherts may have been gel-like and shales soft mud during folding.

One of the striking features of the Marquette synclinorium is that strain gradient increases from south to north. The largest strain ratios correspond to a narrow belt within the MRSG that parallels the northern structural boundary of the synclinorium. This boundary between Archean and Proterozoic rocks is the apparent continuation of the Carp River Falls Shear Zone (Puffett, 1974, Plate 4). Archean greenstone (Mona Schist) is generally confined to a west-trending belt that is sandwiched between blocks of granitoid gneiss. The granitoid blocks north and south of the synclinorium are not necessarily parts of a single igneous mass (Compeau Creek and Bell Creek Gneiss). These have not been sufficiently dated, nor are isotopic data available to clearly demonstrate the relationship between granitoid blocks. Hammond and Van Schmus (1978) show that granitoids in the northern complex are probably younger than 2.75 Ga, and report one date from the southern complex of 2.4 Ga. Also suggested (Hammond and Van Schmus, 1978) on the basis of a single $Sr^{87}/^{86}$ ratio (0.7200), is that the younger granitoids may represent anatectic melts of the more primitive Archean granitiod crust. Even if the

crystalline rocks are part of the same batholith, the Carp River Falls shear zone is a major structure. One possibility suggested by Cambray (1977) is that this structural setting has characteristics of a slice of oceanic crust that is trapped between eroded arc remnants. If this is the case, the Carp River Falls Shear Zone is indeed a major structure.

Zones of high strain in the MRSG are localized along a narrow belt that parallels the Carp River Falls shear zone. Folds are tight to slightly overturned, while in the southern part of the synclinorium, open folds dominate the structural style. The localization of large magnitude extensions along the northern margin of the synclinorium is further evidence that heterogeneous strains are recorded in the MRSG at the foldbelt scale. It appears that the Carp River structure acts like a buttress, and that the bulk of vertical motion is partitioned along this structural trend (Figure 61).

Consider the simple case offered by Johnson (1970, p. 97) of initial development of buckle folds in a member stressed from one end (Figure 62). This type of model is extended to describe the morphology of folds related to drag along high angle thrust faults. Johnson (1970, p. 102) illustrates an outcrop in southwestern Utah as an analog for the theoretical case (Figure 63). A similar situation is suggested to account for the asymmetry of folds in the MRSG, as well as the heterogeneous strain style.

Figure 61. Diagram illustrating the heterogeneous strain model. Note strains localized along trend of the contact between Archean greenstone and granitoid gneiss, and proposed pop-up structure beneath Ski Hill anticline.

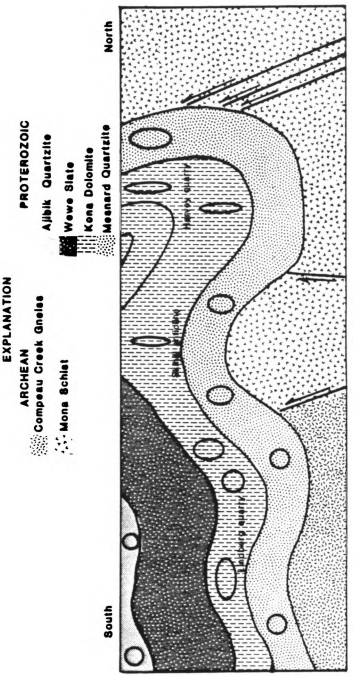
EXPLANATION
ARCHEAN
Compeau Creek Gneiss
Mona Schist
PROTEROZOIC
Ajibik Quartzite
Wewe Slate
Kona Dolomite
Mesnard Quartzite
South
North
NOT TO SCALE

Figure 61.

Figure 62. Simple buckling of an unconfined member on elastic media; deformed from stress at one end (from Johnson, 1970, p. 97). (B and Bo, elastic moduli for member, and elastic media, respectively, T is thickness of member, p is stress, and k is a constant).

Figure 63. Geologic section, showing sketch of fold geometry and natural analog for model illustrated in Figure 62 (from Johnson, 1970, p. 102).

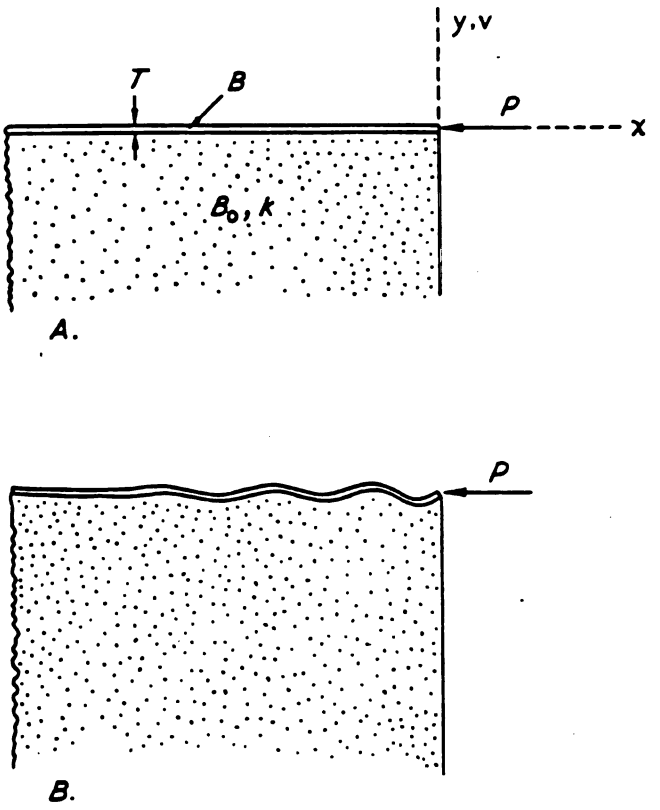

Figure 62.

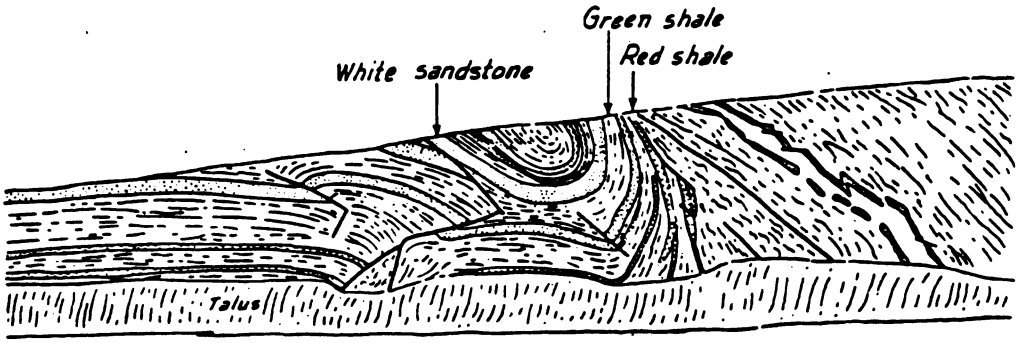

Figure 63.

There are details shown on geologic maps of the synclinorium that indirectly support the involvement of the Archean blocks. One of the more interesting is a sliver of Mona Schist that trends from Lake Superior westward along the Marquette city boundary (see Plate 1, and Gair and Thaden, 1968, Plate 4). This Archean block cores the Ski Hill anticline. The greenstone block is shown in fault contact (queried contact, indicating some uncertainty regarding the structural relations) with the MRSG on the north. I suggest that this is a flower or pop-up structure, and the Ski Hill anticline is a product of this feature. Inspection of geologic maps for the Marquette-Ishpeming area illustrate that features like the Ski Hill anticline are not uncommon, and it is suggested the these undulations are the product of structures in Archean blocks that are covered by the supracrustal package.

There are also observations at the outcrop scale that can be attributed to interaction of Archean and Proterozoic rock units. Figure 64 is an equal area stereogram that shows the distribution of poles to slaty cleavage (Harvey slates) and poles to crenulation cleavage for Mona Schist (same locality). Although it can be argued that crenulation cleavage existed before folding, and hence has no relationship, structures of this type are only observed near the contacts between Archean and Proterozoics units.

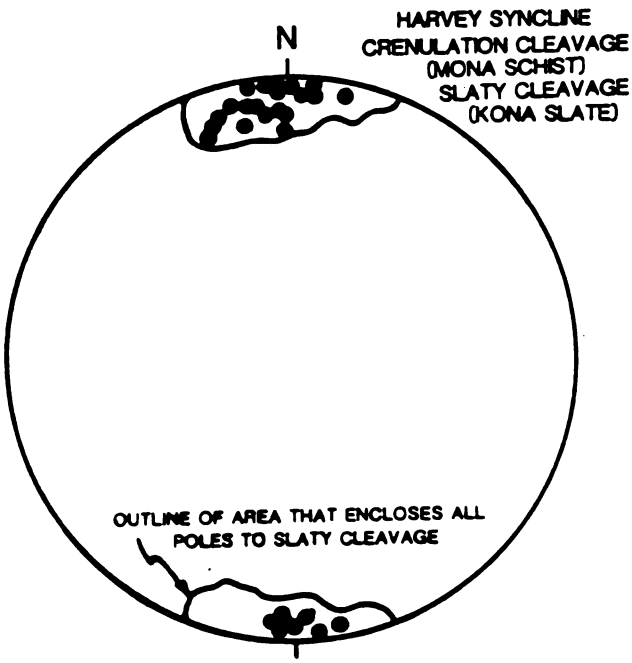

Figure 64. Equal area stereonet plot of area enclosing 179 poles to slaty cleavage orientations (Kona salte, Harvey syncline north limb). Filled circles are poles to crenulation cleavage orientations (28 poles), measured in Mona Schist at the south limb of the Harvey syncline.

CONCLUSIONS

All aspects of a detailed microfabric and macrofabric study of textures in slates and quartzites support the conclusion that a flattening style (X>Y>1>Z) of deformation characterizes internal distortions suffered by the MRSG, but this style of strain is restricted to a narrow trend that parallels the major structural boundary between Archean and Proterozoic rocks. The internal distortions developed in a orderly manner progressively with fold development. Strain magnitudes for slates are approximately twice those observed for quartzites for structural settings in the northern part of the synclinorium. In the south, quartzites show no indication of being strained, while along the Carp River Falls shear zone, strains are very heterogeneous and range from slight constriction to slight flattening. Argillites have suffered predominantly compactional strain, and slight distortions related to the development of open flexures. Strains are heterogeneous, particularly along contacts between units that have large ductility contrasts. Angular shear strains estimated from boudinaged veins show extensions approach 200 percent at contacts between quartzite and slate. These large magnitude extensions are

viewed as real, but hinge on assuming knowledge of pretectonic vein orientations. These areas of high strain are very localized in slates beds, and are not representative of strain for the MRSG at the regional scale.

Major structural features from the Archean rock units are inherited by the supracrustal package, and fold geometry is controlled by translations and rotations along faults and shear zones in the basement blocks. The concept of extrusion tectonics (Topponnier and others, 1982) is disputed by some (Rowley, oral commun., 1988, for example) as a model for explaining large magnitude crustal shortening in the Himalayas, but this mechanism is consistent with the strain style observed. Horizontal shortening in slates estimated previously (Westjohn, 1978) are realistic, but the predominant mechanism controlling internal distortions of reduction spots appears to be pressure dissolution and volume loss. However, the overall magnitude of crustal shortening for the entire MRSG sequence appears to be minor, and localized along a narrow structural zone. The 10 percent horizontal shortening estimated from deformed quartzites with in this structural zone is viewed as a realistic estimate for tectonic related distortions. Extension suggested by Carter (1989) and Westjohn (1978) are exaggerated because volume loss plays an important role in internal distortions and fabric development.

Internal distortions in quartzites produced during

bending were probably accommodated by pressure dissolution precipitation mechanisms accompanied by dynamic recrystallization. Internal distortions (dislocation creep, grain defect slip, etc.) were recorded only in the advanced stage of fold development. Internal distortions in slates are recognized in the early stages of folding, since veins are slightly buckled and stretched, even in weakly deformed argillites.

It is not possible to delineate different strain patterns between the Chocolay and Menominee groups. Strain ratio are approximately the same for Kona and Siamo slates; the same is true for Mesnard and Ajibik quartzites. It is interpreted that penetrative deformation developed after the bulk of sedimentation, or that finite strains are so small that the methods cannot discriminate inherent differences.

A sequence of events that is consistent with the deformation style (see Figures 59 and 61) observed in the MRSG includes (1) early layer-normal shortening (23 percent) related to compaction during continued sedimentation; (2) continued extension during sedimentation along normal faults in Archean basement, with coeval development of east-trending vein sets and sandstone dikes that resulted as the sedimentary pile dewatered; (3) additional tectonic related volume redistribution (approximately 40 percent) and rotation of early structures (veins and sandstone dikes) with the development of early buckle folds or proto-folds during trough closure; initial

bending strains in quartzites during this stage accomplished by pressure dissolution and dynamic recrystallization, (4) onset of flattening strains earlier in slates than quartzites and continued vein and sand-dike rotation driven by angular shear related to flexural-slip folding, (5) continued vertical movement along steep reverse faults (shears) in the Archean, but localized along the greenstone trend, with concomitant development of flower structures below the deforming pile, and (6) minor readjustment along the northern trough margin involving left-lateral shear with the local production of superposed folds, and the development of brittle extension veins in quartzites.

APPENDIX A

APPENDIX A

Computer programs, M.S.U structural geology lab.

Program	Source	Input/function	Output
DIGROCK	Bill Enslin M.S.U.	digitize XY coordinate pairs	file read by RPPH2
RFPH2	J.T. Wilband M.S.U.	XY coordiante pairs	Rf/Phi data pairs
PE	Commercial	delete Y=0 values	clean Rf/Phi data
PASE7	R. Bauer Columbia Univ.	ellipse ratios	3-D solution
FRY2	R. Bauer Columbia Univ.	ellipse long and short axes end points	Fry vacancy field plot
INSTRAIN	Commercial	XY coordinates from digrock	normalized Fry plot
SYMMETRY	P.J. Carter	Rf/Phi data	statistics Lisle (1985) equations
PHICON	B. Cunniff	Rf/Phi data	Rf/Phi data plus 90 degrees
AXICON	B. Sack	Rf/Phi data	Rf/Phi data, mean Phi = 0
XYPL/COPYPLT	J.T. Wilband	any XY or XYZ data	Rf/Phi plots Flinn plots
ROCKWARE/ STEREO	Commercial	orientation data	stereo plots

APPENDIX A

Flow chart showing steps taken to process strain data.

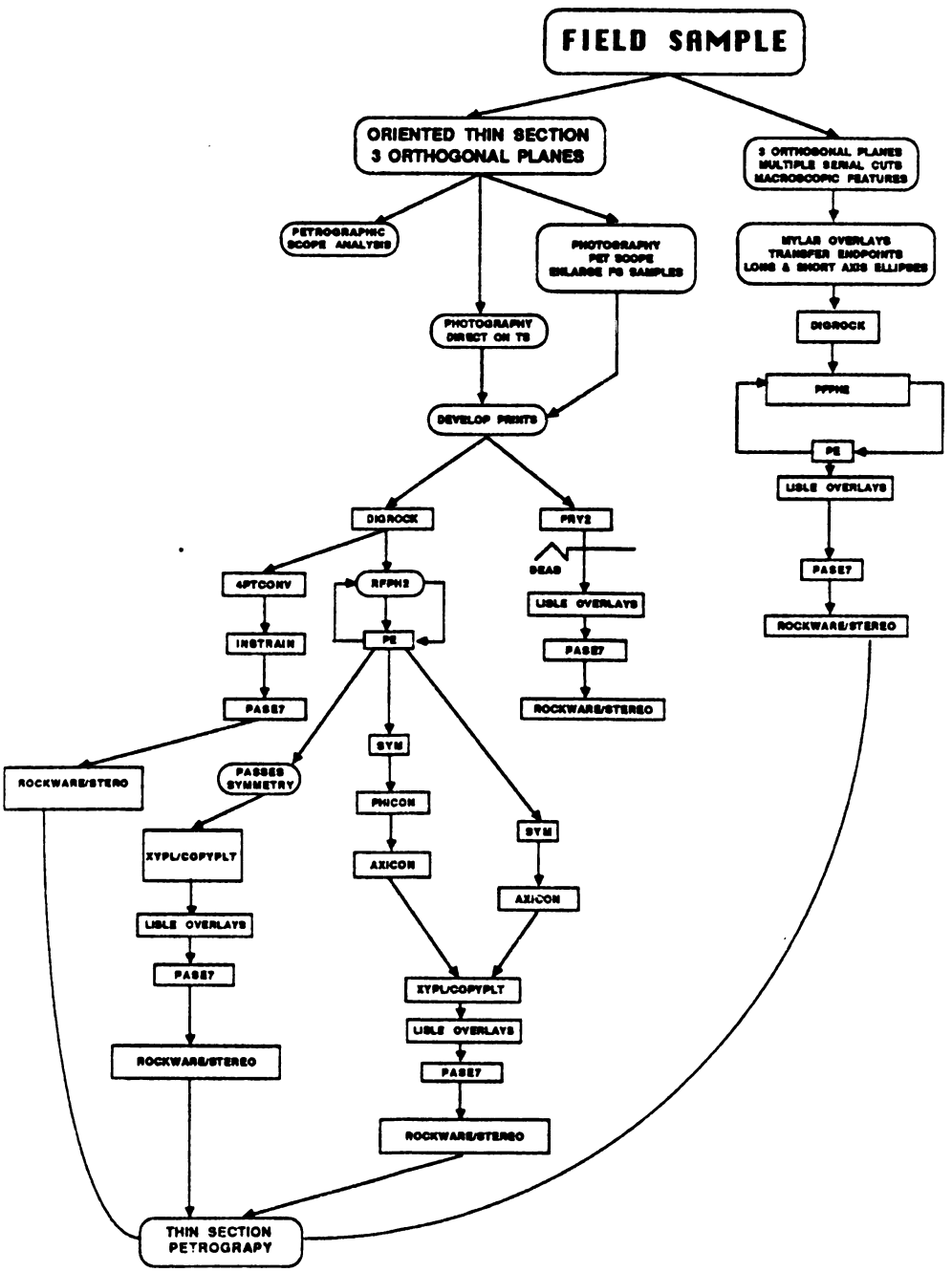

APPENDIX B

APPENDIX B

Summary of Rf/Phi data for quartzite samples

Sample #	Rf max	Rs	Rf (Hm)	Phi (m)	Sym	features (#)
10301E	2.21	1.45	1.36	-0.8	.93	229
10301C	3.15	1.78	1.56	9.4	.87	165
10301BG	3.02	1.77	1.55	-6.8	.88	186
10301D	2.79	1.68	1.53	-0.6	.90	241
914872BC	1.85	1.23	1.24	-0.5	.96	301
914872BA	2.32	1.47	1.45	-3.6	.87	326
914872BB	2.24	1.51	1.43	5.3	.84	301
72851A	2.24	1.50	1.52	-3.2	.93	219
72851AF	2.50	1.57	1.48	-11.4	.88	154
72851F	1.79	1.28	1.27	-9.0	.97	111
72851GF	2.28	1.45	1.38	-14.4	.88	201
72851N	1.80	1.29	1.20	-2.6	.93	155
72851JF	2.96	1.56	1.38	-0.2	.84	230
NGRS1AF	2.07	1.48	1.45	-0.9	.90	211
NGRS1FF	1.95	1.34	1.26	-8.1	.83	77
NGRS1IF	1.80	1.26	1.20	-5.6	.90	160
914875A	2.06	1.44	1.39	0.6	.92	142
914875B	1.92	1.33	1.28	13.5	.84	105
914875C	2.00	1.34	1.26	19.6	.81	198
9145A	2.76	1.56	1.40	-4.0	.85	361
9145B4	2.95	1.37	1.45	0.6	.91	335
9145C4	3.08	1.63	1.37	6.3	.98	412
915875C	2.34	1.41	1.38	3.8	.91	219
915875B	2.71	1.55	1.51	-9.1	.98	398
915875A	2.56	1.50	1.49	-10.1	.95	316
915876B	3.01	1.75	1.50	-4.5	.97	304
915876C	2.80	1.66	1.50	11.8	.93	231
915876A	2.89	1.69	1.66	-13.5	.89	303
916873A	2.61	1.54	1.36	0.6	.97	359
916873B	3.29	1.77	1.42	35.9	.93	308
916873C	2.25	1.41	1.38	30.5	.92	289

APPENDIX B (continued)

Summary of Rf/Phi data, quartzite samples.

Sample #	Rf max	Rs	Rf (Hm)	Phi (m)	Sym	features (#)
103111A	2.51	1.57	1.43	21.4	.97	239
103111B	2.31	1.52	1.42	3.8	.97	238
103111C	2.30	1.42	1.33	5.0	.96	254

APPENDIX C

APPENDIX C

Error Analysis

Errors related to field measurements, transfer of field orientation measurements to rock saw cut surfaces, contact goinometry measurements, and stereonet analysis are the same as reported in Westjohn (1978).

One source of additional error related to techniques that were developed after the preliminary work of Westjohn (1978) is in the selection of Lisle (1985) nomograms for each Rf/Phi plot. For most Rf/Phi plots, it is not possible to select with certainty the "exact" overlay, as data point distributions may fit nomograms that have strain ratios (Rs) that differ by 0.05 units. Where Rs values for two planes (single sample) are the same, or differ by 0.05 units, changing the Rs value input into the Bauer Rf/Phi computer program (see Appendix A) results in a shift in Flinn A and B parameters. This seemingly minor change may shift the strain ratios from one strain field to another. This is primarily because the strain ratios in quartzites are very small.

An additional source of error is that the mean Phi angle derived from the SYMMETRY program (Appendix A) is used in the 3-D calculation of strain geometry. In cases where the Lisle nomogram value (Rs) is very small, the standard deviation for the angle Phi is large (see Appendix B). If the angle the long axis makes with the reference plane is changed by 5 degrees for example, the result may be a much better fit (or a poor fit) regarding the 3-D solution. The program provided by Bauer (personnal commun., 1985) has a subroutine that calculates a value for "internal inconsistency". The internal inconsistency is a value that indicates how well the 3-D solution fits the 2-D data input from the three orthogonal planes. Internal inconsistency values for all data range from 0.00 to 33.71 percent. Strain determinations for QGSF constitute the range reported. The Bauer program iterates five times to find the best fit solution. In cases where the internal inconsistency is less than 5 percent, the strain axes orientations from each iteration plot in the same area of the stereonet, and often only one point for each axis is plotted by the stereo subroutine. In cases where the internal inconsistency value exceeds 10 percent, stereonet plots generated by the Bauer program show substantial scatter in the orientation of the calculated strain axes orientations, and the variation is as much as 30 degrees. In cases where the internal inconsistency value exceeds 20 percent, X and Y, or Y and Z axes may plot in the same area

of the stereonet. In all cases, the best fit solution (best of five iterations) is used; this eliminates any subjectivity. The following is a list of internal inconsistency values, and corresponding 2-D data input per samples. For ease of reference, the geographic name of the outcrop sampled is listed, and the sampled number can be derived from Plates 1-4 if the reader wishes to compare the data to strain ratios or other structural data.

OUTCROP	INTERNAL CONSISTENCY	2-D PARAMETERS PLANE	Rs	ANGLE
Kona slate	3.72%	1	2.24	87.0
Harvey N. limb		2	1.36	81.0
		3	2.79	3.0
Kona slate	4.52%	1	2.34	87.0
Harvey N. limb		2	1.41	82.0
		3	2.96	1.0
Kona slate	8.62%	1	3.30	97.0
Harvey core		2	1.42	25.0
		3	3.00	0.0
Kona slate	6.34%			
Lindbery quarry				
Kona slate	18.97%			
Eagle Mills				
Kona slate	4.32%			
Section 4, Sands Quad.				
Ajibik Quartzite	6.79%	1	1.32	358
Eagle Mills		2	1.58	69
72851 QGSF		3	1.24	348
Ajibik Quartzite	1.87%	1	1.32	348
Eagle Mill		2	1.58	111
72851 reduction spots		3	1.24	348
Ajibik Quartzite	25.32%			
On Teal Lake				
Reduction spots				

Mesnard Quartzite Eagle Mills 915875 QGSF	0.97%	1	1.05	90
		2	1.60	100
		3	1.60	0
Mesnard Quartzite Crest of Eagle Mills ridge QGSF	12.50%	1	1.50	94
		2	1.80	13
		3	1.50	101
Ajibik Quartzite Cooper Lake QGSF	9.41%	1	1.25	90
		2	1.45	68
		3	1.35	0
Ajibik Quartzite Eagle Mills reduction spots 914874	2.33%	1	1.30	95
		2	1.30	95
		3	1.60	0
Ajibik Quartzite Eagle Mills QGSF 914874	3.70%	1	1.30	90
		2	1.15	90
		3	1.60	0
Mesnard Quartzite DNR outcrop QGSF	1.90%	1	1.70	91
		2	1.10	88
		3	1.80	1
Mesnard Quartzite DNR outcropQGSF 1.00 90	0.0%	1	1.80	90
				2
		3	1.80	0
Mesnard Quartzite DNR outcrop QGSF	4.9%	1	1.80	90
		2	1.10	90
		3	1.80	90
Abibik Quartzite Eagle Mills QGSF 914872	35.71%	1	1.10	0.7
		2	1.40	81.4
		3	1.40	84.7

LIST OF REFERENCES

LIST OF REFERENCES

Bachman, R.T., and Edwin, L.H. 1976. Density, porosity, and grain density of samples from deep sea drilling project site 222 (leg 23) in the Arabian Sea. J. Sed. Pet., 46, 654-658.

Baragar, W.C.A., and Scoates, R.F.S., 1981. The Circum-Superior Belt: A Proterozoic plate margin? In: Precambrian Plate Tectonics, A. Kroner, ed., Elsevier Press, New York, p. 297-330.

Beach, A., 1979. Pressure solution as a metamorphic process in deformed terrigeneous sedimentary rocks. Lithos 12, 51-8.

Beach, A., 1974. A geochemical investigation of pressure solution and the formation of veins in deformed greywacke. Contrib. Mineral. Petrol. 46, 61-8.

Bell, A.M. 1985. Strain paths during slaty cleavage formation-the role of volume loss. J. Struct. Geol. 7, 563-568.

Beutner, E.C., 1978. Slaty cleavage and related strain in Martinsburg slate, Delaware Water Gap, New Jersy. Am. J. Sci. 278, 1-23.

Beutner, E.C, Jancin, M.D., and Simon, R.W., 1977. Dewatering origin of cleavage in light of deformed calcite veins and clastic dikes in Martinsburg slate, Delaware Water Gap, New Jersey. Geology 5, 118-122.

Bokman, J., 1959. Comparison of two and three dimensional sphericity of sand grains. Bull. Geol. Soc. Am. 68, 1689-1692.

Borradaile, G.J., 1977. On cleavage and strain: results of study in West Germany using tectonically deformed sand dykes. J. Geol. Soc. Lond., 133, 146-164.

Borradaile, G.J., 1974. Bulk finite tectonic strain estimates from the deformation of Neptunian dykes. Tectonophysics, 22, 127-139.

Bouchez, J.L. 1977. Plastic deformation of quartzites at low temperature in an area of natural strain gradient. Tectonophysics 39, 433-437.

Cambray, F.W., 1984. Proterozoic geology of the Lake Superior south shore. Geol. Assoc. Can. Field Trip Guide 5, 55 p.

Cambray, F.W., 1978. The origin and timing of cleavage formation in the Siamo Slate, of Precambrian X age, Marquette, Michigan. Geol. Soc. Am. Abstr. with Programs.

Cambray, W.F., 1977. Field guide to the Marquette district, Michigan. Michigan Basin Soc. Annual Field Trip. 62 p.

Cannon, W.F., 1973. The Penokean orogeny in Northern Michigan. Geol. Assoc. Can. Spec. Paper 12, 251-271.

Cannon, W.F., and Gair, J.E., 1970. A revision of stratigraphic nomenclature for middle Precambrian rocks in northern Michigan. Geol. Soc. Am. Bull., 81, 2843-2846.

Carter, P.J., 1989. Finite strain estimations for Archean Mona Schist pillows and early Proterozoic Enchantment Lake Formation metawackes in the eastern upper peninsula of Michigan. Unpublished Masters Thesis, Michigan State Univ., East Lansing, Michigan, 97 p.

Clark, L.D., Cannon, W.F., and Klasner, J.S., 1975. Geologic map Negaunee SW Quadrangle. U.S. Geological Survey, Map GQ-1226.

Coward, M.P., 1976. Archaean deformation patterns in south Africa. Phil. Trans. R. Soc. Lond. A283, 313-331.

Crespi, J.M., 1986. Some guidelines for the practical application of Fry's method of strain analysis. J. Struct. Geol., 8, 799-808.

De Boer, R.B., 1977. On the thermodynamics of pressure solution-interaction between chemical and mechanical forces. Geochim. Cosmochim. Acta 41, 249-256.

De Boer, R.B., Nagtegaal, P.J.C., and Duyvus, E.M., 1977. Pressure solution experiment on quartz sand. Geochim. Cosmochim. Acta 41, 257-264.

De Paor, D.G., 1980. Some limitations of the Rf/phi technique of strain analysis. Tectonophysics 64, T29-31.

Donath, F.A., 1970. Some information squeezed out of rocks. Amer. Sci. 58, 54-72.

Donath, F.A., Faill, R.T., and Tobin, D.G., 1971. Deformation mode fields in experimentally deformed rock. Geol. Soc. Am. Bull. 82, 1441-1462.

Donath, F.A., and Parker, R.B., 1964. Folds and folding. Geol. Soc. Am. Bull. 75, 45-62.

Dunnet, D., 1969. A technique of finite strain analysis using elliptical particles. Tectonophysics 7, 117-136.

Dunnet, D., and Siddans, A.W.B., 1971. Non-random sedimentary fabrics and their modification by strain. Tectonophysics 12, 307-325.

Elliot, D. 1970. Determination of finite strain and initial shape from deformed objects. Bull. Geol. Soc. Am. 81, 307-325.

Erslev, E.A., 1988. Normalized center-to-center strain analysis of packed agregates. J. Struct. Geol., 10, 201-209.

Etheridge, M.A., Wall, V.J., Cox, S.f. and Vernon, R.H., 1984. High fluid pressures during regional metamorphism and deformation: implications for mass transport and deformation mechanisms. J. Geophys. Res. 89, 4344-4358.

Etheridge, M.A. and Vernon, R.H., 1981. A deformed polymictic conglomerate: the influence of grain size and composition on the mechanism and rate of deformation. Tectonophysics 79, 237-254.

Flinn, D., 1962. On folding during three-dimensional progressive deformation. Q. J. Geol. Soc. Lond. 118, 385-428.

Fry, N., 1979. Random point distributions and strain measurement in rocks. Tectonophysics 60, 89-105.

Gay, N.C., 1969. The analysis of strain in the Barberton Mountain Land, eastern Transvaal, using deformed pebbles. J. Geol. 77, 337-396.

Gair, J.E., 1975. Bedrock geology and ore deposits of the deposits of the Palmer quadrangle. U.S. Geological Survey Professional Paper, 769, 195 p.

Gair, J.E., and Thaden, R.E, 1968. Geology of the Marquette and Sands quadrangles, Marquette county, Michigan. U.S. Geological Survey Profesional Paper 397, 77 p.

Griggs, D.T., 1940. Experimental flow of rocks under conditions favoring recrystallization. Geol. Soc. Am. Bull., 51, 1001-1022.

Hammond, R.D., and Van Schmus, W.R., 1978. Geochronology of Archean rocks in Marquette County, Upper Michigan. Abstr. and Proc., 24th Ann. Inst. Lake Superior Geol., p 14.

Holst, T.B., 1982. The role of initial fabric on strain determination from deformed ellipsoidal objects. Tectonophysics 82, 329-350.

Holst, T.B., and Fossen, H., 1987. Strain distribution in a fold in the West Norwegian Caledonides. J. Struct. Geol. 9, 915-924.

Houseknecht, D.W., 1988. Intergranular pressure solution in four quartzose sandstones. J. Sed. Pet., 58, 228-246.

James, H.L, Clark, L.D., Lamey, C.A., and Pettijohn, F.J., 1961. Geology of central Dickinson county, Michigan. U.S. Geological Survey Professional Paper 310, 176 p.

Johnson, A.M., 1970. Physical Processes in Geology. Freeman Cooper, San Francisco, 577 p.

Klasner, J.S., 1978. Penokean deformation and associated metamorphism in the western Marquette range, northern Michigan. Geol. Soc. Am. Bull. 89, 711-722.

Klasner, J.S., and Cannon, W.F., 1974. Geologic interpretation of gravity profiles in the western Marquette district, northern Michigan. Geol. Soc. Am. Bull., 85, 213-218.

Larue, D.K., 1983. Early Proterozoic tectonics of the Lake Superior region: Tectonostratigraphic terranes near the purported collision zone. Geol. Soc. Am. Mem. 160, 33-47.

Larue, D.K., and Cambray, F.W., 1979. Cross folding in the Precambrian X strata of the eastern Marquette trough. Abst. and Proc. 25th Ann. Inst. Lake Superior Geol. p. 27.

Lisle, R.J., 1985. Geological Strain Analysis: A Mannual for the Rf/phi Method. Pergamon Press, 99 p.

Lisle, R.J., 1979. Strain analysis using deformed pebbles: The influence of initial pebble shape. Tectonophysics 60, 263-277.

March, A., 1932. Mathematische Theorie der Regelung nach der Korngestalt bei affiner Deformation: Zeitschr. Kristallographie, 81, 285-298.

McClay, K.U.R.L., 1977. Pressure solution and cobble creep in rocks: a review. J. Geol. Soc. London 134, 57-70.

McEwen, T.J., 1978. Diffusional mass transfer processes in pitted pebble conglomerates. Contrib. Mineral. Petrol. 67, 405-415.

Mendum, J.R., 1976. A strain study of the Strathan Conglomerate, North Sutherland. Scott. J. Geol., 12, 135-146.

Meyer, R., 1983. A strain study of the Kona Formation, Marquette County, Michigan. Unpublished masters thesis, Michigan State University, East Lansing, Michigan, 65 p.

Miller, D.M., and Oertel, G., 1979. Strain determination from pebble shapes: a modification. Tectonophysics 55, T11-13.

Milton, N.J., 1980. Determination of the finite strain ellipsoid from measurements on any three sections. Tectonophysics 64, T19-27.

Mitra, S., 1977. A quantative study of deformation mechanisms and finite strain in quartzites. Contr. Min. Petrol., 59, 203-206.

Morey, G.B., and Sims, P.K., 1976. Boundary between two Precambrian W terranes in Minnesota and its geological significance. Geol. Soc. Am. Bull., 87, 141-152.

Moser, S., 1976. Pressure solution as a deformation mechanism in Pennsylvanian conglomerates from Rhode Island. J. Geol. 84, 355-364.

Moser, S., 1980. Pressure solution deformation of conglomerates in shear zones, Narragansett Basin, Rhode Island. J. Struct. Geol. 2, 219-225.

Mykura, H., and Hampton, B.P., 1984. On the mechanism of formation of reduction spots in the Carboniferous/Permian red beds of Warwickshire. Geol. Mag. 121, 71-74.

Oertel, G., 1978. Strain determination from the measurement of pebble shapes. Tectonophysics 50, 73-78.

Onasch, C.M., 1984. Application of the Rf/phi technique to elliptical markers deformed by pressure solution. Tectonophysics 110, 157-165.

Owens, W.H., 1984. The calculation of a best-fit ellipsoid from elliptical data on arbitrarily oriented planes. J. Struct. Geol. 6, 571-578.

Patterson, S.R., 1983. A comparison of methods used in measuring finite strains from ellipsoidal objects. J. Struct. Geol. 5, 611-618.

Peters, W.C., 1978. Exploration and Mining Geology. John Wiley and Sons, New York, 696 p.

Powell, C. McA., 1972. Tectonic dewatering and strain in the Michigamme Slate, Michigan. Geol. Soc. Am. Bull., 83, 2149-2158.

Puffett, W.P., 1974. Geology of the Negaunee Quadrangle, Marquette county, Michigan. U.S. Geological Survey Professional Paper 788, 51 p.

Ramsay, J.G., 1967. Folding and Fracturing of Rocks. McGraw-Hill, New York, 568 p.

Ramsay, J.G., and Huber, M.I., 1983. The Techniques of Modern Structural Geology. Academic Press, London, 307 p.

Ribeiro, A., Kullberg, M.C., and Possolo, A., 1983. Finite strain estimation using "anti-clustered" distributions of points. J. Struct. Geol. 5, 233-244.

Rutter, E.H. 1983. Pressure solution in nature, theory and experiment. J. Geol. Soc. Lond. 140, 725-740.

Sack, W.R., 1988. Geometrical analysis and kinematics of folding associated with overthrusting: Blue Ridge Province, Tennessee. Unpublished Masters Thesis, Michigan State Univ., East Lansing, Michigan, 158 p.

Sanderson, D.J., 1976. The superposition of compaction and plane strain. Tectonophysics 30, 35-54

Sharp, D., 1847. On slaty cleavage. Q. J. Geol. Soc. 3, 74-105.

Sibley, D.F., and Blatt, H., 1976. Intergranular pressure solution and cementation of the Tuscarora orthoquartzite. J. Sed. Pet., 46, 881-896.

Siddans, A.W.B. 1981. Some limitations on the Rf/phi technique of strain analysis: discussion. Tectonophysics 72, 155-157.

Siddans, A.W.B., 1980. Elliptical markers and non-coaxial strain increments. Tectonophysics 67, T21-25.

Sims, P.K., and Peterman, Z.E., 1983. Evolution of Penokean foldbelt, Lake Superior region, and its tectonic environment. Geol. Soc. Am. Mem. 160, 3-14.

Sorby, H.C., 1855. On slaty cleavage as exhibited in the Devonian limestones of Devonshire. Phil. Mag. 11, 20-37.

Sorby, H.C., 1853. On the origin of slaty cleavage. Edin. New Philos. J. 55, 137-148.

Stephens, M.B., Glasson, M.J., and Keays, R.R., 1979. Structural and chemical aspects of metamorphic layering development in metasediments from Clunes, Australia. Am. J. Sci., 279, 129-160.

Talbot, C.J. 1970. The minimum finite strain ellipsoid using deformed quartz veins. Tectonophysics, 9, 47-76.

Taylor, G.L., 1973. Stratigraphy, sedimentology, and sulfide mineralization of the Kona dolomite. Unpublished doctoral dissertation, Michigan Technological Univ., Houghton, Michigan.

Tregus, S.H., 1987. A history of cleavage and folding: An example from the Goldenville Formation, Nova Scotia. Discussion. Geol. Soc. Am. Bull. 100, 152-153.

Toponnier, P., Peltzer, G., Le Dain, A.Y., Armijo, R., and Cobbold, P., 1982. Propagating extrusion tectonics in Asia: New insights from simple experiments with plasticine. Geology 10, 611-616.

Tullis, T.E., and Wood, D.S., 1975. Correlation of finite strain from both reduction bodies and preferred orientation of mica in slate from Wales. Geol. Soc. Am. Bull. 86, 632-638.

Ueng, Wen-long C., and Larue, D.K., 1988. The early Proterozoic structural and tectonic setting of the south central Lake Superior region. Tectonics, 7, 369-388.

Van Hise, G.H., and Leith, C.K., 1911. The geology of the Lake Superior region. U.S. Geological Survey Mon. 52, 641 p.

Van Schmus, W.R., 1976. Early and middle Proterozoic history of the Great Lakes area, North America. Phil. Trans. R. Soc. Lond. A280, 605-628.

Van Schmus, W.R., and Bickford, M.E., 1981. Proterozoic chronology and evolution of the midcontinent region, North America. In: Precambrian Plate Tectonics, A.Kroner, ed., Elsevier Press, New York, p. 261-296.

Voight, B., 1964. Boudinage: A natural strain and ductility gauge in deformed rocks. Geol. Soc. Am. Programs with Abstracts, p. 213-214.

Waldron, H.M., and Sandiford, M.S., 1988. Deformation volume and cleavage development in metasedimentary rocks from the Ballarat slate belt. J. Struct. Geol. 10, 53-62.

Wall, V.J., and Cephlecha, J.C., 1976. Deformation and metamorphism in the development of gold-quartz mineralization in slate belts [abst.]. 25th International Geological Congress, Sidney, Australia.

Westjohn, D.B., 1989. Application of geophysics in the delineation of the freshwater/saline-water interface in the Michigan basin. Monograph series, 24th Annual American Water Resources Association, 32 p.

Westjohn, D.B., 1987, Strain partitioning in Proterozoic supracrustal rocks of the Marquette Range Supergroup, Marquette County, Michigan, U.S.A. Geological Society of America Abstracts with Programs, v. 19, no. 4, p. 251.

Westjohn, D.B., 1986, A comparison of finite strains in quartzites and slates of the Marquette Range Supergroup, Marquette County, Michigan, U.S.A. [abs.] 32nd Annual Institute on Lake Superior Geology.

Westjohn, D.B., 1978. Finite strain in the Precambrian Kona Formation, Marquette county, Michigan. Unpub. M.S. thesis, Michigan State Univ., E. Lansing, Michigan, 72 p.

Williams, P.F., 1977. Foliation: A review and discussion. Tectonophysics 39, 305-354.

Williams, P.F., 1976. Relationships between axial-plane foliations and strain. Tectonophysics 30, 181-196.

Wood, D.S., 1974. Current views of the development of slaty cleavage. Annual Reviews Earth Planetary Sci. 2, 368-401.

Wood, D.S, 1973. Patterns and magnitudes of natural strain in rocks. Phil. Trans. R. Soc. Lond. A. 274, 373-382.

Wright, T.O., and Platt, L.B., 1982. Pressure dissolution and cleavage in the Martinsburg shale. Am. J. Sci., 282, 122-135.

Geology from Gair and Thaden, 1968

NORTHERN COMPLEX GRANITOIDS

Contact between Archean greenstone and Archean granitoid

Diabase dikes

MARQUETTE

LAKE SUPERIOR

MONA SCHIST

MT. MESNARD
POLES TO PLANAR QUARTZ VEINS

1030868

1030861

DNR GGSF

MESNARD QUARTZITE DNR OUTCROP GGSF

CONSTRICTION FIELD
PLANE STRAIN
FLATTENING FIELD

ARCHEAN PROTEROZOIC CONTACT

SKIHILL SPOTS

SKIHILL REDUCTION SPOTS

1030868
MT. MESNARD
1030861
1030862

1030863

COMMON SECTION CORNER

T48N / T47N — 36 31 1 6 — R26W | R25W

SKI HILL ANTICLINE

HARVEY SYNCLINE

MARQUETTE QUADRANGLE

SANDS QUADRANGLE

914878

HARVEY SPOTS & VEINS

HARVEY REDUCTION SPOTS & VEINS

Z(RS)
Y(V)
X(V)
X(RS)
Y(RS)
Z(V)

SHALLOW DIPPING KONA ARGILLITE VEIN TRENDS

1031867
1031868

1031869

SECTION 4 (RS)

914878

SECTION 4 SAND AND HARD QUADS REDUCTION SPOTS KONA SLATE

AJIBIK (15 DEGREES)

HARVEY CORE (RS)

HARVEY CORE KONA REDUCTION SPOTS

72853
72852

LINDBERG QUARRY

LINDBERG (RS)

LINDBERG REDUCTION SPOTS

KONA SLATE HARVEY SYNCLINE

121 POLES TO BOUDINAGED VEINS

179 POLES TO CLEAVAGE

COMPEAU CREEK MRS CONTACT

TALBOT VEIN SOLUTIONS

Overall Area of Elongation Solution B

SOLUTION C OVERALL AREA OF ELONGATION

SOUTHERN COMPLEX GRANITOIDS

EXPLANATION

- sample number and location
- contact between geologic units
- trend of diabase dike
- axis of syncline
- axis of anticline
- trend of fault or shear zone

MRSG — Marquette Range Supergroup

Accg — Archean Compeau Creek Gneiss

Ams — Archean Mona Schist

SCALE 1:24 000

1 MILE

0 1000 2000 3000 4000 5000 6000 7000 FEET

0 1000 1 KILOMETER

0 .5 1

PLATE 2

Geology from Gair, 1975

NEGAUNEE QUADRANGLE

T48N

12 7
13 18

R27W R26W

EXPLANATION

- sample number and location
- contact between geologic units
- trend of diabase dike
- axis of syncline
- axis of anticline
- trend of fault or shear zone

MRSG Marquette Range Supergroup

Accg Archean Compeau Creek Gneiss

Ams Archean Mona Schist

AJIBIK & MESNARD QUARTZITES
EAGLE MILLS SYNCLINE TO COOPER LAKE
FLINN PLOT

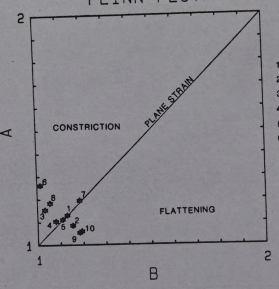

EXPLANATION

1 72851 Ajibik Spots
2 914873 Ajibik Spots
3 914873 Ajibik QGSF
4 72851 Ajibik QGSF
5 Teal Lake Spots
6 915875 Mesnard QGSF
7 10318611 Ajibik QGSF
8 915876 Mesnard QGSF
9 914872 Ajibik Spots
10 914872 Ajibik QGSF

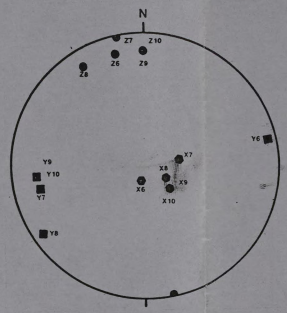

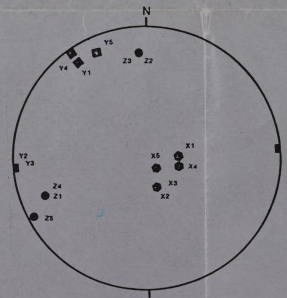

EAGLE MILLS (RS)

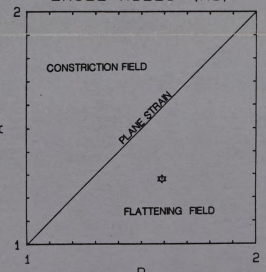

EAGLE MILLS SYNCLINE
KONA SLATE
REDUCTION SPOTS

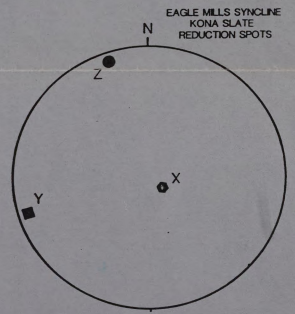

ARCHEAN METAVOLCANICS

CARP RIVER FALLS SHEAR ZONE

MARQUETTE RANGE SUPERGROUP

915871
915872
111861
915876a
915876b
Teal Lake Spots
712851
111862
916871
72851
72852
912871
912872
914871
914872
914873
914874
914875
914876
915873
915874
915875
TEAL LAKE

EAGLE MILLS SYNCLINE

PLATE 3

Geology from Puffett, 1974

PALMER QUADRANGLE

EXPLANATION

- sample number and location
- contact between geologic units
- trend of diabase dike
- axis of syncline
- axis of anticline
- trend of fault or shear zone
- MRSG Marquette Range Supergroup
- Accg Archean Compeau Creek Gneiss
- Ams Archean Mona Schist

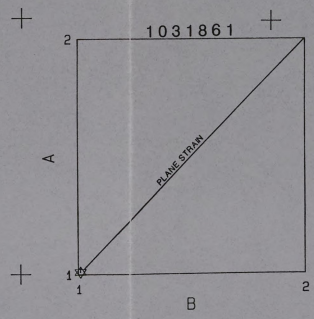

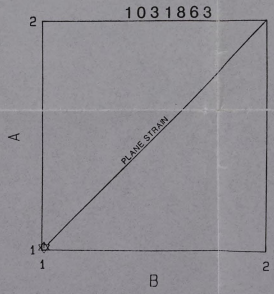

1031861

GOOSE LAKE

1031863 1031862

Accg

MRSG

MRSG Accg

MRSG Accg

MRSG Accg

MRSG Accg

T47N R26W

26 25
35 36

ARCHEAN COMPEAU CREEK GNEISS

Geology from Clark and others, 1975

NEGAUNEE SOUTHWEST QUADRANGLE

PLATE4

EXPLANATION

- ⊠ sample number and location
- contact between geologic units
- trend of diabase dike
- axis of syncline
- axis of anticline
- trend of fault or shear zone

MRSG Marquette Range Supergroup

Accg Archean Compeau Creek Gneiss

Ams Archean Mona Schist

T48N R27W

9,10
16 15

MAJOR SHEAR ZONE

AJIBIK & MESNARD QUARTZITES
EAGLE MILLS SYNCLINE TO COOPER LAKE
FLINN PLOT

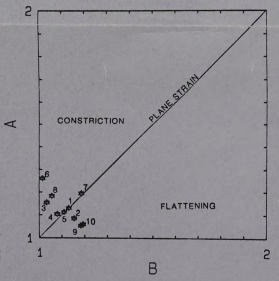

EXPLANATION

1 72851 Ajibik Spots
2 914873 Ajibik Spots
3 914873 Ajibik QGSF
4 72851 Ajibik QGSF
5 Teal Lake Spots
6 915875 Mesnard QGSF
7 10318611 Ajibik QGSF
8 915876 Mesnard QGSF
9 914872 Ajibik Spots
10 914872 Ajibik QGSF

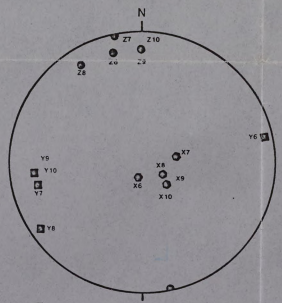

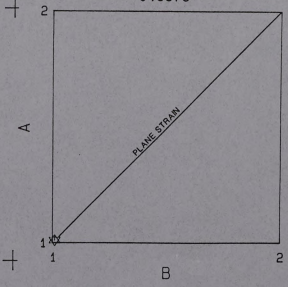

CARP RIVER FALLS SHEAR ZONE

916872

TEAL LAKE

10318610

916874b

916873

916874a

10318611

T48N

KITCHI SCHIST

3631
T6

Common Section Corner

T47N

R28W R27W

MARQUETTE RANGE SUPERGROUP